FISSION YIELD DETERMINATIONS

C. Fred Moore, et al

Texas University at Austin

Prepared for:

Office of Naval Research
Advanced Research Projects Agency

1973

FINAL TECHNICAL REPORT

FISSION YIELD DETERMINATIONS

Sponsored by

ADVANCED RESEARCH PROJECTS AGENCY

Form Approved Budget Bureau No. 22-R0293

Program Code Number	0F10
ARPA Order Number	1571
Name of Contractor	The University of Texas at Austin
Date of Contract	1 January 1973
Contract Number	N00014-67-A-0126-0012
Amount of Contract	$120,000
Contract Expiration Date	31 December 1973
Short Title of Work	Fission Yield Determinations
Principal Investigators	C. Fred Moore, Professor of Physics
	G. W. Hoffmann, Assistant Professor of Physics

Disclaimer: The views and conclusions contained in this document are those of the authors and should not be interpreted as necessarily representing the official policies, either expressed or implied, of the Advanced Research Projects Agency or the U.S. Government.

107

TABLE OF CONTENTS

I. INTRODUCTION 1

II. EXPERIMENTAL PROGRAMS 7

A. X-Ray Measurements 7

B. Electrostatic Particle Guide 30

C. High Resolution-Charged-Particle Mass Identification Using Time-Of-Flight 37

D. Internal Conversion Spectrometer 44

E. Studies of p + ^{92}Mo Induced Internal Conversion Electrons 52

F. X-Ray-Gamma Coincidence Studies from Spontaneous Fission of ^{252}Cf 61

I. INTRODUCTION

In this introduction, a summary of the work done to date in connection with fission yield measurements and fission related studies is given. The sections following this introduction then provide fuller discussion of topics only briefly mentioned.

During the past three years, research aimed at the ultimate extraction of isotopic fission yields from neutron induced fission of $^{233,235,238}U$ and ^{239}Pu has been contracted between the University of Texas' Center for Nuclear Studies and the Advanced Research Projects Agency of the United States Government and administered through the Office of Naval Research.

The task of isotopic fission yield determination is, in fact, a monumental one. Simultaneously, for each fission fragment, one must obtain both its nuclear (not atomic) charge and its mass. Many avenues of approach have been explored as to the most reliable experimental technique (indeed, if any) from which the needed information can be obtained. As far as the nuclear charge determination is concerned, clearly X-rays emitted from excited fission fragments may be observed, and these, in fact, can, and have been, used to determine the nuclear charge of those fragments from which X-rays are detected. See Section II.A for some of the results of coincidence X-ray studies from fission.

The problem of relating these measured charge values to the actual fission quantized charge distribution is complicated by the uncertainty of the mechanism of X-ray emission. If this mechanism is one of nuclear de-excitation in origin, such as internal conversion, which for K X-ray emission seems to predominate, then normalization of the change yield, at this point, is virtually impossible, because internal conversion is very nuclear structure dependent, and essentially no information is at hand, from which a systematic normalization procedure can be constructed. On the other hand, if X-ray emission is atomic in nature, such as that which may result from electronic transitions after inner-shell ionization by passing energetic fission fragments through thin metallic foils, then the unfolding of the charge distribution from the observed X-ray spectra can be managed since inner-shell electron ionization for such processes is understood. Hence, this is a promising technique for determining fission quantized charge distributions and, in fact, is the technique we undertook for fission yield charge distributions.

Of course, at the same time that the fragment charge is determined, the mass of the fragment must be measured. Many techniques have been used in the past, but they all suffer in that masses have never been determined to better than 1 mass unit, so quantized mass yields are still to be determined. Many possible techniques for determining quantized mass yields have been explored. It was felt that the most promising of these was an energy-time-of-flight measurement on the fragment itself from which the mass may be calculated from (classically,

for example) $m = 2Et^2/d^2$. Such an experiment requires, if m is to be determined to better than 1 mass unit, a very long flight path with excellent fast timing to make $\Delta t/t$ small, as well as excellent energy resolution in a solid state detector such that $\Delta E/E$ is very small. The problem of timing over a long flight path with a reasonable effective solid angle was solved with the use of an electostatic particle guide of the type described by Oakey and Macfarlane. See Section II.B for a comprehensive discussion of the electrostatic particle guide. The problem of excellent energy resolution from a solid state charged particle detector is more serious. An inherent difficulty in accurately determining the kinetic energy of a fission fragment (typical A = 100 amu, and E = 100 MeV) is that the large value of the charge of the fragment (say 20) makes the energy uncertainty (ΔE) from the detector larger than, say, for protons, deuterons, alphas, or other light charged particles, because the much larger number of ion pairs produced in the detector for the heavier fission fragment means that more atomic recombination will occur before all ion pairs are collected, and hence, more energy uncertainty. However, this problem can be circumvented to some degree by two techniques. The first is to 'channel' the heavy fragments with a special silicon surface barrier detector. The much improved energy resolution for those particles that do channel (about 75% in practice) then makes energy determination to the accuracy needed for quantized mass determination via $m = 2Et^2/d^2$ more feasible. The other technique is to degrade the fission fragment energy with a thin foil. Then the smaller energy can be measured more

accurately than the larger energy and hence dE/E will be reduced. Since the particle energy is degraded before entering the particle guide, the time measured by the guide is that for a particle of reduced energy but the same mass as the particle incident upon the foil, so degrading the energy if it improves dE/E, must improve dM/M.

During the period of the ARPA Contract, several very novel basic nuclear physics experiments grew directly from our efforts to measure fission yields.

The proto-type of the electrostatic particle guide has been installed on one of the beam lines from the University of Texas EN Tandem Accelerator, where it is being used for high energy resolution mass identification for charged particle induced reaction products. It is operated essentially in the same way as the fission electrostatic particle guide. There are two modes of operation: (1) pulsing and bunching the beam from the accelerator itself gives a periodic structure to the beam from which time-of-flight measurements utilizing the particle may be made, and (2) by running the accelerator with a DC beam and having the charged reaction products go through a thin plastic film before entering the guide for transport. The film is 'observed' by a photo-multiplier system, and thus, the photons created by the particle traversing the plastic film initiate a very fast signal in the photomultiplier from which the particle can be timed as it traverses the guide. This technique using an electrostatic particle guide for high energy resolution and high mass resolution is ideal, for, say, (d,p) reactions studies to highly

excited states in the residual nucleus, and heavy ion transfer reaction studies, where the use of a single energy detector is mandatory if one expects reasonable energy resolution. This application of the electrostatic particle guide is more fully discussed in Section II.C of this report.

Gamma decay from fission fragments has also been investigated in an attempt to extract fission yields. Our measurements have involved gamma-gamma coincidence studies, and more than 500 gamma transitions have been identified as to particular fission isotope. Section II.F reports on some of these experiments.

A very sophisticated PDP-15 computer system has been developed during the course of the fission experiments. An on-line multiparameter (up to 4) data acquisition program as well as an off-on-line multiparameter data analysis program now exist to provide the experimenter essentially any degree of flexibility for his particular experiment.

II. EXPERIMENTAL PROGRAMS

A. X-Ray Measurements

This section reports the observation of internal conversion cascades in nuclei formed by the fission of ^{252}Cf. The measurement involves the detection of the X-rays following internal conversion transitions. The development in recent years of high efficiency, high resolution solid state detectors to measure the X-rays produced in a fission event in coincidence with other processes has renewed interest in the study of fission yields. The fission process produces highly excited fragments with unstable nuclei having very short halflives. Their electromagnetic radiations as well as their beta-decay and their internal conversion electrons form complicated spectra that can be analyzed most efficiently by coincidence techniques.[1,2,3] These have been used to determine the charge, mass and energy of the fragments in order to identify the isotopes with short lives that are produced during the fission.[4,5,6,7]

The most rudimentary X-ray coincidence measurement to make, but one which has not been reported previously,[8] is that of (X-ray, X-ray). The present measurement gives the result that not only do the complementary fission products produce coincident K X-rays, but also coincident K X-rays from the same Z element are produced with comparable and more often much greater magnitude. This obviously can happen only by some means of multiple <u>successive</u> K shell ionizations in the same

element, since double K shell ionization will shift the X-ray energies appreciably for the first of the two K X-ray transitions.

Source and Detectors

A small ^{252}Cf source (approximately 550 fissions/sec) was sandwiched between two pieces of cellophane tape ($C_{10}H_8O_4$) and placed between the faces of two semi-conductor detectors with 1.0 mm and 5.0 mm Beryllium windows. The cellophane tape stopped the fission fragments and as far as can be determined prevented Doppler distortions in the X-ray spectra while obtaining the maximum coincidence rate.

The X-rays were detected by high resolution Ge(Li) and Si(Li) detectors. The Ge(Li) detector had an approximate active volume of 0.14 cc and the Si(Li) detector approximately 0.03 cc. A resolution of about 325 eV full width at half maximum at 18 keV was obtained with both detectors.

The efficiency, in the range of operation from 10 keV to 40 keV was 100% for the Ge(Li) detector and from 100% to 28% for the Si(Li) detector. Corrections due to counter efficiency have been made with respect to measurements dependent on the Si(Li) detector. The solid angle of each of the two detectors was about 0.5 sr. This experiment was repeated with two 100% Ge(Li) detectors and the results agree within statistics.

Coincidence System

Pulses generated in the Si(Li) and the Ge(Li) detectors by the X-rays were amplified and passed through constant fraction timing

discriminators as shown in Fig. 1. The timing signals from the fast discriminators were sent to a time-to-pulse-height converter (TPHC). It was required that the X-rays be detected within the time interval of 50 nanoseconds in order to generate a gating signal through a signal-channel analyzer (SCA). The linear X-ray pulses from both detectors and the output of SCA were routed to three 1024 channel analog-to-digital converters (ADC). A two-parameter analysis was then performed on line via a PDP-7 and PDP-15 computer system. The gated linear signals from the Ge(Li) detector were sorted and stored in 1024 channel spectra according to windows set in the computer on the X-ray peaks in the gated spectrum from the Si(Li) detector.

Calibration

The two X-ray spectra were calibrated with ^{55}Fe and ^{133}Ba sources and by observing the position of the known peaks of the X-rays of the light and heavy fission fragments. The energies of the other peaks were determined by a least squares' fit to a third order polynomial function. The gains of the amplifiers were checked at every 10-hour run by noting the position of the prominent peaks of each spectrum. The set-up was stable enough that no gain adjustments were required.

Windows

When the peaks in the X-ray spectrum of the Si(Li) detector contained a sufficient number of counts, gates were set on the $K\alpha_{1,2}$ X-ray peaks of 14 fission fragments (as indicated in Fig. 2) by the channel location in which these X-ray peaks were stored in the spectrum.

After a 107-hour run the 7 pairs of spectra: Y-Pr, Zr-Ce, Nb-La, Mo-Ba, Tc-Cs, Ru-Xe and Rh-I were graphed and compared with the total X-ray coincident spectrum obtained from the Ge(Li) detector. Figs. 3a-g show these spectra.

Results

Numerical results of this experiment are tabulated in Table I. The intensities are given relative to Tc and corrected for the efficiency of the Si(Li) detector which varies from 100% for Y to 28% for Pr. The intensity of the K_α X-ray from the light fragment is usually about the same whether the window is on the heavy or on the light fragment X-ray. The inverse is usually not so. The intensity of the heavy fragment X-ray is usually much greater in self coincidence. Exceptions to this are Tc-Cs and Ru-Xe pairs. In the fourth column of Table I are listed the intensity ratios of the K_α X-ray lines of each of the fission products with the K_α X-ray of the complementary fission product. In most cases the ratio of self coincidence to complementary coincidence is greater than one for the heavy fragments and less than one for the light fragments; the only exceptions are Tc and Ru with the ratios greater than one. Fig. 4 shows a bar graph of the results tabulated in Table I.

The coincidence X-ray spectra given in Figs. 3a-g show the total X-ray spectrum compared with the coincidence spectra for the complementary pairs. The prominent peaks are the characteristic K_α and K_β lines. The self coincidence is usually more prolific than the complementary X-ray production. There are several spectra where prominent peaks apparently

due to low energy gamma rays are observed, e.g. Y (Fig. 3a) where a peak appears at about the Ru K_α energy, but no Ru K_β is seen.

The remainder of the discussion will be devoted to explanations of processes which may give rise to multiple X-ray yield from a single fragment. The various possibilities one may consider are: (1) K X-ray production by the primary fission process followed by internal conversion, (2) multiple K X-ray production in the stopping process of the fission products, (3) K shell ionization resulting from β-decay of the fission fragments followed by internal conversion in the same fragment, and (4) multiple internal conversion processes from cascading transitions. These will be discussed below.

(1) The presently accepted source of K X-ray production in fission processes is the X-ray following an internal conversion electron transition in the nuclear de-excitation of a fission product.[4,5] The primary fission process itself is thought to be adiabatic in the rearrangement in the K shell electron configurations for the fission products. This is believable since the velocity of the K shell electron is much faster than the velocity of the fission product itself. Thus the two K electrons would fill their respective shells in each of the fission products as they emerge from the electron cloud of the californium atoms, and consequently no primary K X-ray would be produced. If this were a source of the X-ray production, the X-rays would be Doppler shifted and would not appear as a single narrow line in our spectra. The fission product will stop in 10^{-12} seconds, and the lifetimes of the K X-ray transitions are of the order of 10^{-16} seconds.

(2) In the present experiment the fission fragments were stopped in $C_{10}H_8O_4$ (cellophane tape) which was in contact with the source. The stopping process of the fission products in the tape is not a likely source of K X-ray prodtction. From cross section calculations using the tables of Khandelwal et al.[9] for the case of the most probable mass and energy of technetium (104 u, 100 MeV), it was found that the number of K X-rays expected from these fragments when they are stopped was about 10^{-6} X-rays per fragment or 70 K X-rays after a 107-hour run, which is negligible.

(3) A third possible explanation for double K X-ray production leading to X-ray self coincidence is K shell ionization produced by nuclear beta-decay of the fission fragment followed by internal conversion. The probability that beta-decay causes K shell ionization has been studied both theoretically[10,11,12] and experimentally.[13,14] An accurate estimate of this probability can be made using Migdal's result which is $P_k = 0.64/Z^2$. The $1/Z^2$ dependence favors K ionization for the light fragments, thus an optimistic estimate of the effect can be made by considering the case of a Zr fission fragment. For this case P_k is 4×10^{-4}. With such a small probability it seems unlikely that this can be the source of K X-ray self coincidence.

(4) Multiple internal conversion involves two or more internal conversions in cascade. In the literature there are a few cases where internal conversion cascades are likely, e.g., the decay of ^{117}Sn (317

keV, 158 keV).[15] For the 158 keV M1 transition, the K shell internal conversion coefficient α_K was measured to be 0.137 which compared well with calculated values. The 317 keV M4 transition feeding the 158 keV level has a 14 day halflife and e/γ is listed as being very large.[16] Thus for low energies, internal conversion cascades can compete favorably with gamma decay cascades even for multipole orders as low as M1.

The following considerations show that the latter process[4] can explain the data even though it may intuitively seem unlikely:

(a) The experiment discussed above and tabulated values[17] for α_K show that internal conversion is probable for low-energy transitions in the mass range of the fission fragments.

(b) Recent experiments show a large number of low-energy gamma rays in coincidence with K X-rays from ^{252}Cf fission.[2,7]

(c) The odd Z elements have the largest number of low-energy transitions, but in general the multipolarities are not known so the internal conversion probabilities cannot be given with certainty. One case where two gamma rays with known multipolarities are known to be in cascade[18,19] is for the 97 keV $2^+ \rightarrow 0^+$ and 209 keV $4^+ \rightarrow 2^+$ transitions in ^{150}Ce. The respective E2 K shell conversion probabilities $P_K = \frac{\alpha_K}{1+\alpha_K}$, neglecting L shell conversion, are 0.58 and 0.11.[17]

(d) The results shown in Table I show large variations with Z and are without any noticeable systematic trend. Thus a nuclear process, internal conversion, is more likely. An atomic process would be expected to show a smooth dependence with Z.

(e) The predominance of self coincidence seems to indicate that the majority of the observed X-rays occur following isomeric transitions or after β-decay so that they are not in prompt coincidence with X-rays from the complementary fragment.

Correlation Effects

Prompt fission X-ray coincidence yields for random population of nuclear levels in the fission products will be proportional to (total X-ray yield for complementary light fragment). This result dictates that the ratio (K_L/K_H) complement = 1.0, since complementary X-ray coincidence production can arise only from prompt processes. This result is approximately born out, as seen in Table I, for the ratios Y/Pr, Mo/Ba, Ru/Xe, and Rh/I. However, the ratios Zr/Ce, Nb/La, and Tc/Cs are far from unity. The last column in Table I shows the result one should obtain for random X-ray events using the yields obtained by Watson et al.[2] The last column shows little agreement with the relative intensities in column 3. This is evidence that nuclear level population in fission fragments is strongly correlated. That is, if one fragment de-excites via internal conversion, the probability of the complementary fragment being in a state which also decays by internal conversion is not random. This is consistent with conservation laws, but has never been shown.

Conclusion

The results of this work leave many questions which can be answered only by further experimentation. Certainly more detailed knowledge of the structure of these nuclei is needed.

Nuclear shell effects are evident in the almost complete lack of X-rays from Te (Z = 52) and the low intensity of X-rays from Xe (Z = 54) which have proton numbers near the closed shell at 50. Those isotopes of Te and Xe observed in ^{252}Cf binary fission also have neutron numbers near the N = 82 closed shell.[18] Thus their low-lying levels are more widely spaced resulting in higher energy transitions and correspondingly much lower probabilities for internal conversion.

It seems that multiple internal conversion is the process dominating the observation of K X-rays in self coincidence. Electron-electron coincidence experiments involving internal conversion electrons would help confirm this hypothesis.

REFERENCES

1. R. L. Watson, Phys. Rev. 179 (1969) 1109.
2. R. L. Watson, H. R. Bowman and S. G. Thompson, Phys. Rev. 162 (1967) 1169.
3. T. Alvager, R. A. Naumann, R. F. Petry, G. Sidenius and T. Darrah Thomas, Phys. Rev. 167 (1968) 1105.
4. L. E. Glendenin and J. P. Unik, Phys. Rev. 140 (1965) B1301.
5. J. B. Wilhelmy, Ph.D. dissertation, University of California, Berkeley, (1969).
6. D. R. Ruegsegger, Jr., and R. Roy, Phys. Rev. C1 (1969) 631.
7. F. F. Hopkins, G. W. Phillips, J. R. White, C. F. Moore and Patrick Richard, to be published.
8. Work on X-ray, X-ray coincidences is concurrently being carried at Trombay, Bombay, India, (S. S. Kapoor, private communication).
9. G. S. Khandelwal, G. H. Choi, and E. Merzbacher, Atomic Data 1 (1969) 103.
10. A. Migdal, J. Phys. (USSR) 4 (1941) 449.
11. E. L. Feinberg, J. Phys. 4 (1941) 424.
12. J. S. Levinger, Phys. Rev. 90 (1953) 11.
13. T. B. Novey, Phys. Rev. 86 (1952) 619.
14. Yasuhito Isozumi and Sakae Shimizu, Phys. Rev., to be published.
15. J. P. Bocquet, Y. Y. Chu, G. T. Emery, and M. L. Periman, Phys. Rev. 167 (1968) 1117.
16. C. M. Lederer, J. M. Hollander, I. Perlman, Table of Isotopes, Sixth Ed., John Wiley & Sons, (1968).

17. R. S. Hager and E. C. Seltzer, Nuclear Data 4A (1968) 1.

18. J. B. Wilhelmy, S. G. Thompson, R. C. Jared, and E. Cheifetz, Phys. Rev. Letters, 25 (1970) 1122.

19. E. Cheifetz, R. C. Jared, S. G. Thompson and J. B. Wilhelmy, Phys. Rev. Letters, 25 (1970) 38.

Table I: ^{252}Cf Fission X-ray Coincidence Normalized Intensities and Intensity Ratios with $I_{Tc} = 1$, for Self Coincidence.

Window Set On	Relative Intensities $(K_\alpha)_{self}$	Relative Intensities $(K_\alpha)_{complement}$	$\frac{(K_\alpha)_{self}}{(K_\alpha)_{comp}}$	P[a]
Y	0.11±.01	0.13±.01	0.86±0.09	0.02±0.004
Pr	0.97±.06	0.10±.01	9.7 ±1.2	
Zr	0.04±.01	0.17±.01	0.24±0.03	0.06±0.007
Ce	0.62±.04	0.06±.01	11.0 ±1.7	
Nb	0.10±.01	0.33±.02	0.31±0.02	0.10±0.013
La	1.55±.08	0.11±.01	14.0 ±1.4	
Mo	0.08±.01	0.18±.01	0.45±0.39	0.11±0.013
Ba	0.16±.02	0.13±.02	1.2 ±0.16	
Tc	1.00±.04	0.60±.03	1.7 ±0.08	0.38±0.046
Cs	1.68±.07	0.39±.03	4.3 ±0.23	
Ru	0.37±.02	0.06±.01	5.8 ±0.55	0.06±0.008
Xe	0.10±.01	0.06±.01	1.7 ±0.25	
Rh	0.13±.01	0.15±.01	0.85±0.07	0.06±0.008
I	0.16±.06	0.10±.01	11.6 ±1.2	

[a] P is the product of K X-ray yields of complementary fragments from primary ^{252}Cf fission products normalized to the Ru/Xe K_α complement from column 3. The yields were taken from ref. 2, Table I.

FIGURE CAPTIONS

Fig. 1 Schematic diagram of electronics.

Fig. 2 Windows set on light and heavy fragments X-rays.

Fig. 3 X-ray spectra obtained in coincidence with windows set on

(a) Yttrium Praseodymium, compared with the total X-ray spectrum;

(b) Zirconium and Cerium, compared with the total X-ray spectrum;

(c) Niobium and Lanthanum, compared with the total X-ray spectrum;

(d) Molybdenum and Barium, compared with the total X-ray spectrum;

(e) Cesium and Technetium, compared with the total X-ray spectrum;

(f) Ruthenium and Xenon, compared with the total X-ray spectrum;

(g) Rhodium and Iodine, compared with the total X-ray spectrum.

Fig. 4 Results tabulated in Table I are shown as a bar graph. X-ray production from each fission product is compared to its complement.

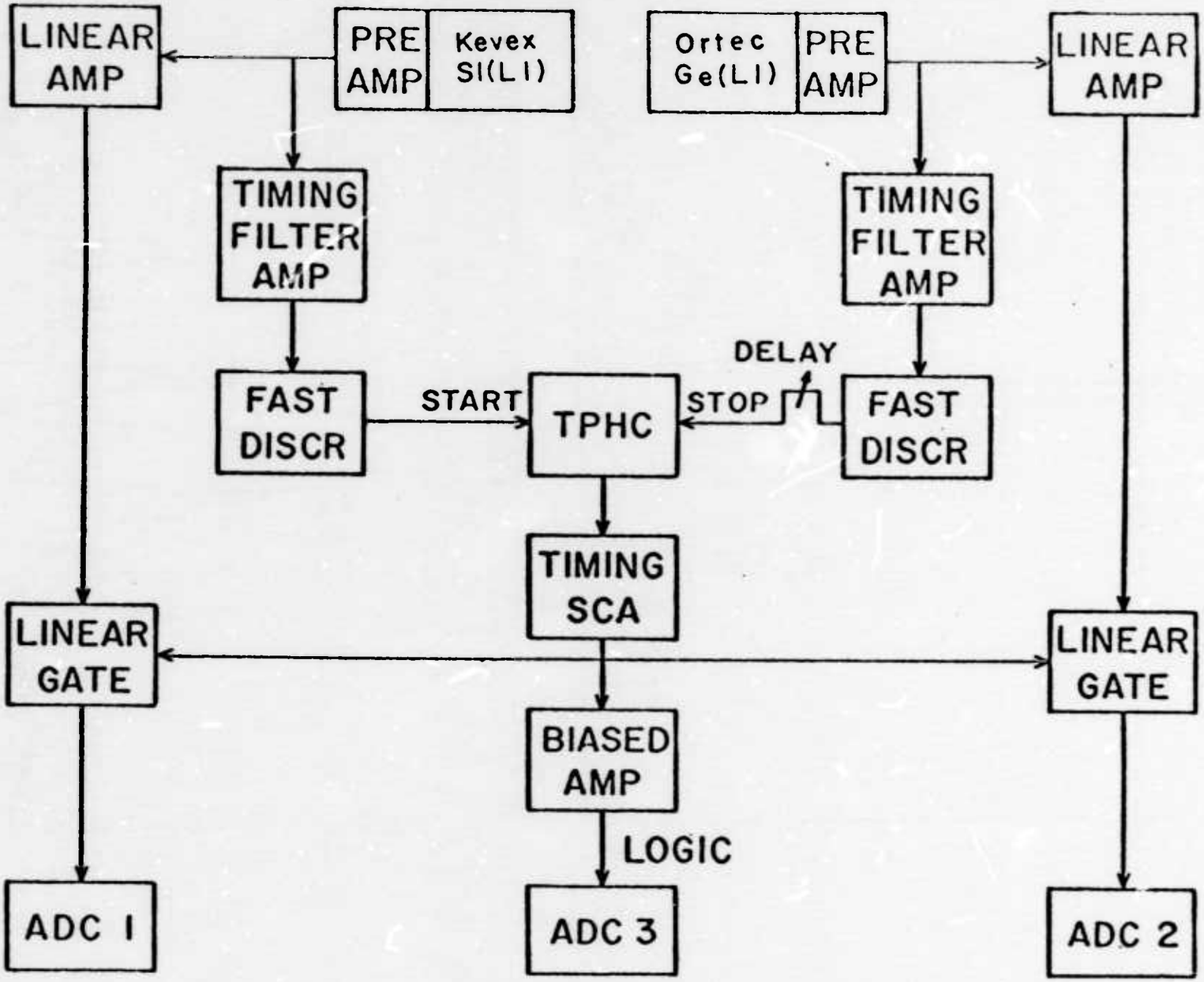

CIRCUITRY USED IN COINCIDENCE EXPERIMENT.

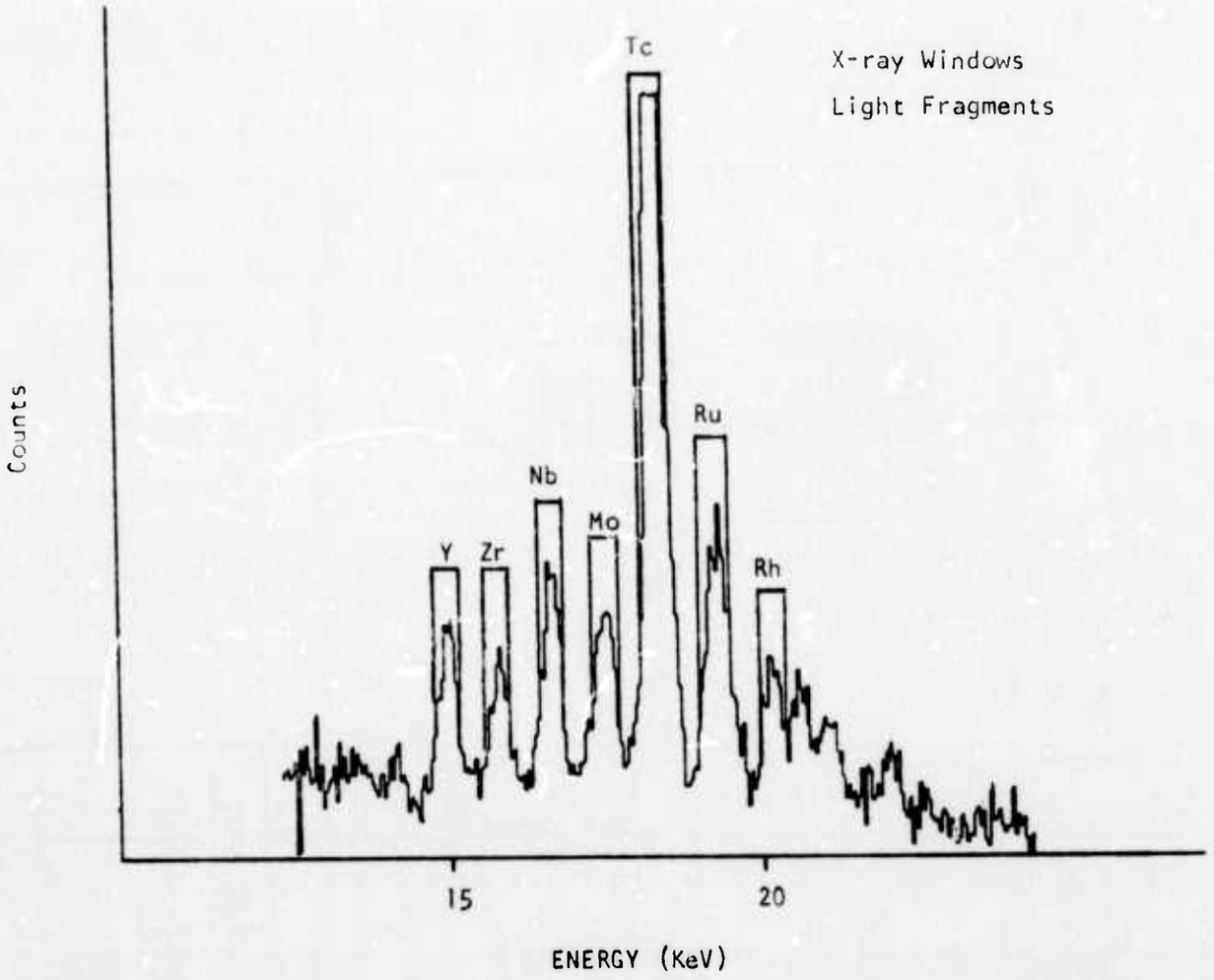
X-ray Windows
Light Fragments
Counts
Tc
Ru
Nb
Mo
Y
Zr
Rh
15
20
ENERGY (KeV)

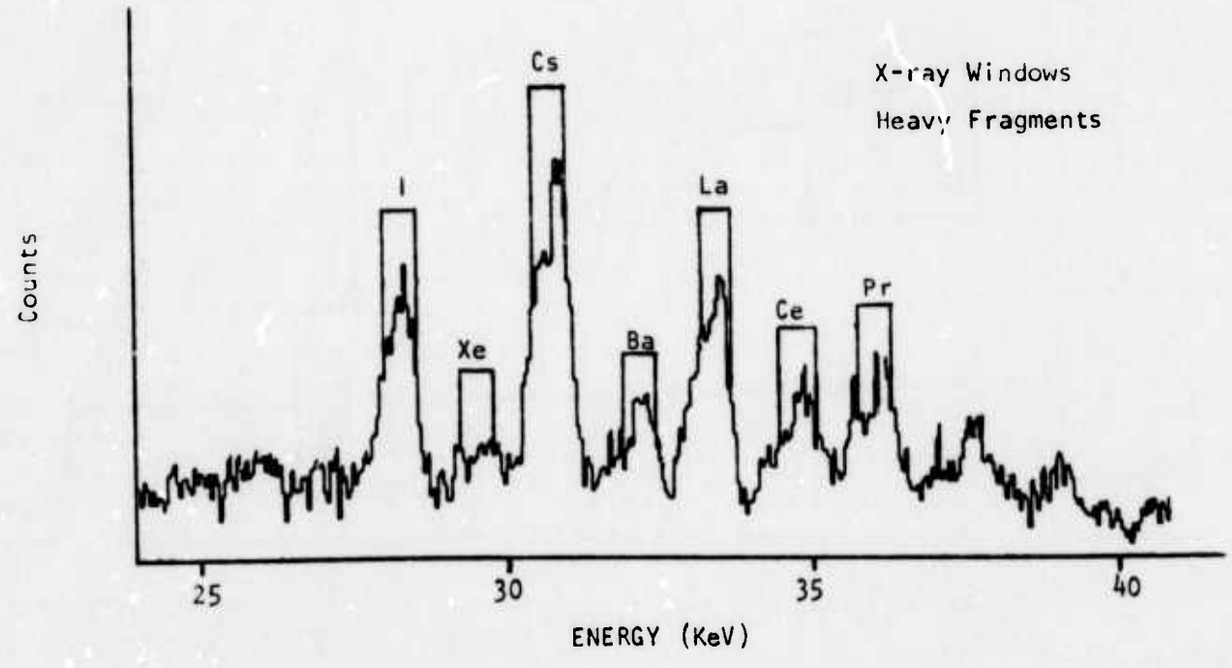
X-ray Windows
Heavy Fragments
Counts
Cs
I
La
Xe
Ba
Ce
Pr
25
30
35
40
ENERGY (KeV)

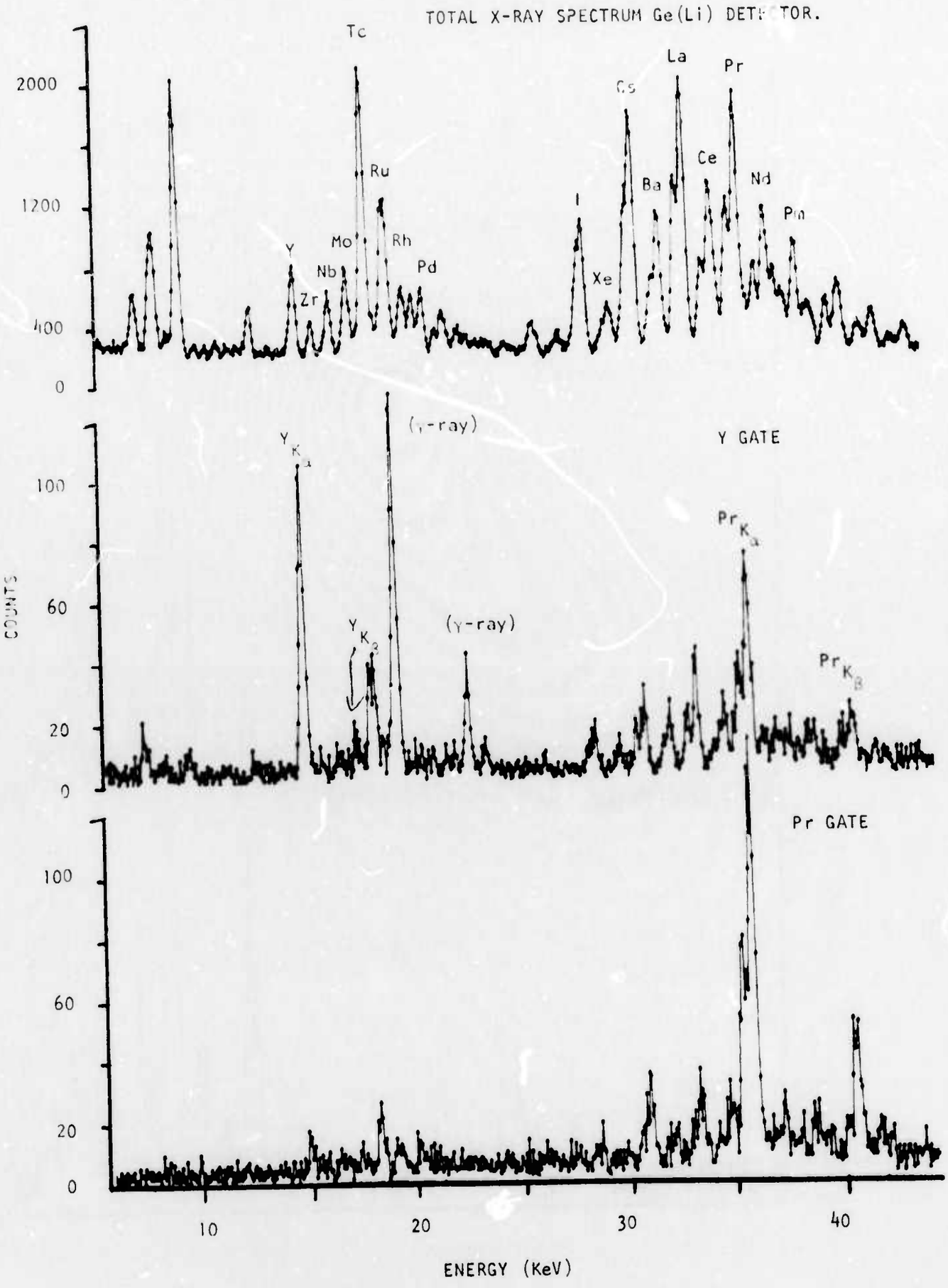
TOTAL X-RAY SPECTRUM Ge(Li) DETECTOR.
Tc
La
Pr
Cs
Ce
Ba
Nd
Pm
Ru
Rh
Mo
Nb
Y
Zr
Pd
I
Xe
2000
1200
400
0
Y GATE
(γ-ray)
Y_{K_α}
Y_{K_β}
Pr_{K_α}
Pr_{K_β}
100
60
20
0
COUNTS
Pr GATE
10
20
30
40
ENERGY (KeV)

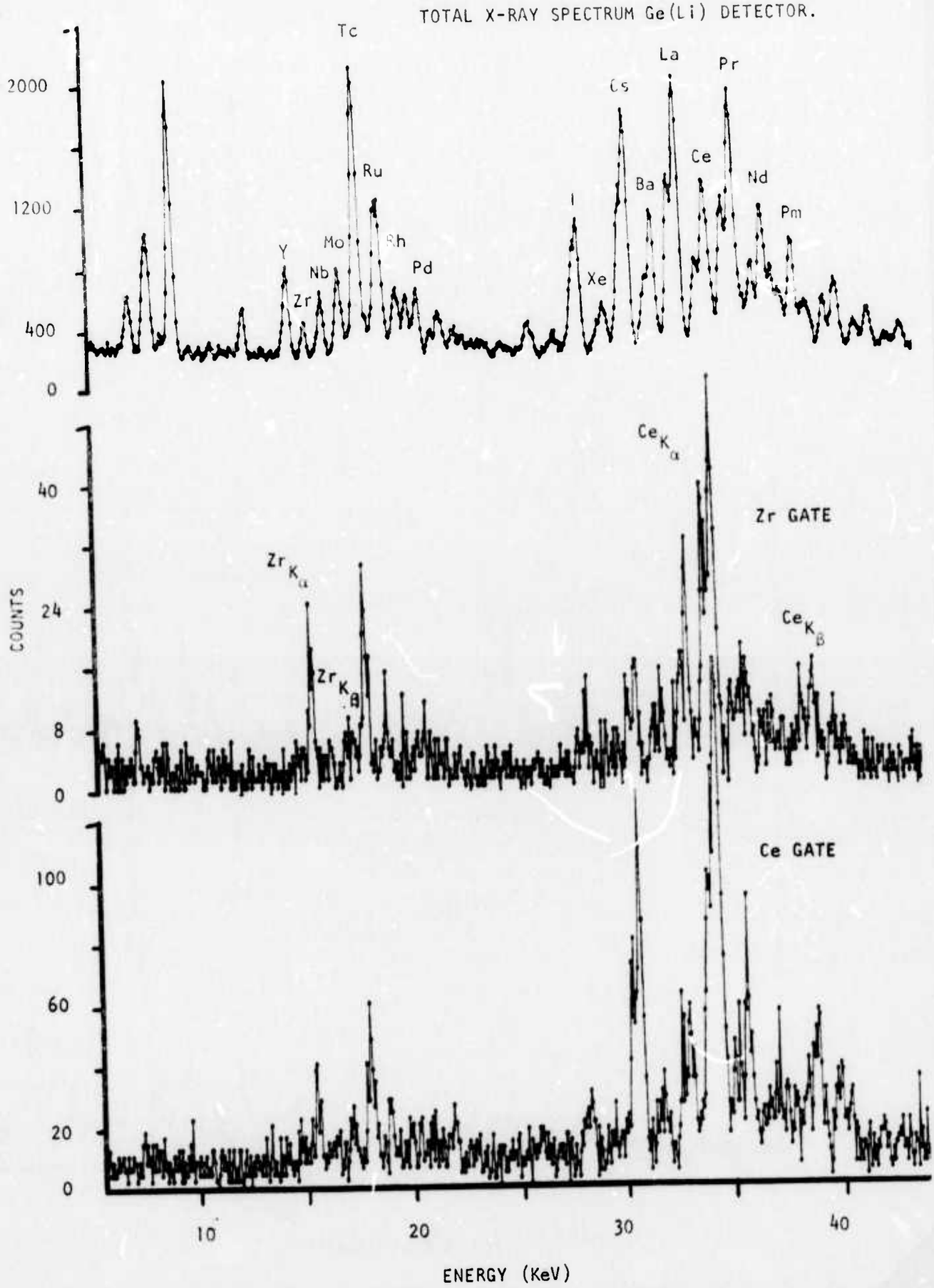
TOTAL X-RAY SPECTRUM Ge(Li) DETECTOR.
2000
1200
400
0
Tc
Ru
Y
Mo
Rh
Nb
Zr
Pd
I
Xe
Cs
Ba
La
Ce
Pr
Nd
Pm
Ce_{K_α}
Zr GATE
Zr_{K_α}
Ce_{K_β}
Zr_{K_β}
COUNTS
40
24
8
0
Ce GATE
100
60
20
0
10
20
30
40
ENERGY (KeV)

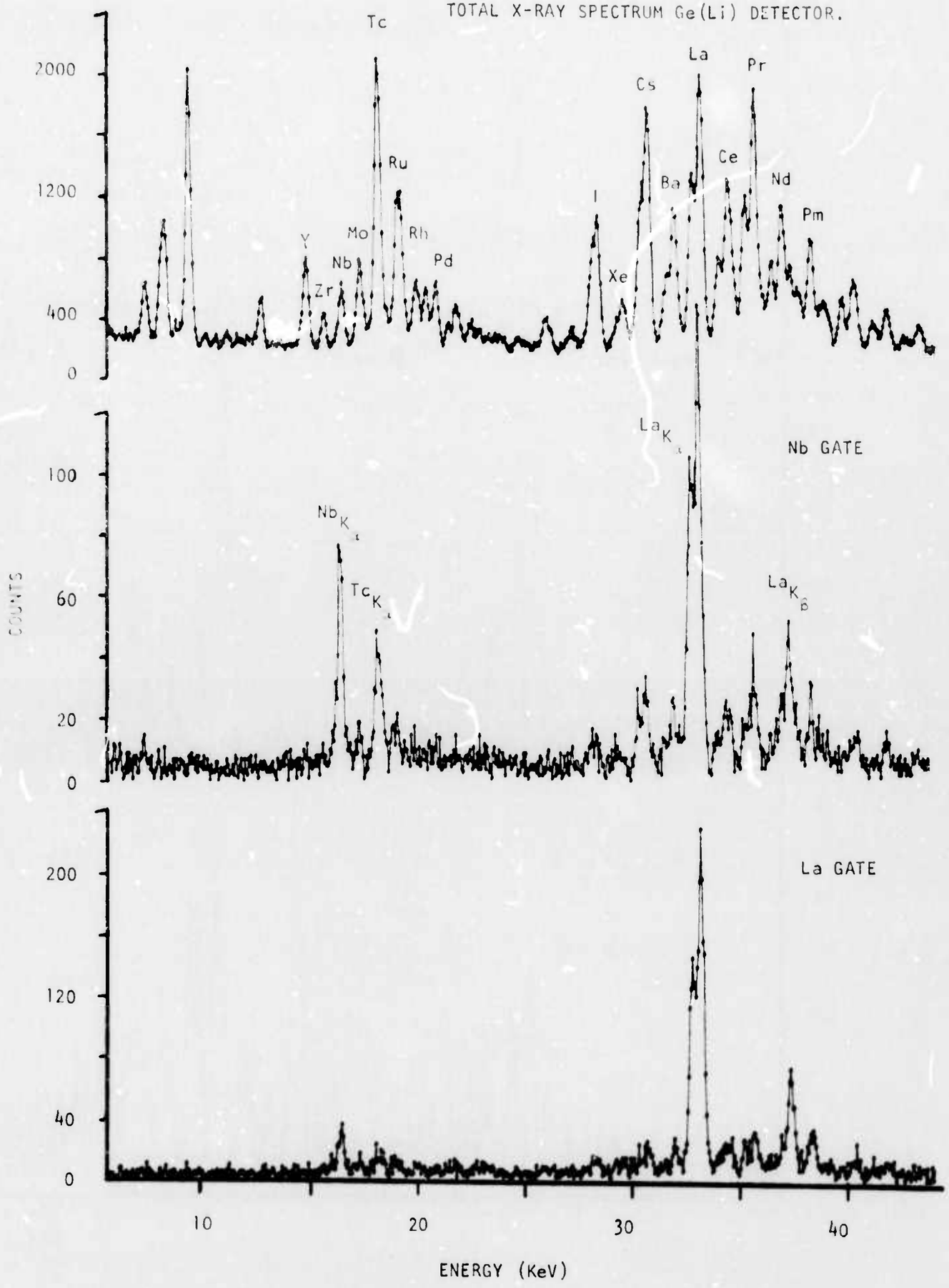
TOTAL X-RAY SPECTRUM Ge(Li) DETECTOR.
Tc
La
Cs
Pr
Ru
Ce
Ba
Nd
I
Pm
Mo
Rh
Y
Nb
Pd
Zr
Xe
2000
1200
400
0
La_{K_α}
Nb GATE
100
Nb_{K_α}
Tc_{K_α}
La_{K_β}
60
20
0
COUNTS
La GATE
200
120
40
0
10
20
30
40
ENERGY (KeV)

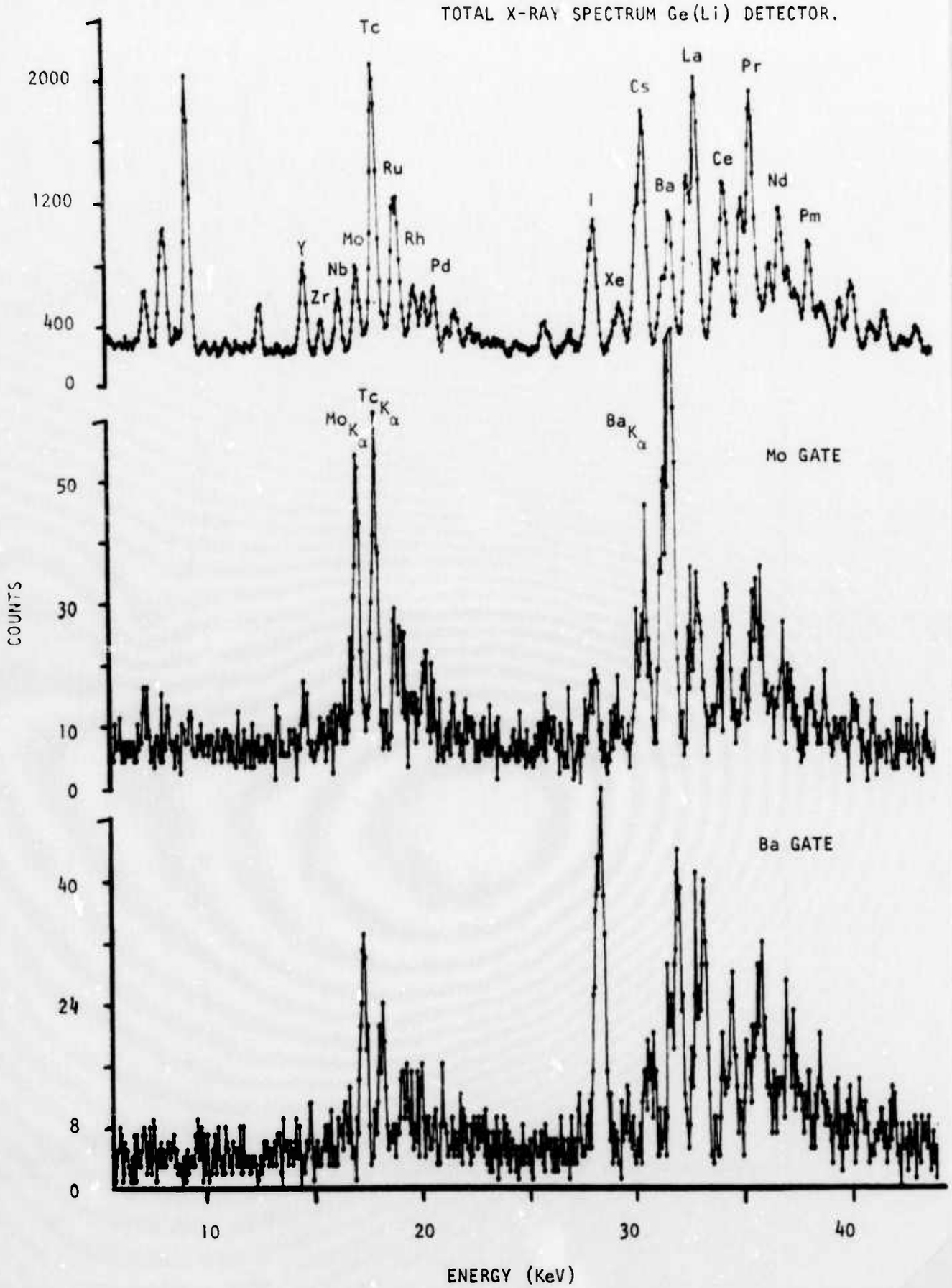
TOTAL X-RAY SPECTRUM Ge(Li) DETECTOR.
Tc
La
Pr
Cs
Ce
Ba
Nd
Pm
Ru
Rh
Mo
Nb
Pd
Y
Zr
I
Xe
2000
1200
400
0
Mo GATE
Ba GATE
COUNTS
50
30
10
40
24
8
10
20
30
40
ENERGY (KeV)

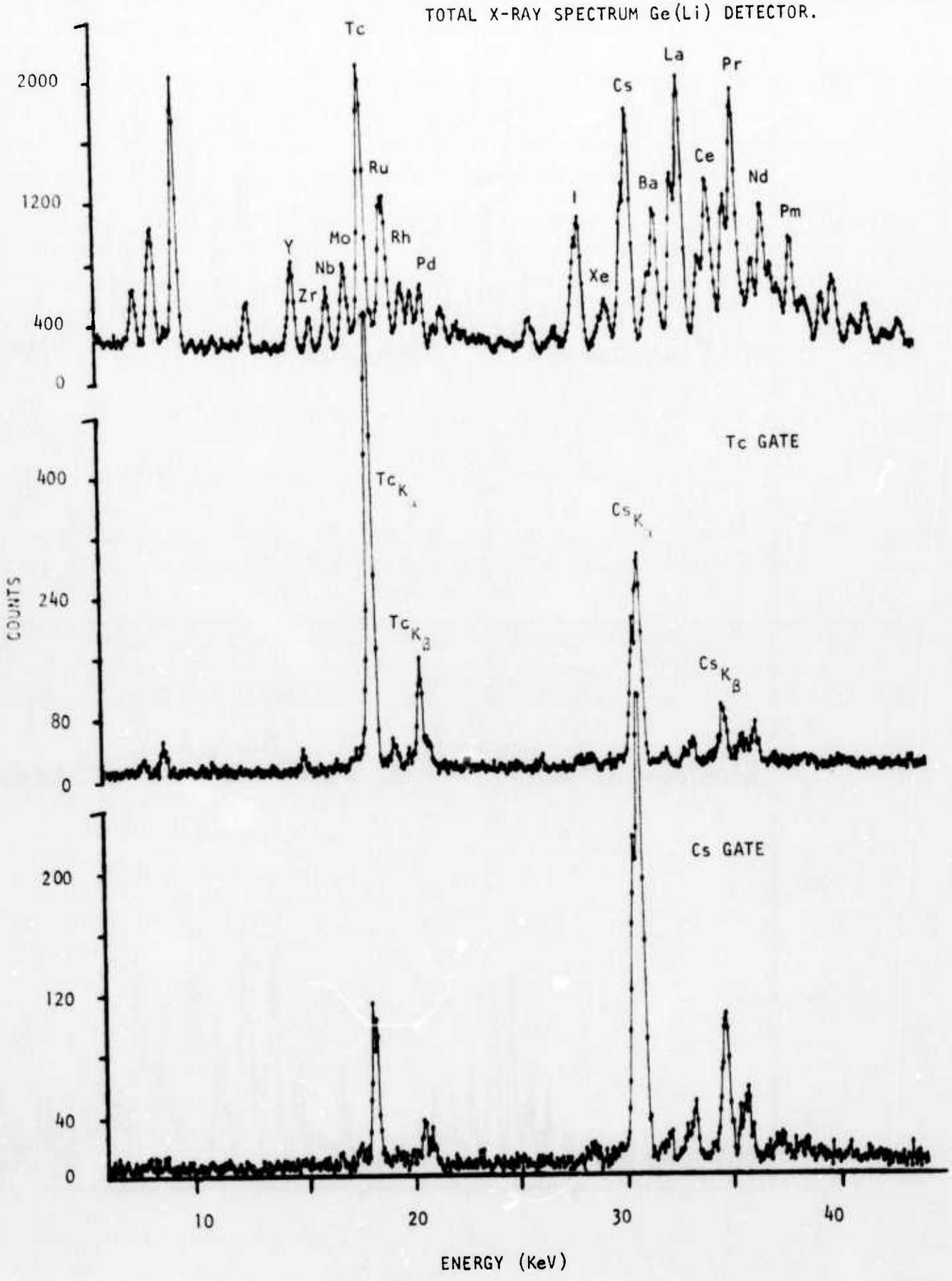
TOTAL X-RAY SPECTRUM Ge(Li) DETECTOR.
Tc
Ru
Rh
Pd
Mo
Nb
Zr
Y
I
Xe
Cs
Ba
La
Ce
Pr
Nd
Pm
2000
1200
400
0
Tc GATE
Tc$_{K_\alpha}$
Tc$_{K_\beta}$
Cs$_{K_\alpha}$
Cs$_{K_\beta}$
400
240
80
0
COUNTS
Cs GATE
200
120
40
0
10
20
30
40
ENERGY (KeV)

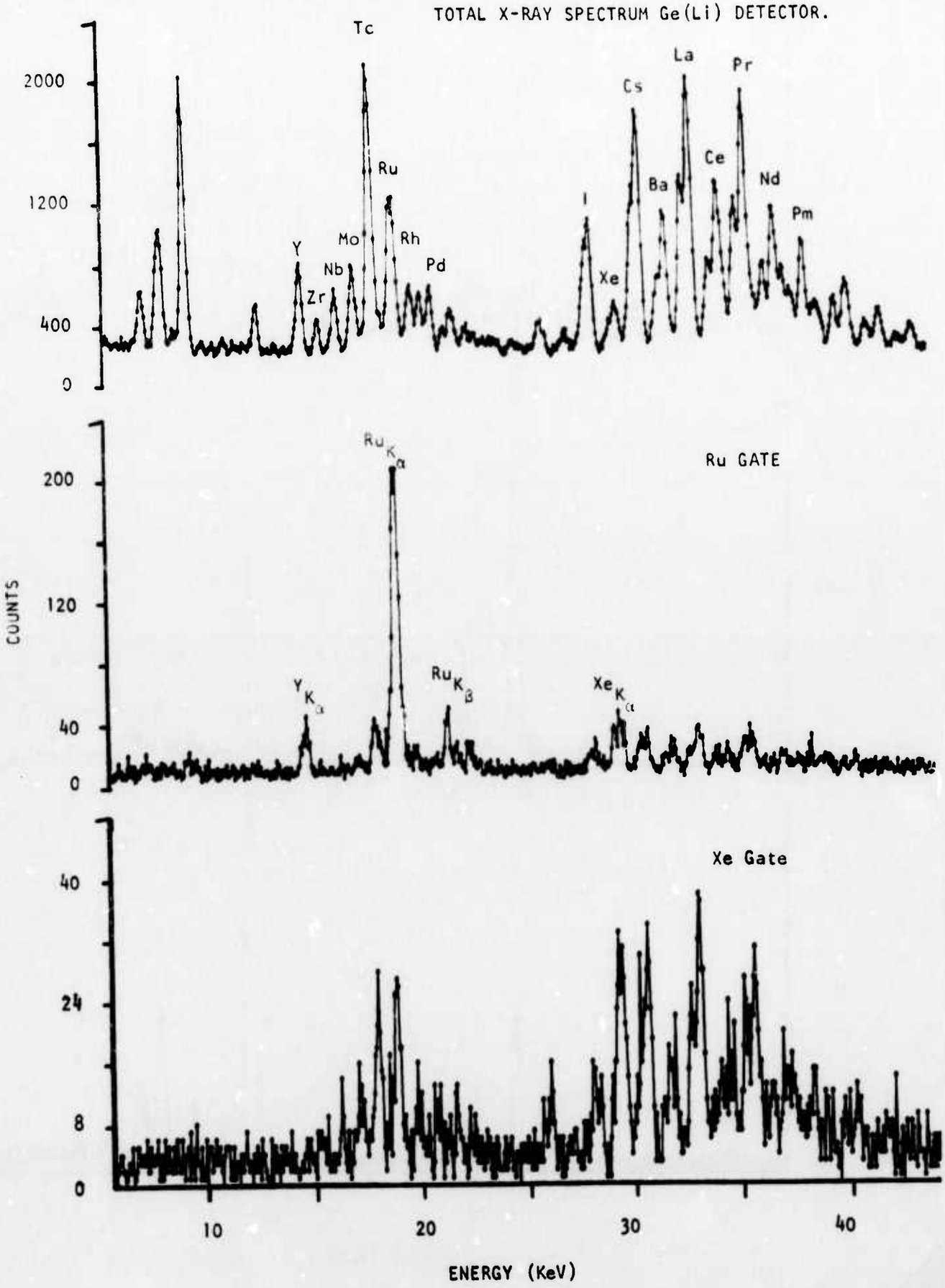
TOTAL X-RAY SPECTRUM Ge(Li) DETECTOR.
2000
1200
400
0
Tc
Ru
Y
Mo
Nb
Zr
Rh
Pd
I
Xe
Cs
Ba
La
Ce
Pr
Nd
Pm
Ru GATE
200
120
40
0
COUNTS
Ru Kα
Y Kα
Ru Kβ
Xe Kα
Xe Gate
40
24
8
0
10
20
30
40
ENERGY (KeV)

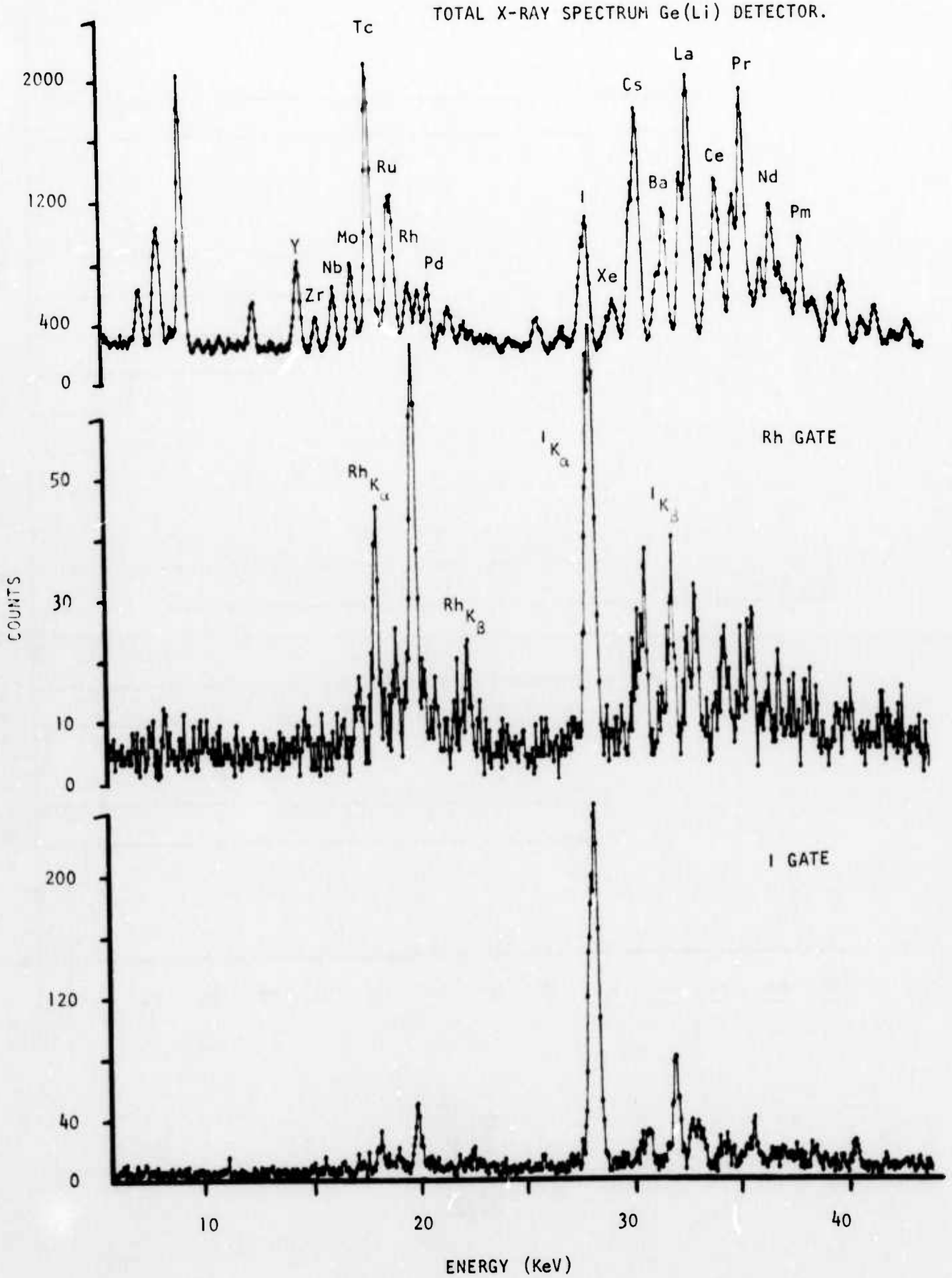
TOTAL X-RAY SPECTRUM Ge(Li) DETECTOR.
Tc
Ru
Mo
Rh
Pd
Y
Zr
Nb
I
Xe
Cs
Ba
La
Ce
Pr
Nd
Pm
2000
1200
400
0
Rh GATE
Rh_{K_α}
Rh_{K_β}
I_{K_α}
I_{K_β}
50
30
10
0
COUNTS
I GATE
200
120
40
0
10
20
30
40
ENERGY (KeV)

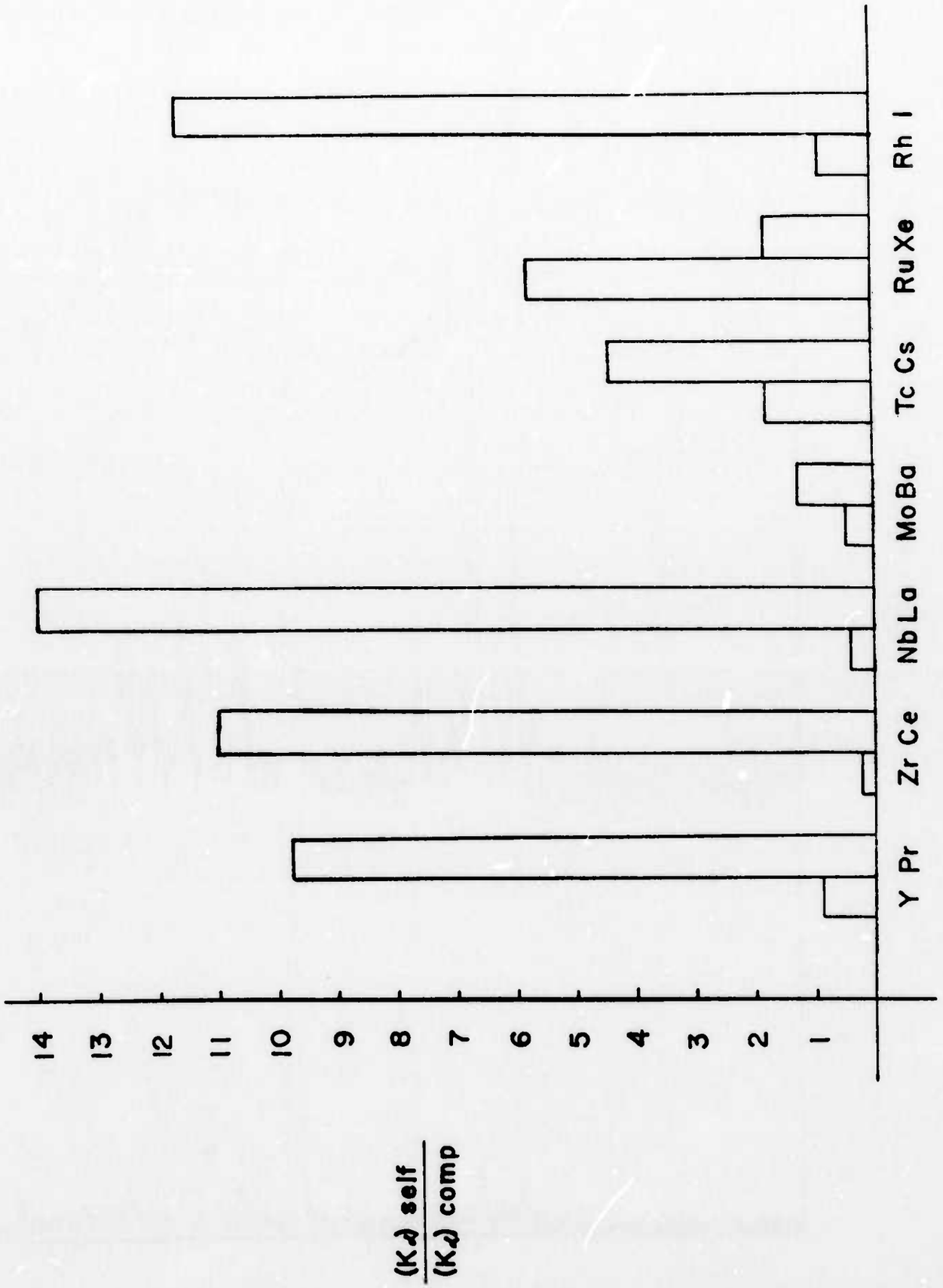
(Kd) self / (Kd) comp
14
13
12
11
10
9
8
7
6
5
4
3
2
1
Y Pr Zr Ce Nb La Mo Ba Tc Cs Ru Xe Rh I

B. Electrostatic Particle Guide

In the case of the time-of-flight technique the experimental mass resolution is a function of (1) the energy resolution of the fragment detectors, (2) the timing resolution of the electronics, and (3) the angular resolution of the time-of-flight measurements. Fig. 1 shows how these quantities enter in the calculation of the mass resolution. Fig. 2 shows the contributions to the mass resolution for the uncertainties ΔT = 1 ns, ΔE = 1 MeV, and with $\Delta\theta = 2^{o}$, E = 100 MeV, D = 10 m, M = 100 u. The large solid angle for such a long flight path will be discussed later. The expected mass resolution $\langle \Delta M/M \rangle \cong 1$ u (FWHM) which is due almost entirely to the energy uncertainty indicates that with this time of flight technique the integral nuclear mass distribution (i.e., quantized A yields) may be unfolded from the experimental mass spectrum with a great degree of certainty. Of course, the long flight path of 10 m implies a vanishingly small solid angle (4×10^{-2} msr for a 300 mm^2 detector). Hence such a technique is impossible because of count rate considerations. However, by using an electrostatic particle guide, consisting of a wire at a negative high voltage running down the center of a cylinder the length of the flight path, ions may be confined to trajectories around this wire as they traverse the guide. A tremendous increase in solid angle may be gained by using such a device. Fig. 3 shows the calculated electrostatic guide efficiency for both a point source a radial distance r from the center of the guide and an extended uniform source over the entire guide cross section. The collection efficiency in the case of the point source is proportional to

the fragment energy, as expected. As is seen from Fig. 3 an increase in solid angle of several orders of magnitude is expected over the case of no particle focusing. We feel that the time-of-flight technique using such a guide is a very practical means of extracting fission fragment integral (A values) mass yields. Such a guide has now been constructed at the University of Texas Center for Nuclear Studies. A 10 m long stainless steel tube with an inside diameter of 5.05 cm has a 5 mil wire running its length. The high voltage is provided via a 50 keV high voltage feedthrough to which a voltage from 0 to 50 keV may be applied.

A preliminary experiment was performed to investigate the relative collection efficiency of this guide for fragments from spontaneous fission of ^{252}Cf. A small ^{252}Cf source (approximately 10^6 fissions/minute) was placed on axis about 2 inches from one end of the guide. A 300 mm^2 lithium drifted silicon detector with a depletion depth of 100 μm was placed centered on axis about 2 inches from the other end of the guide. At a pressure of 1×10^{-5} torr the voltage on the wire was varied from 0 to 20 keV, and the number of fission fragments detected by the particle detector in 100 seconds was observed at each voltage setting. The results of these measurements are shown in Fig. 4. Indeed, these measurements indicate that such an electrostatic particle guide increases the "effective" solid angle over the 10 m flight path by many orders of magnitude as suggested by the calculations.

FIGURE CAPTIONS

Fig. 1 Quantities involved in calculating mass resolution.

Fig. 2 Contributions to mass resolution for ΔT = 1ns and ΔE = 1 MeV.

Fig. 3 Calculated electrostatic guide efficiency for point source and extended source.

Fig. 4 Experimental plot of count rate versus voltage on central wire of particle guide.

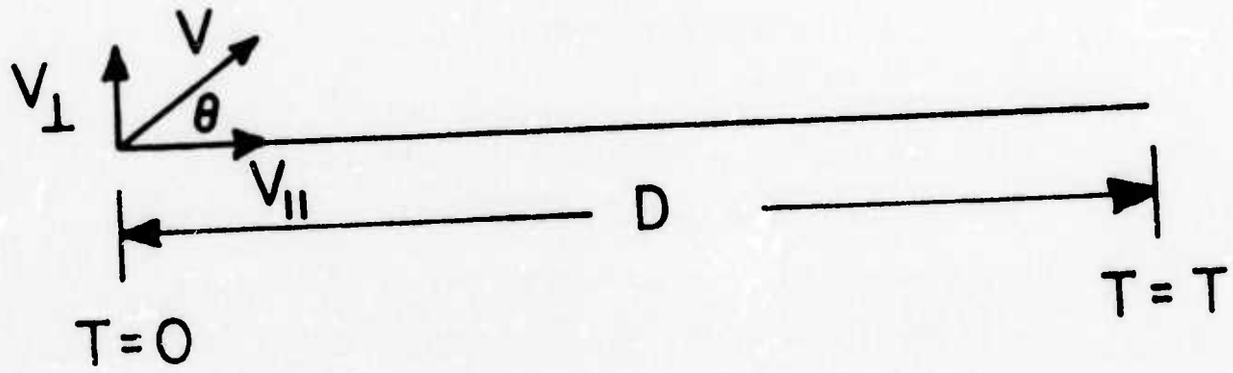

$$V_{||} = \frac{D}{T} , \quad V_\perp = V \sin\theta \doteq V\theta$$

$$M = \frac{2E}{V^2} = \frac{2E}{V_\perp^2 + V_{||}^2} = \frac{2E}{V^2\theta^2 + \frac{D^2}{T^2}}$$

$$M(E, T, D, \theta) = 2E\frac{T^2}{D^2}(1 - \theta^2)$$

$$\frac{\Delta M}{M} = \frac{\Delta E}{E} + 2\frac{\Delta T}{T} - 2\frac{\Delta D}{D} - 2(\Delta\theta)^2$$

(1) (2) (3)

(1) $\frac{\Delta E}{E} \doteq 10^{-2}$ (typical)

(2) $2\frac{\Delta T}{T} = 2\frac{c}{D}\sqrt{\frac{2E}{Mc^2}}\Delta T \doteq 2.5\ 10^{-3}$

for $E = 100$ MeV, $D = 10$ m, $M = 100$ u, and $\Delta T = 1$ ns

(3) $2(\Delta\theta)^2 \doteq 2.5\ 10^{-3}$

for $\Delta\Omega = 0.005$ sr $(\Delta\theta \doteq 2^\circ)$

$$\left\langle \frac{\Delta M}{M} \right\rangle_{exp} \doteq 1.06\ 10^{-2}$$

ELECTROSTATIC PARTICLE GUIDE EFFICIENCY

point source

$$F(r) = (1/4)(q|V|/E)\left[\ln(r/R)/\ln(s/R)\right](1 - r^2/R^2)^{-1/2}$$

for $r \doteq s \ll R$, $F(r) \doteq (1/4)(q|V|/E)$

$E \doteq 100$ MeV , $q \doteq 20\,e$, $V \doteq 30$ keV

$F(r) \doteq 1.5 \cdot 10^{-3}$ or 19 msr

extended target

$$F \doteq 0.153\ q|V|/\left[E \ln(R/s)\right]$$

for $R = 2"$, $s = 0.005"$

$F \doteq 2 \cdot 10^{-4}$ or 2.5 msr

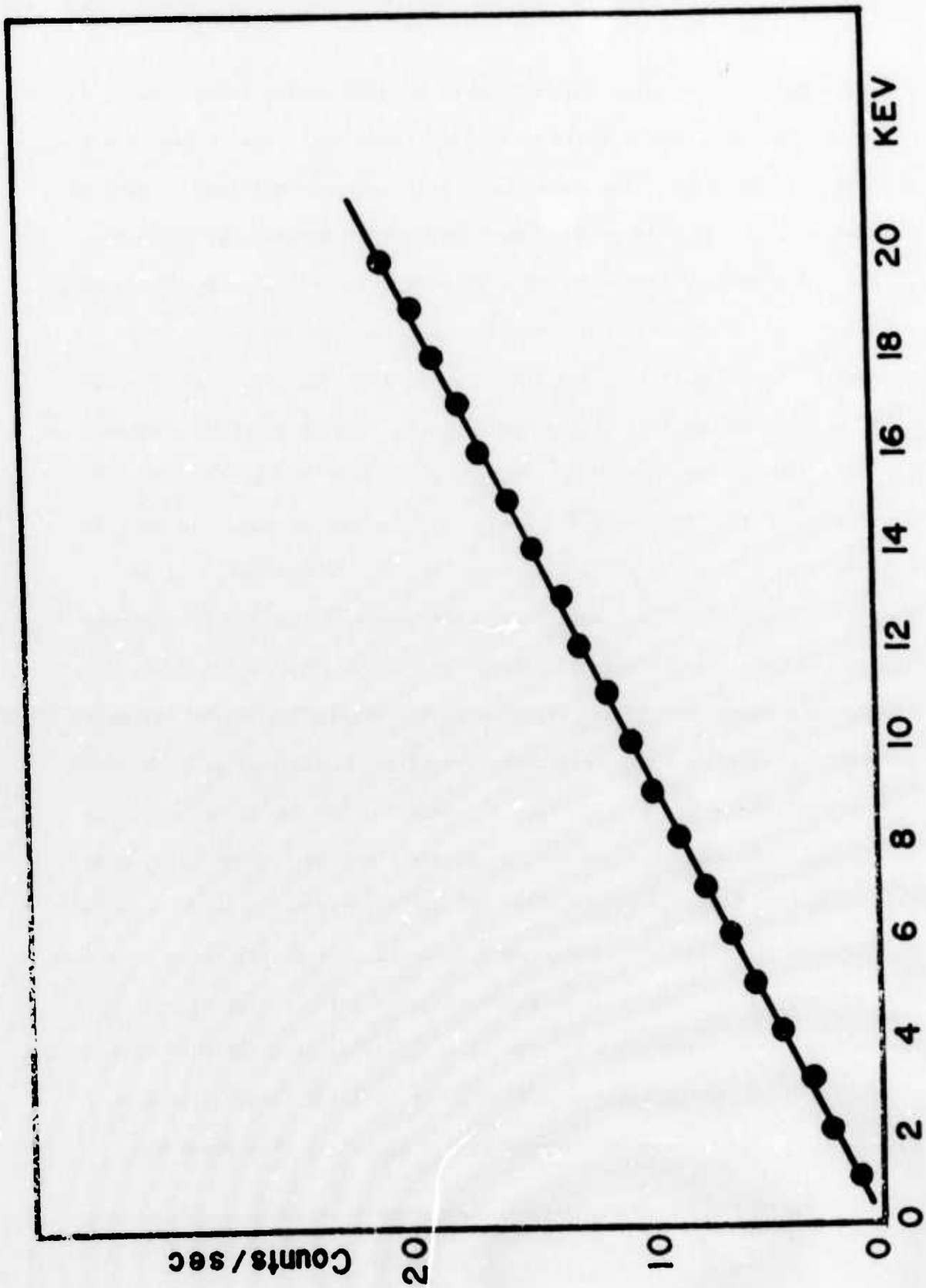
Counts/sec
0
10
20
0
2
4
6
8
10
12
14
16
18
20
KEV

C. High Resolution-Charged-Particle Mass Identification Using Time-of-Flight

Research in the field of low energy nuclear physics has generated a variety of techniques for charged particle mass identification, such as conventional particle telescopes, magnetic spectrographs, and time-of-flight. A simple technique is reported here which exploits an electrostatic particle guide similar to that described by Oakey and Macfarlane[1] to transport charged particles and permit time-of-flight measurements over quite long flight paths. By placing a single, high-resolution charged-particle detector at the end of the guide, the mass may be determined from the obvious relation $m = 2Et^2/L^2$ where E is the energy deposited in the detector and t is the time for the particle to traverse the guide of length L. Where excellent mass resolution together with the best energy resolution from charged particle detectors is desired this single-detector energy-mass-identifier is far superior to conventional particle telescope systems, because for these telescopes two or more detectors must be used, and also by virtue of the fact that the detector for the guide system is safely far from the region of the target and the beam. Since ions, once trapped by the logarithmic potential[2] of the electrostatic guide, continue to traverse the guide no matter what its length (except for those colliding with the very thin, high-voltage wire along the guide's center), the guide may be made almost arbitrarily long, so that any desired velocity resolution may be obtained, while still maintaining a relatively large collection efficiency.[1] The mass resolution of such a system is then given by

$$\frac{\Delta M}{M} = \left[\left\langle\frac{\Delta E}{E}\right\rangle^2 + \left\langle\frac{2\Delta t}{t}\right\rangle^2 + \langle 2\Delta\theta\rangle^2\right]^{\frac{1}{2}}$$

where $\Delta E/E$ represents the resolution of the energy measurement, $\Delta t/t$ represents the resolution of the time measurement, and $\Delta\theta$ is the angle of the cone of acceptance of the guide. For the system and test to be described $\Delta M \ll 1$ amu.

The device consists of a 7.1 m long stainless steel tube of inside diameter 5.08 cm with a 20 mil tungsten wire along its center. A standard high-voltage feed-through provides up to 20 keV negative voltage to the wire. The wire is terminated about 5 cm from the target, and the detector is placed about 2.5 cm from the other end of the wire. The guide is mounted on a rotating arm, radial to the center of a 10.0 cm scattering chamber. The present system can cover scattering angles between 0^{o} and 60^{o}. The beam is stopped on a small Faraday cup located 2 cm behind the target, in the scattering chamber.

To test the usefulness of this system for mass identification, a thin carbon foil was bombarded with a 9.0 MeV pulsed deuteron beam from the University of Texas EN Tandem Accelerator. Beam pulses of about 4 ns width occur every 400 ns. A Sherman-Roddick preamplifier[3] was used with an Ortec 2 mm surface barrier detector of active area 100 mm^2 to generate the linear energy signal for the energy amplifier as well as a fast (rise time about 2 ns) timing signal. The fast signal was taken as the start and a fast pulse generated from the source oscillator wave train was used as the stop for input to an Ortec time to amplitude converter (TAC) to generate a signal proportional to the time for the particle to traverse the guide. The output of the TAC and the linear energy

signal were fed to a PDP-15 computer where the data was accumulated in the two-parameter mode of our on-line data acquisition program SUPERVISOR. A total of 21 on-line windows were selected on the time-of-flight spectrum so that the performance of the system as a high resolution mass identifier could be evaluated. For events whose time fell within each of these windows a separate 1024 channel energy spectrum was updated.

The figure shows the total coincidence time-of-flight and energy spectra for the test run at 25^{o} laboratory scattering angle. For this run, -5 keV was applied to the wire. For a discussion of the effective solid angle of such a device the reader is referred to ref. 1. For our system the electrostatic guide accepts an effective solid angle of 2 msr for an applied voltage of -5 keV. The energy resolution is 22 keV at 9.0 MeV, while the time resolution is 6.8 ns as determined by inserting a fixed time delay of 50 ns into the TAC circuitry. The windows placed on the time spectrum were quite generous since at these energies protons and deuterons of the same energy are separated in time by an interval about an order of magnitude greater than the time resolution. The energy and time spectra were then calibrated and masses were calculated off line for those peaks appearing in the gated energy spectra using $m = 2Et^2/L^2$. The calculation was done twice, once for the lower and once for the upper time limit on the time-of-flight gate. For protons the calculated mass was always between 0.9 and 1.1 amu while for deuterons masses were generally between 1.9 and 2.1 amu. Several alpha particle groups were

also observed with a mass resolution between 3.8 and 4.2 amu. The lower spectrum in the figure shows a gated energy spectrum for the time window between channels 443 and 459 of the time-of-flight spectrum corresponding to flight times between 179 and 193 ns. Note that only protons appear in this spectrum, and that a much improved background is provided.

Since the collection efficiency of the guide is proportional to the inverse of the particle's energy,[1] this system is particularly useful for studying products of reactions with large negative Q values. Higher energy particles due to other reactions are selectively filtered. This technique is also quite applicable for the detection and identification of heavy ion reaction products where particle telescopes cannot be used and excellent energy resolution is required. This system is simple, very inexpensive, and can compete favorably with the much more expensive magnetic spectrograph which can only measure the charge to mass ratio.

REFERENCES

1. N. S. Oakey and R. D. Macfarlane, Nucl. Instr. Method 49 (1967) 220.

2. W. G. Mourad, T. Pauly, and R. G. Herb, Rev. Sci. Instr. 35 (1964) 661.

3. I. S. Sherman and R. G. Poddick, IEEE Trans. Nucl. Sci. NS-17 (1970) 252.

FIGURE CAPTION

(Top and Middle) Total energy and time-of-flight coincidence spectra at 25^{o} for ^{12}C + d at 9.0 MeV incident deuteron energy. (Bottom) Gated energy spectrum for the time window between channels 443 and 459 (vertical arrows) or the time spectrum corresponding to flight times between 179 and 193 ns.

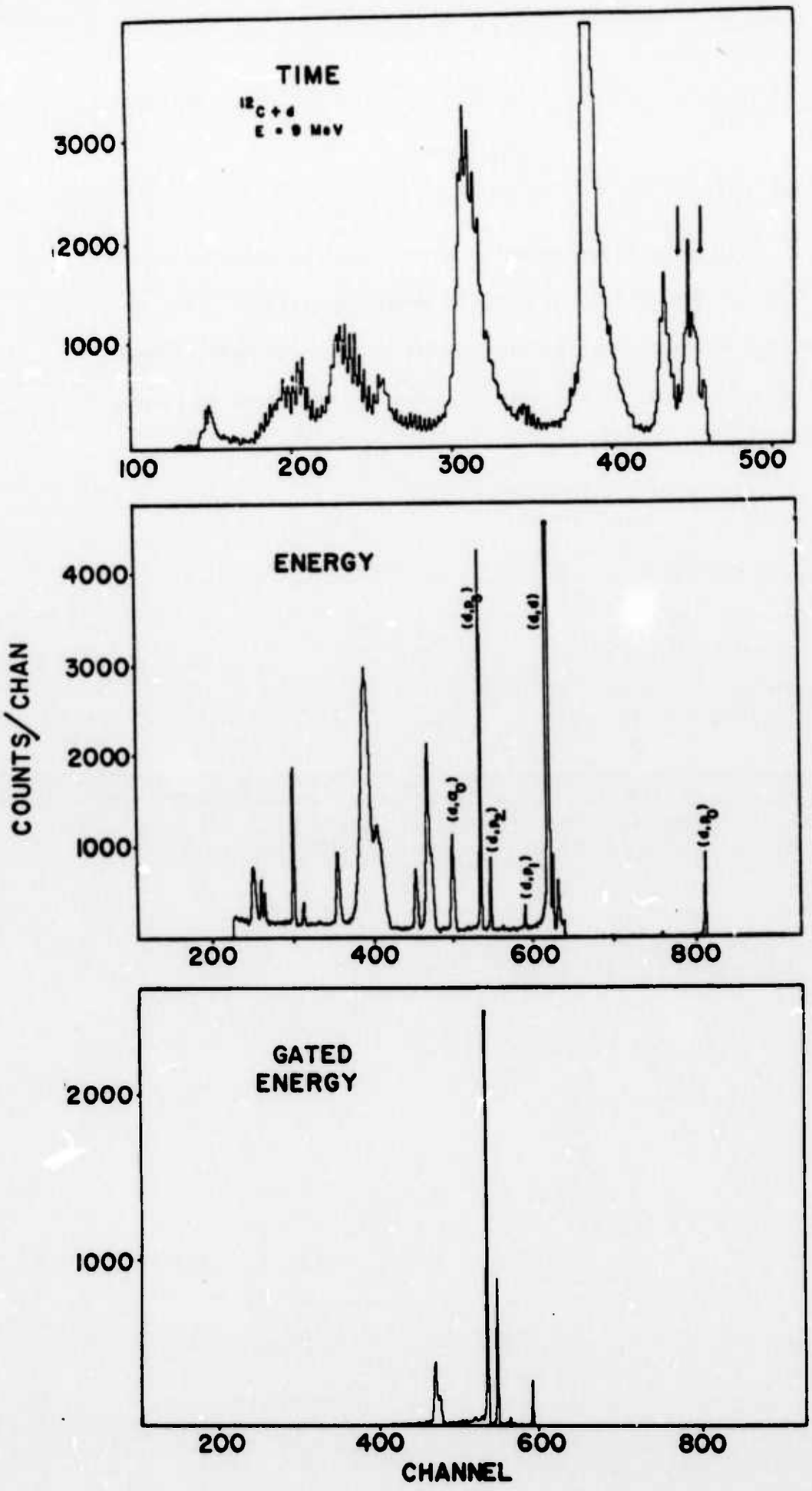
TIME
$^{12}C + d$
E = 9 MeV
3000
2000
1000
100
200
300
400
500
ENERGY
4000
3000
2000
1000
COUNTS/CHAN
(d,p$_0$)
(d,p$_2$)
(d,d)
(d,p$_1$)
(d,p$_0$)
200
400
600
800
GATED
ENERGY
2000
1000
200
400
600
800
CHANNEL

D. Internal Conversion Spectrometer

In-beam studies of internal conversion (IC) constitute a relatively unexplored area of experimental nuclear physics.[1-4] Such conversion electron studies allow investigation of short-lived levels in nuclei that are not normally populated by long-lived radioactive decay, but only by nuclear reactions. In-beam measurements also are advantageous because nuclear reactions provide large effective source strength, and allow control of the thickness, size, and uniformity of the source. Besides giving the usual information on spins and parities of nuclear levels, in-beam IC studies also may be exploited to measure nuclear lifetimes directly.

A major problem associated with any attempt at in-beam detection of electrons is the necessity of separating the electrons from the gamma-rays in order to minimize background levels arising from Compton scattering in the electron detector, while still obtaining high transmission of electrons to the detector.[1-3] An axial β-ray spectrometer was designed and built for use with the University of Texas EN Tandem Van de Graaff accelerator. To test its usefulness for in-beam conversion electron studies a ^{90}Zr target was bombarded with 11.2 MeV protons at a current of 300 nA, and the conversion electron spectra were studied. These spectra demonstrate that the transmission (3.5%) and low background provided by this instrument will make it a useful tool for future experimental investigations at this laboratory.

A schematic drawing of the experimental apparatus is shown in Fig. 1. The two large outer coils consist of 238 turns each. A stainless steel chamber 1.55 m long and 38.1 cm in diameter houses a lead rod 5 cm in diameter and 1.3 m long, placed along the axis of the chamber. A smaller coil of 107 turns is placed around the lead rod in the center of the cylinder. The three coils are wired in series such that the field produced by the central coil 'bucks' the field produced by the two larger coils. The beam enters at a 135^{o} angle to the axis of the apparatus to strike the target which is housed in a triangular stainless steel compartment welded onto the end of the chamber and centered on the axis and with respect to the depth of the coil at that end (i.e., the target is centered in all three dimensions of the coil).

The stainless steel compartment contains two ports, one for attachment of a beam dump and another for a Ge(Li) detector, used in direct determination of internal conversion coefficients. A 70 mm^2 x 2 μm Si(Li) detector with 2 to 4 keV resolution is centered on all three coil dimensions at the other end of the chamber, thus completing the configuration for optimum electron transmission (3.5%) as indicated by calculations. The lead rod along the line joining the target and the detector reduces considerably the number of gamma-rays reaching the detector. Those radiations scattering off the walls are diminished in intensity since the distance between the target and detector is reasonably large. The spectrometer is dispersive and for a given coil

current (up to 70 A) focuses electrons of an energy $E_0 \pm \Delta E$, where ΔE is about 7% of E_0. Electrons of energies up to about 400 keV can be focused by the present system. Immediate plans are for a larger power supply to bring $E_{0,max}$ to about 1 MeV. The system is operated at a pressure of 5×10^{-7} torr provided by a liquid nitrogen trapped oil diffusion pump.

Provisions have been made for a computer-controlled sweep of the current range of the spectrometer to allow for more convenient observation of the electron lines originating in a given reaction. Extensive use of the PDP-7 system for control of future measurements of conversion electrons is planned.

To test the usefulness of the internal conversion electron spectrometer for in-beam studies, a ^{90}Zr target was bombarded with 11.2 MeV protons, and the electron spectrum was scanned. Since the threshold for the $^{90}Zr(p,n)^{90}Nb$ reaction is about 7 MeV, it was expected that conversion electrons from transitions between states in ^{90}Nb as well as between states in ^{90}Zr (excited by (p,p') inelastic scattering and $(p,n\beta^+)$ decay) would be observed.

Fig. 2 shows a composite spectrum of the electron groups observed. The individual spectra for the various coil current settings are joined and overlapped to display a continuous spectrum. The vertical scale has been changed at each tick mark on the horizontal axis to give the reader the best view of any particular transition. The energy range of the spectrometer is limited at the lower end by an overwhelming number of knock-out

electrons (delta-rays) and at the upper end by the current delivered by the power supply. A range from about 90 to 400 keV can be covered at present. The data shown in Fig. 2 were accumulated in about 2-3 hours of running time. The average beam current for any one run was approximately 300 nA.

In Fig. 2 a total of 16 electron groups is seen. There is perfect correspondence between 14 of these groups and the known gamma-ray transition energies in ^{90}Zr and ^{90}Nb in the range 100-400 keV.[5-8] In addition, an electron group of energy 218.5 keV is observed which can be explained as an internal conversion (K shell) transition between the (3.31(35) MeV) 2^+ and (2.077 MeV) 4^+ states in ^{90}Zr.[8] A corresponding E2 gamma transition has not been reported to our knowledge. Also, another electron group of energy 152.4 keV is quite consistent with an internal conversion (K shell) transition between the (0.8226 MeV) ? and (0.6512 MeV) 3^+ states in ^{90}Nb; the corresponding gamma transition, to our knowledge, has not been observed.[8]

In conclusion, this axial β-ray spectrometer has been found to provide a larger transmission with comparable resolution and lower background for in-beam internal conversion studies than in earlier reported experiments, and should provide an important tool in the future study of nuclear structure.

REFERENCES

1. C. F. Moore, J. G. Kulleck, W. R. Coker, R. G. Clarkson, J. J. Kent, and W. J. Courtney, Nucl. Instr. and Meth. 79 (1970) 353.
2. W. J. Courtney and C. Fred Moore, Phys. Letters 31B (1970) 131; and W. J. Courtney, Thesis, University of Texas (1971), unpublished.
3. B. L. Cohen, Progress Report - University of Pittsburgh (1970).
4. K. W. Robert, J. R. Linn, and T. E. Durham, Nucl. Instr. and Meth. 79 (1970) 251.
5. C. M. Lederer, J. M. Hollander, and I. Perlamn, Table of Isotopes (John Wiley and Sons, Inc. N. Y., 1967) 401.
6. A. B. Tucker and S. O. Simmons, Nucl. Phys. A156 (1970) 83.
7. J. E. Glenn, H. W. Baer, and J. J. Kraushaar, Nucl. Phys. A165 (1971) 533.
8. J. B. Ball, M. W. Johns, and K. Way, Nuclear Data Tables (Academic Press, New York and London, 1970) 407.

FIGURE CAPTIONS

Fig. 1 Schematic drawing of axial ß-ray spectrometer used for in-beam internal conversion measurements.

Fig. 2 Composite in-beam electron spectrum observed for 11.2 MeV proton bombardment on ^{90}Zr. The individual spectra for the various coil current settings are joined and overlapped to display continuous spectrum. The vertical scale has been changed at each tick mark on the horizontal axis to give the reader the best view of any particular transition. The 16 electron groups correspond to internal conversion transitions in ^{90}Zr and ^{90}Nb in the energy range 100-400 keV.

AXIAL BETA RAY

SPECTROMETER

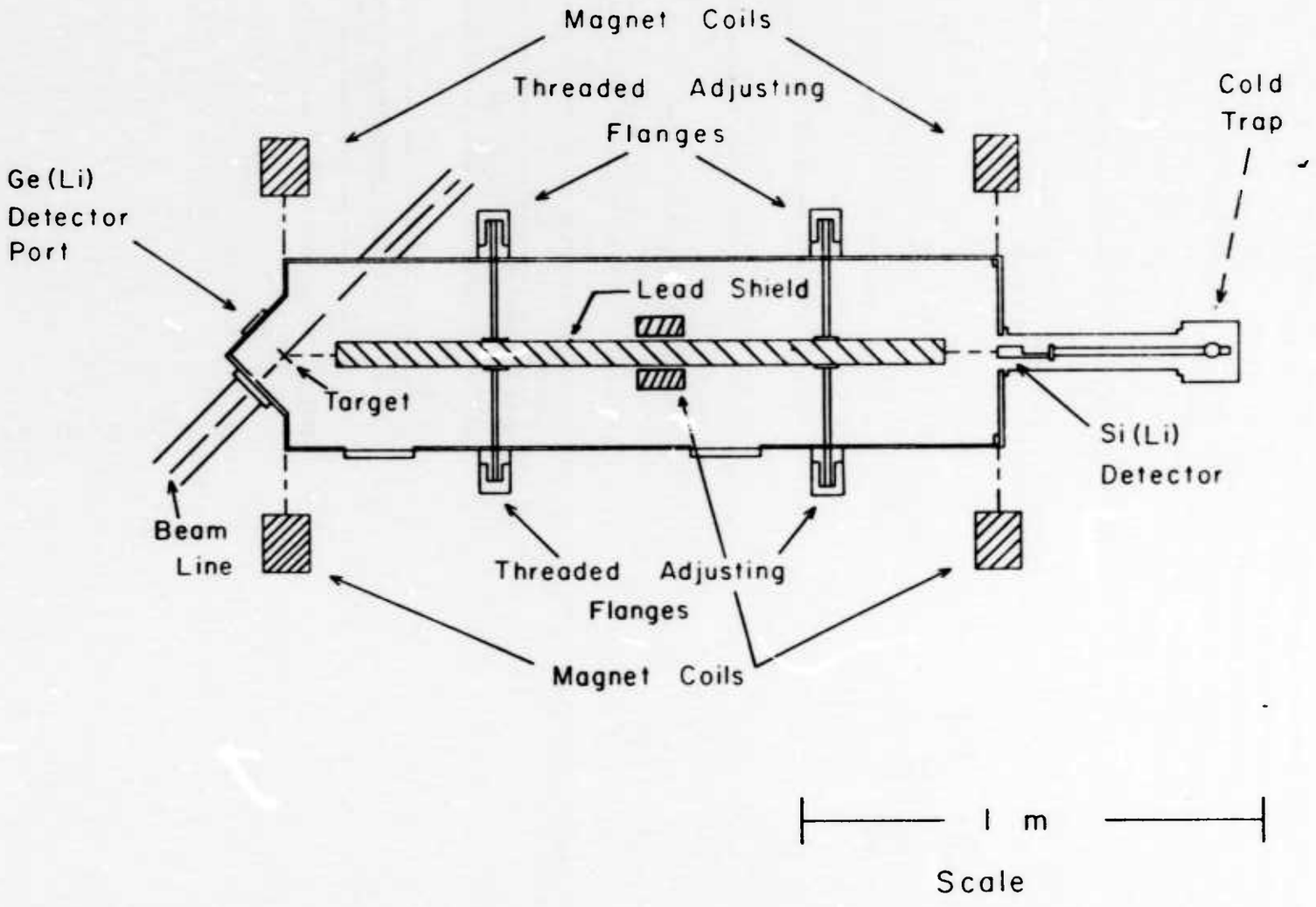

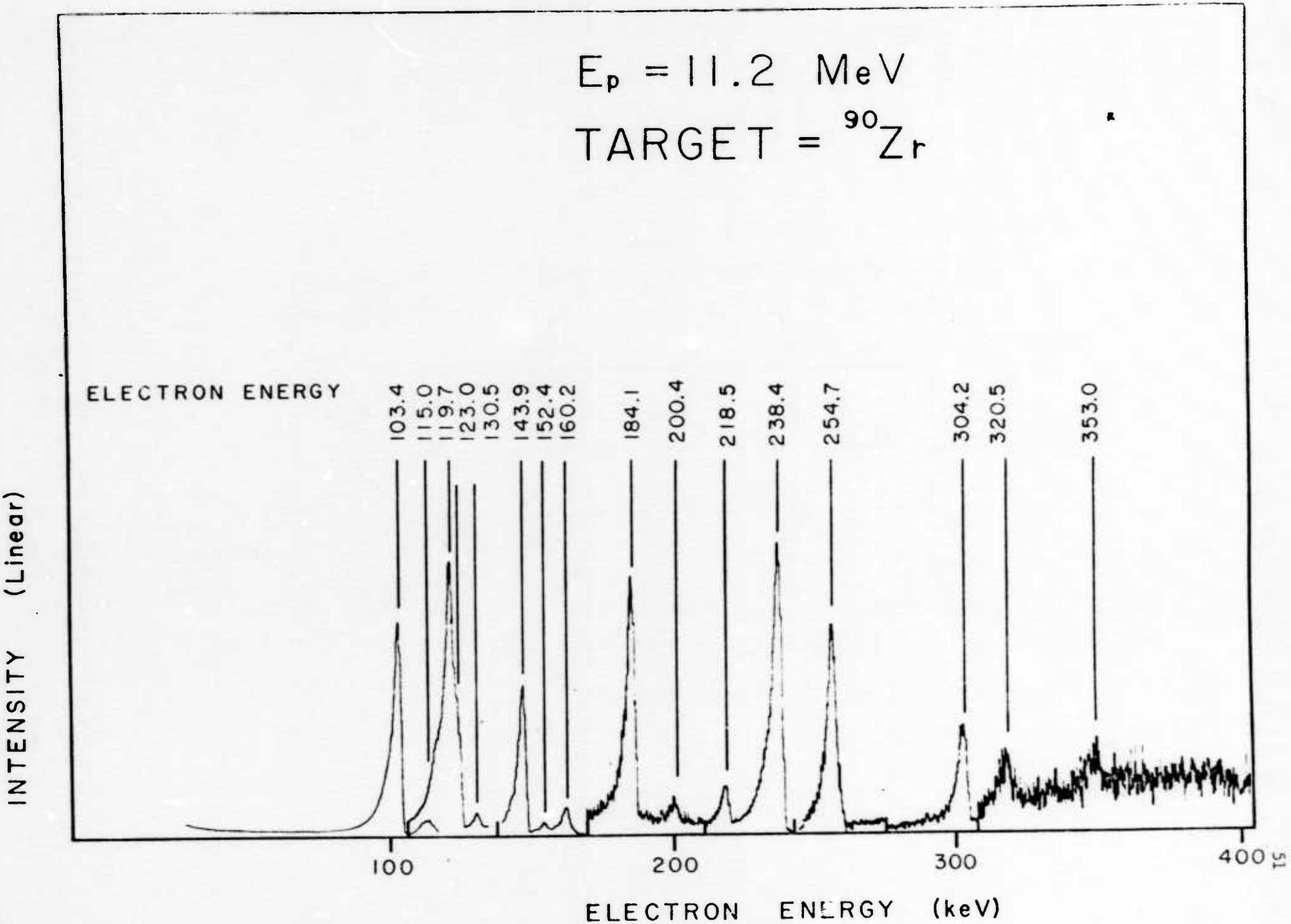
E_p = 11.2 MeV
TARGET = ^{90}Zr
ELECTRON ENERGY
103.4
115.0
119.7
123.0
130.5
143.9
152.4
160.2
184.1
200.4
218.5
238.4
254.7
304.2
320.5
353.0
INTENSITY (Linear)
100
200
300
400
ELECTRON ENERGY (keV)

E. Studies of p + ^{92}Mo Induced Internal Conversion Electrons

The very first information concerning nuclear energy levels in the history of physics was obtained from the study of internal conversion electrons,[1,2] and such studies have continued to play a vital role in nuclear spectroscopy. We report here on in-beam studies of conversion electrons from ^{92}Mo and ^{92}Tc, using an axial electron spectrometer of unique design.[3] In-beam internal conversion (IC) electron spectroscopy solves many of the difficulties of conventional β-ray spectroscopy, but introduces some new experimental problems which it shares with in-beam γ-decay experiments. Since the time required to accumulate a spectrum is long compared to β-decay lifetimes, it is often difficult to assign very weak lines. Coincidence requirements thus become highly desireable, as in the in-beam γ-ray studies.

In our examination of IC electrons from p + ^{92}Mo, which was partially a test of the capabilities of our new spectrometer, we have not imposed coincidence requirements. As will be seen, the solid angle and resolution of the instrument permit identification of a number of new transitions in ^{92}Mo and ^{92}Tc.

Experimental Procedure

The design of the spectrometer is described in ref. 3. Electrons were detected by a 2 μm Si(Li) detector with an active area of 50 mm^2, cooled to liquid nitrogen temperature. The resolution of the detector was about 4 keV for electrons of the energies considered here, 100-500 keV. By design the spectrometer admits electrons of energy $E_0 \pm \Delta E$,

where E_0 is fixed by the spectrometer coil current and ΔE is about 7% of E_0. Thus the observed IC lines, at a given coil current setting, appear on a background distribution which has relatively steep slopes and a width an order of magnitude larger than the detector resolution.

The target was a 98% enriched, rolled ^{92}Mo foil of 600 $\mu g/cm^2$. Two complete scans of the IC spectrum were carried out, one at 8.0 MeV incident proton energy, the other at 11.0 MeV incident proton energy.

Results

The threshold for the $^{92}Mo(p,n)^{92}Tc$ reaction is 8.84 MeV, so that the IC groups observed in the 8 MeV run can be mainly assigned to transitions in ^{92}Mo excited by proton inelastic scattering. One could, however, also imagine the possibility of proton capture to highly excited states in ^{93}Tc followed by a cascade to lower states and subsequent internal conversion. We see at least one transition of the latter type.

For bombarding energies of 9 MeV or more we expect to observe IC transitions in ^{92}Tc as well. Further β-decay of ^{92}Tc will feed specific transitions in ^{92}Mo. In fact, at the energy of 11.0 MeV we observed fewer ^{92}Mo transitions than at 8.0 MeV. However, the 11.0 MeV runs were considerably shorter than those at 8.0 MeV because of the strong electron yields from transitions in ^{92}Tc and our main interest in these.

In Figs. 1 and 2 are shown the composite spectra of the electron groups observed, at 8.0 and 11.0 MeV respectively. The various spectra for the range of coil current settings used have been joined piece by piece and overlapped to display a continuous spectrum. The vertical

scale has been changed at each tick mark on the horizontal axis so that the best presentation of any particular group is obtained.

The energy range of the spectrometer is limited at the lower end by the large number of knock-out electrons from the target, and at the upper end by the maximum current which our present power supply can deliver. A range of from 100 to 500 keV can be covered at present.

In Fig. 1 a total of 14 electron groups is seen. Five of the transitions correspond to previously observed[4] γ-ray transitions in ^{92}Mo. In addition, a transition corresponding to the 390 keV γ-decay of ^{93}Tc[5] is observed. Other transitions, which have not previously been reported, are seen at 140.6, 144.0, 171.2, 182.2, 214.5, 306.5, and 337.5 keV. These are presumably transitions in ^{92}Mo, as can be verified directly by the K to L separation in the case of the 140.6, 171.2, 214.5, 306.5, 337.5 keV transitions. These transitions, however, do not fit into the known level scheme of ^{92}Mo, and thus may be transitions at higher excitation energies than covered by the known level scheme. Finally the transition at 363.6 keV is consistent with decay of the 3.369 MeV level in ^{92}Mo to the 3.005 MeV level.

Turning next to Fig. 2, the 11.0 MeV spectrum displays transitions at 135.0, 213.5, and 259.5 keV which are consistent with known γ-decay transitions in ^{92}Tc.[4] Also observed are the 148.0, 244.0, 330.0, and 392.0 keV transitions seen at 8.0 MeV and corresponding to known transitions in ^{92}Mo. One additional transition, at 116.0 keV, is assigned to ^{92}Tc.

The table summarizes the transitions observed. The number of new transitions observed in this limited energy region is encouraging. A clear stimulus is provided for further study of the nuclei ^{92}Mo and ^{92}Tc with this technique. In future work, internal conversion-electron-proton coincidence and internal conversion-electron-γ-ray coincidence studies will be invaluable in locating the newly observed transitions within an expanded level scheme.

REFERENCES

1. F. Danysz, Le Radium 10 (1913) 4.

2. E. Rutherford and A. Robinson, Phil. Mag. 26 (1913) 717.

3. J. Michael Picone et al., Nucl. Instr. Methods 105 (1972) 377.

4. D. C. Kocher and D. J. Horen, Nuclear Data Sheets B7 (1972) 299.

5. Nuclear Data Sheets (1959-1965) 644.

Table: The observed internal conversion transitions seen from p + ^{92}Mo at E_p = 8.0 and 11.0 MeV.

E_p (MeV)	Transition Energy (keV)	Nucleus	Transition
8.0	140.6	^{92}Mo	
8.0	144.0	^{92}Mo	
8.0	148.0	^{92}Mo	2.759(8^+)-2.6115(6^+
8.0	171.2	^{92}Mo	
8.0	182.2	^{92}Mo	
8.0	214.5	^{92}Mo	
8.0	235.0	^{92}Mo	4.484(11^-)-4.249(9^-
8.0	244.0	^{92}Mo	2.5262(5^-)-2.2825(
8.0	306.5	^{92}Mo	
8.0	330.0	^{92}Mo	2.6115(6^+)-2.2825(
8.0	337.5	^{92}Mo	
8.0	363.6	^{92}Mo	3.369-3.005
8.0	392.0	^{93}Tc	0.390($1/2^-$)-0.0(9/
8.0	480.0	^{92}Mo	3.572-3.092(2^+)
11.0	116.0	^{92}Tc	
11.0	135.0	^{92}Tc	0.60803-0.47335
11.0	148.0	^{92}Mo	2.7594(8^+)-2.6115(
11.0	213.5	^{92}Tc	0.21394-0.0(7^+)
11.0	244.0	^{92}Mo	2.5262(5^-)-2.2825(
11.0	259.5	^{92}Tc	0.47335-0.21394
11.0	306.5	^{92}Mo	
11.0	330.0	^{92}Mo	2.6115(6^+)-2.2825(
11.0	392.0	^{93}Tc	0.390($1/2^-$)-0.0(9/

FIGURE CAPTIONS

Fig. 1 Composite electron spectrum from p + ^{92}Mo at E_p = 8.0 MeV. The vertical scale has been changed at each tick mark on the horizontal axis to give the reader the best view of the data.

Fig. 2 Composite electron spectrum from p + ^{92}Mo at E_p = 11.0 MeV. The vertical scale has been changed at each tick mark on the horizontal axis to give the reader the best view of the data.

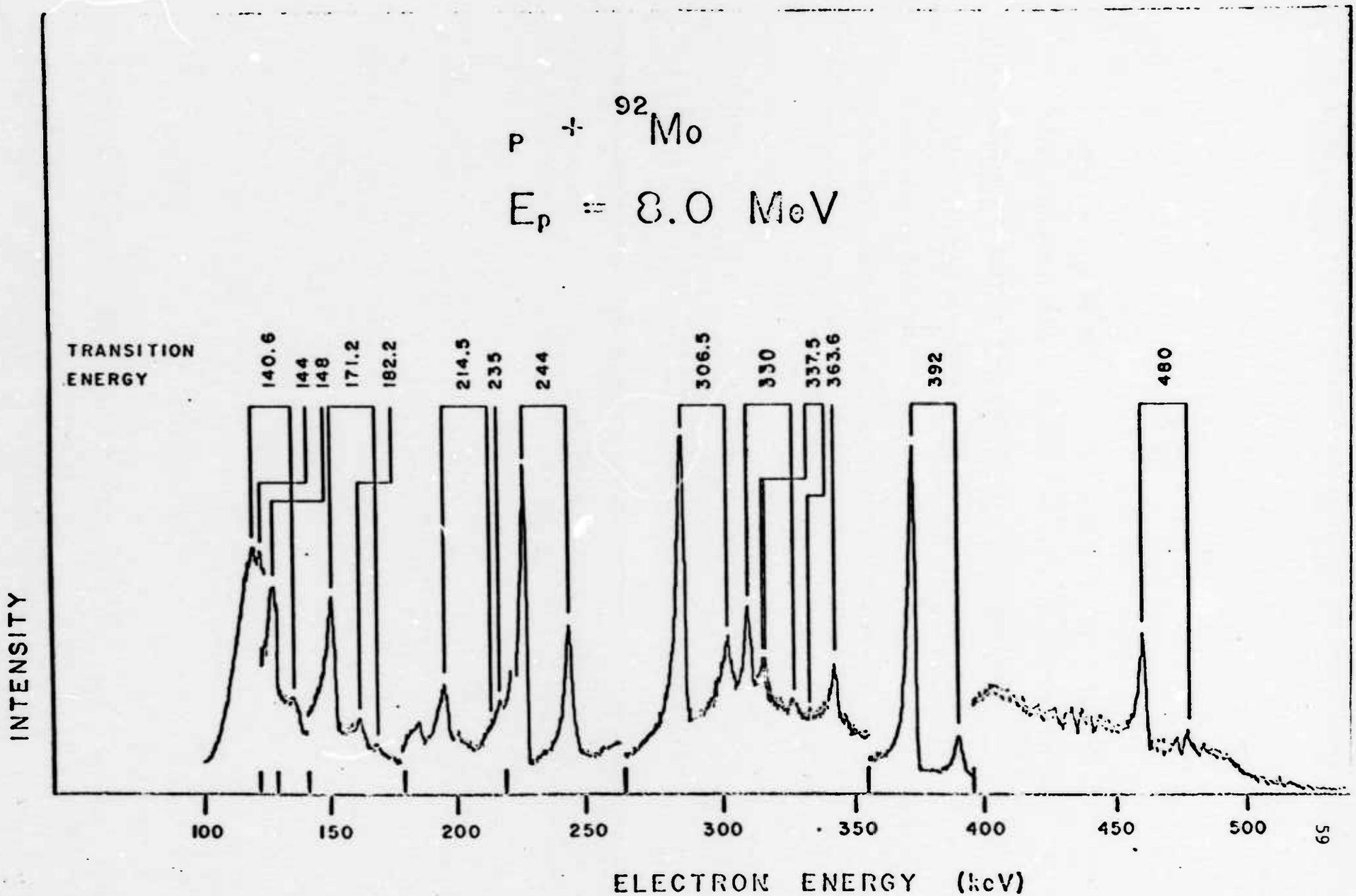
p + 92Mo
Ep = 8.0 MeV
TRANSITION ENERGY
140.6
144
148
171.2
182.2
214.5
235
244
306.5
330
337.5
363.6
392
480
INTENSITY
100
150
200
250
300
350
400
450
500
ELECTRON ENERGY (keV)
59

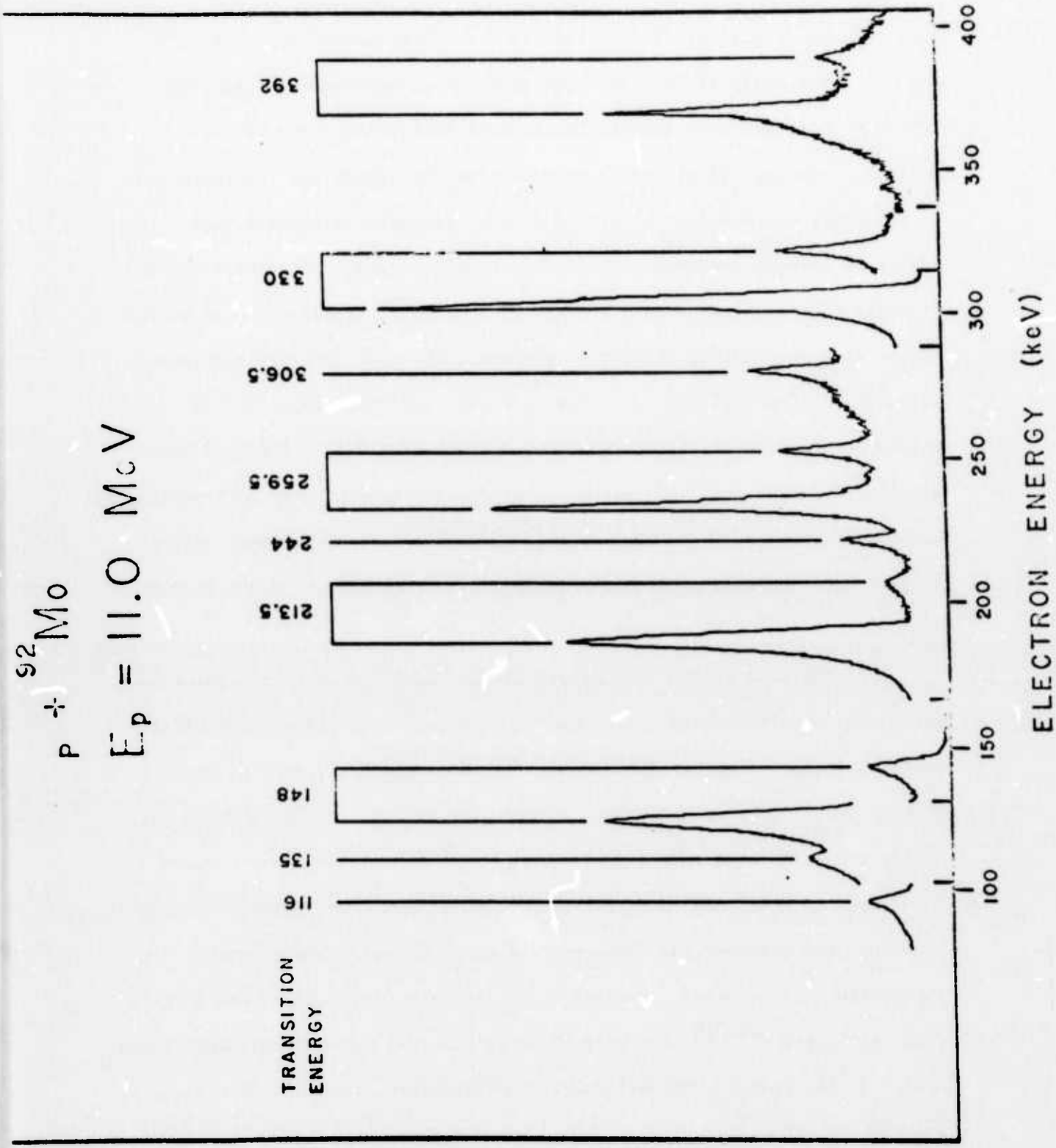
p + 92Mo
Ep = 11.0 MeV
TRANSITION ENERGY
116
135
148
213.5
244
259.5
306.5
330
392
100
150
200
250
300
350
400
ELECTRON ENERGY (keV)
INTENSITY

F. X-Ray-Gamma-Ray Coincidence Studies from Spontaneous Fission of ^{252}Cf

The study of fission, both spontaneous and induced, has often involved coincidence techniques in attempts to correlate the various products. The myriad of states available to the system and the complexity of the decay schemes for the highly excited fragments present a rich source of information which is valuable both as a means of identifying the features of the scission process and as a means of studying the structure of the neutron-rich nuclei thereby produced, which are for the most part accessible in no other manner. The latter has received considerable attention in the case of the spontaneous fission of ^{252}Cf from Cheifetz et al.,[1] Wilhelmy et al.,[2] and Watson et al.[3] These studies of coincidences between fission fragments, internal conversion electrons, X-rays, and/or γ-rays, have revealed much about deformed even-even nuclei in the populated regions.

The mass yields from binary fission of ^{252}Cf have been determined with both coincidence and radiochemical methods.[3,4] In the former experiments, the resolution was about 2 u. A method devised by Schmitt et al.[5] to take into account pulse height effects in solid state detectors as well as neutron boil-off values from Bowman et al.[6] has allowed considerable confidence to be placed in recent mass calculations. The behavior of prompt neutrons, the correlations between the ensuing direct forms of decay, γ-radiation and internal conversion, and the mass yields have been investigated at length.[3,6,7,8] The work presented in this paper is concerned with observing low energy γ-transitions in the fragments from the spontaneous

fission of ^{252}Cf by use of an X-ray, γ-ray coincidence system. This is an effective tool in separating the many radiations involved. Such methods have been used in studying higher energy transitions.[9,10] The continuing improvement in the resolutions of the available X-ray and γ-ray detectors, has made possible these measurements to a degree of accuracy heretofore unmatched.

Experimental Setup

A 0.08 μCi ^{252}Cf source on a nickel backing was sandwiched between two 0.1 mm thick pieces of plastic on an aluminum aperture. The plastic stopped the fragments, thus providing a high coincidence rate and preventing Doppler distortions in the spectra. The source package was placed in contact with the beryllium window on the face of a thin window 0.14 cc Ge(Li) low energy photon detector and with the face of a 0.09 cc Si(Li) X-ray spectrometer about 2 cm away. This geometry provided optimum solid angles such that the count rate limitation of the Si counter, around 4000 counts/sec was reached. The actual resolutions of the respective detectors, 350 eV at the 31 keV line from a ^{133}Ba source and 500 eV at the 81 keV line from the same source, were degraded somewhat by the electronics used as will be described below. Both detectors rested on pliant foundations to reduce pulses due to vibrations in the experimental environment.

Pulses from the detectors were routed through the timing and amplification circuitry presented in Fig. 1. The fast discriminators were set just above the low-level noise. The time-to-amplitude converter (TAC)

was set at a full scale of 100 nsec, and the stop signal from the Ge counter was delayed 40 nsec. The time resolution of the system was 20 nsec FWHM. The TAC output was directed to a single-channel analyzer (SCA) which accepted the 40-90 nsec segment of the total time spectrum which included practically all of the coincidence timing peak. The time requirement was roughly set at 50 nsec since lifetimes were not a major interest in this experiment. The output of the SCA provided a gate signal to allow the linear pulses to enter 1024 channel analog-to-digital converters (ADC).

The X-ray spectrum was calibrated by taking a self-gated ^{252}Cf singles spectrum; the L X-rays from internal conversion in ^{248}Cm following α-decay of ^{252}Cf provided a convenient source of known lines. The γ-ray spectrum was calibrated in a similar manner with ^{57}Co, ^{133}Ba, and ^{153}Gd sources each superimposed on the ^{252}Cf spectrum to maintain count-rate conditions. Both energy calibrations were fit with third order polynomial functions. The total running time was about 10 days with a coincidence rate of about 50 counts/sec. The gains of the amplifiers were checked daily by simply restarting the total coincidence spectra and noting the locations of the prominent peaks. Fortunately no adjustments to the data were required, since no substantial gain drifts were encountered.

Online Data Analysis

A PDP-7 computer was programmed to perform a two-parameter matchup between peaks in the X-ray and γ-ray spectra. The two-parameter program, initiated by a gate pulse at ADC1, accepted the linear pulses at ADC2 and

ADC3 in either order. An additional pulse at the gate ADC before the other two had both received inputs would abort the current sequence and reinitiate the search. The coincident γ-rays were sorted and placed in corresponding storage areas, according to windows set on the pertinent $K\alpha_{1,2}$ peaks in the X-ray spectrum. In this way the γ-rays from a particular set of isotopes and the complementary set of isotopes were separated from the radiation of the other fragments. Each gated spectrum was stored in 1024 channels located in the additional memory of a PDP-15 computer; an interprocessor buffer provided the access between the two computers.

Results

The total coincidence X-ray spectrum in Fig. 2 consists of well separated $K\alpha_{1,2}$ X-ray peaks for the various fragments, with the light and heavy fragment groups centered about Z = 43 (Tc) and Z = 55 (Cs), respectively. The Ni and Ge X-rays in the low energy end of the spectrum were probably the result of γ-fluorescence of the nickel backing and the Ge crystal itself in coincidence with other γ-rays. The efficiency of this detector begins decreasing from 100% at about 15 keV and is about 30-35% in the region of the Cs peak. The intrinsic resolution of the Si(Li) system was degraded due to count rate effects. The "effective" resolution of the system was sufficient to allow sixteen well separated windows to be set accurately as shown in Fig. 3. The gates in each case were roughly equivalent to or slightly less than the FWHM for the $K\alpha_{1,2}$ peaks and, as is evident in the sorted data, allowed little overlapping between adjacent peaks. An additional concern in this arrange-

ment was the location of K_β groups which in several instances were unresolved from neighboring K_α groups. Specifically the Y, Zr, Nb, and Mo K_β X-rays were unresolved from the Nb, Mo, Tc, and Ru K_α X-rays, respectively, in the light fragment region. The I, Xe, Cs, and Ba K_β lines overlapped with the Ba, La, Ce, and Pr K_α X-rays, respectively, in the heavy fragment region. In such cases a comparison of the appropriate sorted spectra, taking into account the relative intensities of the γ-rays as well as the fact that the K_β X-rays were much weaker than most of the corresponding K_α X-rays, reveals the extent of the overlap. Except for Pd and Sb, these settings recorded spectra for seven pairs of complementary fragments: Y-Pr, Zr-Ce, Nb-La, Mo-Ba, Tc-Cs, Ru-Xe, and Rh-I. The cross referencing within each pair proved highly informative in analyzing the data.

The total coincidence γ-spectrum which has 0.21 keV/channel, Fig. 4, has as its most noticeable features the large number of X-rays in the low-energy end and a 68.8 keV γ-ray which dominates the region of interest in this work, 45-230 keV. Energies below 45 keV lie in the range of some of the X-ray groups and so are open to ambiguity. The light fragment X-rays were only partially recorded whereas the heavy fragment group is entirely present, though compressed due to the gain. Immediately above this group is a series of closely spaced γ-rays of various intensities and energies, the strongest being the one at 68.8 keV. The efficiency of this detector, 100% at 60 keV, 50% at 80 keV, and dropping to 28% at 160 keV and about 20% at 220 keV, must be considered in order to get a true picture of the relative strengths.

The sorted γ-ray spectra corresponding to the windows on the light fragment X-rays and the complementary spectra from windows on the heavy fragment X-rays are shown in Figs. 5-11. Figs. 12 and 13 show the spectra from windows on Pd and Sb X-rays, respectively, for which no complementary spectra were taken. The criterion for determining peaks was a minimum of thirty counts above background in the peak channel and a somewhat Gaussian shape. Large single channel fluctuations were disregarded. The center of a given peak was estimated to the nearest quarter channel. The fit on the calibration was accurate to 0.1 keV and coupled with the error in the choice of the peak channel gave a total error of ±0.15 keV. A point to note in each of the light fragment spectra is the predominance of the X-ray of each fragment's complement in the low energy end, a simple X-ray, X-ray coincidence arising from internal conversion in both fragments, which competes favorably with gamma decay in many of the low energy transitions.

Interestingly, each gate on a heavy fragment X-ray often saw an additional X-ray from that same fragment in the Ge detector. This self-coincidence demands two X-rays from the same fragment within a time span of about 50 nsec, an event which can arise from two internal conversions in the same cascade. This phenomenon is currently being investigated.[11]

The effects of gates on overlapping K_α lines and unresolved K_β-K_α groups are noted by looking at the relative intensites of the peaks in the various spectra involved. The nature of the most heavily produced

group of γ-rays, these seen by the gate on Technetium, is extremely helpful in this respect. The 68.8 keV γ-ray which dominates the total coincidence spectrum belongs to this group and is probably the transition assigned 69 keV by Watson et al.[3] in ^{108}Tc. Any interference between gates in which Tc or its complement is involved can be gauged accurately by the strength of this one line. It appears to a slight extent in all of the spectra, indicating a small background contribution. In the gated spectra from the adjacent Mo and Pd peaks, it is a bit stronger as should be expected. In total, however, it is obvious that this strongest group of lines has been well separated from the others.

The energies of the observed gamma rays are given in Table I, and the two spectra for each complementary set of fragments are compared with each other and with previous data. A few lines which did not quite qualify as peaks but which were definite possibilities are included in parentheses as are any quantities from other works which were reported doubtful. Also lines obviously due to overlap from adjacent spectra or from K_β X-rays have been omitted. Weaker lines have been included if evidence from relative intensities implies that they may be genuine. In many cases the combined information allows a definite assignment of mass and charge. In doubtful cases, where previous results disagree, the assignment is placed in parentheses.

There is generally excellent agreement with the data of Watson et al.[3] Seen in the present work are all low energy transitions in the appropriate ranges of mass and charge to which they give a confidence

level of A or B. In a few cases the present data or the consensus of other references indicates the transition is from a fragment with charge adjacent to that assigned by them.

Agreement is also excellent with the data of John et al.[7] All low energy transitions in the mass range of the present work with halflives less than 80 nsec are seen. However only three isomeric transitions are observed, and two of these are probably members of the same cascade. Since their gamma ray detector was shielded from the second fragment detector, this data gives a reliable indication as to whether the transitions occur in the light or the heavy fragment. Comparison with the work of Cheifetz et al.[1] and Wilhelmy et al.[2] on the decay of even-even nuclei reveals further agreement. This work also explains the weakness of the Xe and Tc X-rays, since the $2^+ - 0^+$ transition energies for these isotopes are generally larger than the others, with correspondingly lower internal conversion probabilities.

Most of the low energy transitions seen by Alvager et al.[12] correspond well to values reported in this paper. Since a mass separator was used, this data generally gives the best mass values. There are two cases of apparent disagreement between Watson et al.[3] and Alvager et al.[12] on the one hand, and John et al.[7] on the other hand, as to whether the transition is from the light or the heavy fragment, possibly indicating doublets. The present data eliminates some ambiguities. For example, John et al.[7] observed a 97.5 keV, mass 150 gamma ray as well as a 98.3 keV, mass 101 gamma ray, either

of which could have been the Zr-Ce 98 keV line. However the latter was attributed by them to be in the same gamma ray cascade as the 91 keV, mass 101 transition (see Table II) which the present data show to be from ^{101}Y. Their use of lifetimes as a guide for grouping transitions in a cascade has been supported by the present data, which in every applicable instance assigns the γ-rays to the same nucleus. This implies the 98.3 keV line is also from ^{101}Y and this is probably the line that Watson et al.[3] attributed to a 99 keV transition in ^{101}Zr but with a confidence level of C.

In the present data, the 112.4 keV gamma ray from Mo-Ba appears strong and sharp in both gates. The energy agrees very well with the gamma ray assigned to mass 104 by John et al.[7] The 119.6 keV gamma ray from Tc-Cs is seen weakly in both spectra. Again the energy agrees well with the gamma ray assigned mass 109 in the same work.

Where they overlap, there is generally little correlation between the present work and the previous gamma ray data of Ruegsegger, Jr. et al.[9] and Eddy et al.[10]; however the latter works covered mainly higher energy gamma rays which lie beyond the energy range of the detector used in the present work.

Discussion

The de-excitation process in each primary fragment is culminated by a γ-cascade and possibly internal conversion. In a given binary fission event, one of the two post-neutron fragments or both can emit X-rays as well as γ-rays, as depicted in Fig. 14. An X-ray, γ-ray coincidence require-

ment does not limit the event to a direct one, as a delayed cascade-internal conversion sequence in a beta-decay product is accepted under this format. The three possibilities, X-ray from one primary fragment and γ-ray from the other, X and γ from the same primary fragment, and X and γ from a beta decay chain member can be separated to an extend by a comparison of the data for gates on two complementary X-rays. A γ-ray appearing in both spectra must be associated with a prompt event some of the time, since a delayed γ-ray would not be in coincidence with an X-ray from the complementary fragment even though it is not certain which is the complementary fragment. However, it is possible, but not necessary, that some of the time, γ-ray can be associated with a delayed event in self coincidence with its cascade internal conversion X-ray. Table I demonstrates the great number of these lines which must be direct in some events. It also indicates that most of the gamma rays assigned to a specific fragment are in coincidence with X-rays from both that fragment and its complement, or from only the complement, implying a direct transition. The lifetime data of John et al.[7] generally support this conclusion. An unidentified γ-ray seen in only one of the spectra could arise from a direct or delayed event.

Excluding those instances where γ-rays have been matched with the data of earlier experiments for a particular Z value, no distinction can be made on the basis of this data between the complementary fragments as possible sources of the radiation. This problem can be resolved only by allowing separation of the fragments by free flight and thereby greatly degrading the geometry.

A gamma-ray from a given fragment will appear in the spectrum gated by X-rays from that fragment, if it is in coincidence with one or more cascade transitions having an appreciable probability for internal conversion. This situation can result from low transition energy or a high multipolarity. However, generally a multipolarity greater than E2 will result in a halflife too long for coincidence with a preceding transition. These features are illustrated in Table II which gives the $2^+ - 0^+$ ground state band transitions observed in the even-even nuclei and the $4^+ - 2^+$ transitions in these bands, according to the data of Cheifetz et al.[1] and Wilhelmy et al.[2] Also given are the nature of the transitions observed in the present data, and the internal conversion probabilities P_K defined in terms of the coefficients α_K, tabulated by Hager and Seltzer,[13]

$$P_K = \frac{\alpha_K}{1+\alpha_K} \quad .$$

P_K is the probability for K-shell internal conversion, neglecting higher shell contributions. For the odd Z nuclei, Table II gives the energy and halflife of transitions attributed to the same cascade by John et al.,[7] which are observed in the present data, and the P_K for E1, M1, or E2 transitions.

The $2^+ - 0^+$ transitions in the even-even nuclei are all observed in the spectrum gated on the complementary X-rays, but the only line seen strongly in the self-gated spectrum is from ^{150}Ce, which has the lowest

energy $4^+ - 2^+$ transition, with by far the largest P_K. The transitions in the odd Z nuclei seem to follow the same trend, as exhibited by the range for P_K over the probable multipolarities, i.e., a γ-ray is seen in the self-gated spectrum when there is evidence that it is in coincidence with a transition with an appreciable internal conversion probability.

A reasonable assumption to make in analyzing this data is that the majority of the strong low energy lines arise from transitions between low-lying states; states higher in excitation would in general tend to emit higher energy radiation. In particular, the comparison of the spectra for the even Z groups with the even-even data of Cheifetz et al.[1] and Wilhelmy et al.[2] suggests that practically all of these low energy γ-rays are coming from even Z - odd A nuclei, in accordance with expectations from nuclear structure. The odd-even and odd-odd nuclei similarly would be expected to give rise to a multitude of low-lying closely-spaced states; the odd Z spectra accordingly display a profusion of low energy lines. In addition, the odd Z - X-rays predominate in the total coincidence spectrum; the relative intensities of the X-ray peaks in this spectrum are very similar to those in the prompt coincidence spectra of Watson et al.[14] and therefore support the assertion that many of the X-rays and γ-rays seen in this experiment are prompt. The predominance in the X-ray production of odd Z over even Z heavy fragments was attributed by the same work to closed shell effects in the Z = 50, N = 82 region. The present work indicates less of an effect for the light fragments, for

which the neutron levels, in the general range N = 58 to N = 68, are well-removed from any major closed shell.

The preconditions for the substantial amount of internal conversion contributing to the decay schemes of these fragments, small energy spacings or large spin differences, were recorded in gross spectra by Kapoor et al.[15] and Kleinheinz and Siegbahn.[16] The former group found that roughly 57% of the X-rays from ^{252}Cf fission fragments represent halflives from 0.1 to 1.0 nsec and 23% are emitted from 1.0 to 50 nsec. The latter work revealed that the lifetimes for transitions 130 to 260 keV in energy are to a large extent compatible with M1 or enhanced E2 transitions. The specific lifetimes reported by Watson et al.[3] for the transitions seen in this work are also in the 1 to 2 nsec range. All of this data concurs with the present data in the fact that a large number of the γ-transitions are M1 or E2 in origin and so, coupled with small transition energy, would give rise to a large number of X-rays as well as low energy γ-rays.

Although quite a few assignments of γ-rays to a specific mass and charge were possible in this work, many of the strong low energy lines have not been seen in previous work and so remain unidentified as to mass. The limitations on the data of John et al.[7] prevented further matching of γ-rays. They analyzed only the strongest lines below 80 keV, omitted the 70–80 keV segment due to lead X-rays, and recorded γ-rays emitted a minimum of 3 nsecs after fission. Transitions reported here which are direct and fall within their energy range but which they

failed to see are probably somewhat less than 3 nsec in lifetime. The lower energy γ-rays were simply beyond the capabilities of their 9 cm^3 Ge(Li) detector. An experiment involving γ-ray fragment mass coincidence is planned as a supplement to this work, and those results will be used to complete the identifications.

REFERENCES

1. E. Cheifetz, R. C. Jared, S. G. Thompson, and J. B. Wilhelmy, Phys. Rev. Lettrs. 25, 38 (1970).
2. J. B. Wilhelmy, S. G. Thompson, R. C. Jared, and E. Cheifetz, Phys. Rev. Letters. 25, 1122 (1970).
3. R. L. Watson, J. B. Wilhelmy, R. C. Jared, C. Rugge, H. R. Bowman, S. G. Thompson, and J. O. Rasmussen, Nucl. Phys. A141, 449 (1970).
4. W. E. Nervik, Phys. Rev. 119, 1685 (1960).
5. H. W. Schmitt, W. E. Kiker, and C. W. Williams, Phys. Rev. 137, B837 (1965).
6. H. R. Bowman, J. C. D. Milton, S. G. Thompson, and W. J. Swiatecki, Phys. Rev. 126, 2120 (1962); 2133 (1963).
7. W. John, F. W. Guy, and J. J. Wesolowski, Phys. Rev. C2, 1451 (1970).
8. H. Nifenecker, J. Frehaut, and M. Soleilhac, Proc. IAEA Conference on the Physics and Chemistry of Fission (Vienna, Austria, 1969) IAEA Vienna, 491 (1965).
9. D. R. Ruegsegger, Jr., and R. R. Roy, Phys. Rev. C1, 631 (1970).
10. N. W. Eddy and R. R. Roy, Phys. Rev. C3, 877 (1971).
11. R. St. Laurent et al., to be published.
12. T. Alvager, R. A. Naumann, R. F. Petry, G. Sidenius, and T. D. Thomas, Phys. Rev. 167, 1105 (1968).
13. R. S. Hager and E. C. Seltzer, Nucl. Data A4, 1 (1968).

14. R. L. Watson, H. R. Bowman, and S. G. Thompson, Phys. Rev. 162, 1169 (1967).

15. S. S. Kapoor, H. R. Bowman, and S. G. Thompson, Phys. Rev. 140, B1310 (1965).

16. P. Kleinheinz and K. Siegbahn, Nucl. Phys. A90, 145 (1967).

TABLE I

YTTRIUM, PRAESODYNIUM

Present E_γ (keV)		Others		Assigned	
		E_γ (keV)	Mass	E_γ (keV)	Mass
Y	Pr				
	48.6				
	52.5				
54.8	54.8				
58.2	58.3				
65.5		66[a]	(^{150}Pr)	65.5	^{150}Pr
	68.9				
	71.7				
	74.2	74[a]	^{150}Pr	74.2	^{150}Pr
	76.6				
	79.9				
82.3	81.9				
	87.6				
90.8	90.8	91.5[b,k]	101^{+0}_{-1}	91.0	^{101}Y
95.1					
98.2	98.2	98.3[b,k]	101^{+1}_{-0}	98.2	^{101}Y
		99[a]	(^{101}Zr)		
100.5	100.7				
102.7					
	103.4				
109.2		109.4[b]	150±0	109.3	^{150}Pr
119.3					

YTTRIUM, PRAESODYNIUM Cont'd

Present E_γ (keV)		Others		Assigned	
		E_γ (keV)	Mass	E_γ (keV)	Mass
Y	Pr				
	122.6	122.0[b]	99^{+1}_{-0}	122.3	^{99}Y
	125.2				
130.2	130.2				
	134.5				
158.2	(158)				

ZIRCONIUM, CERIUM

Present E_γ (keV)		Others E_γ (keV)	Mass	Assigned E_γ (keV)	Mass
Zr	Ce				
	48.0				
	52.2				
53.6	53.2				
55.0	54.7				
	58.0				
	59.1				
64.3	64.3				
	70.2				
	75.2				
82.8					
	87.3				
98.2	98.0	$97.1^{c,d,k}$	^{150}Ce	97.7	^{150}Ce
		97.5^{b}	150±1		
		99^{a}	(^{101}Zr)		
	104.0	$103.2^{b,h,1}$	$^{150}_{-1}$	103.6	^{150}Ce
117.8	117.6				
121.6					
130.2	(130)	$130.9^{b,h,1}$	150±0	130.6	^{150}Ce
133.8	133.4	$135.4^{b,g}$	$^{148}_{-0}$	134.0	^{148}Ce
	(135.9)				
	(141.1)				
143.1	142.4	143^{a}	^{149}Pr		

ZIRCONIUM. CERIUM Cont'd

Present E_γ (keV)		Others		Assigned	
		E_γ (keV)	Mass	E_γ (keV)	Mass
Zr	Ce				
		142.6[b]	$^{149}{}^{+0}_{-1}$	142.7	^{149}Ce
		145.2[f]			
	151.5	151.9[d]	^{102}Zr	151.8	^{102}Zr
		152.1[b]	$^{101}{}^{+1}_{-0}$		
		153[a]	^{102}Zr		
158.8	(158.4)	155.7[f]			
		158.7[c]	^{148}Ce	158.7	(^{148}Ce)
		158.8[b]	$^{147}{}^{+0}_{-1}$		
		158[a]	^{148}Ce		
	209.5	209[d,k]	^{150}Ce	209.5	^{150}Ce
	213.1	212.7[d]	^{100}Zr	212.9	^{100}Zr
		214.8[f]			

NIOBIUM, LANTHANUM

Present E_γ (MeV)		Others E_γ (MeV)	Others Mass	Assigned E_γ (MeV)	Assigned Mass
Nb	La				
46.9	46.4				
56.2	56.0				
58.1	57.9	58.3[b,k]	147±2	58.1	^{147}La
61.2					
	62.8				
64.5	64.2	64[a]	^{146}La	64.3	^{146}La
66.2	65.9				
67.1	66.9				
72.1					
73.6					
	74.0				
77.6	77.6				
81.1					
82.1	81.8	82.8[b,l]	146^{+1}_{-0}	82.2	^{146}La
84.4	84.0				
91.2	90.8				
97.0	96.9				
100.3	99.6	100[a]	(^{145}La)	100.0	^{145}La
102.0					
104.0	103.7	105.0[b]	146±2	104.3	^{146}La
106.7					
	114.8				

NIOBIUM, LANTHANUM Cont'd

Present E_γ (MeV)		Others E_γ (MeV)	Mass	Assigned E_γ (MeV)	Mass
Nb	La				
119.5	119.1				
125.0					
126.4	126.1				
130.7	130.4	130.5[b]	146±0	130.6	^{146}La
		131[a]	^{146}La		
	135.8				
	140.9	140.9[b]	104±0	140.9	^{104}Nb
	(144.5)	144.1[b]	104±1	144.3	^{104}Nb
	150.4				
	153.8				
	156.8				
159.3	158.8	158.8[b,k]	147^{+0}_{-1}	158.9	(^{147}La)
		158[a]	^{148}Ce		
	162.1				
	(164.1)	164.2[b]	130±0	164.2	^{103}Nb
167.7	167.5	167.7[b,l]	146^{+1}_{-0}	167.7	^{146}La
172.2	172.0	175.0[e]		172.2	
	182.8				

MOLYBDENUM, BARIUM

Present E_γ (keV)		Others		Assigned	
		E_γ (keV)	Mass	E_γ (keV)	Mass
Mo	Ba				
45.3					
48.4					
50.1					
58.1					
64.3					
65.9	66.4				
94.8	94.9	95[a]	^{106}Mo	94.9	^{106}Mo
	98.2				
102.4	102.7	100.9[j]	141	102.5	^{141}Ba
109.8	110.0	109.7[b]	145±2	109.8	^{145}Ba
112.4	112.6			112.4	(^{104}Mo)
		113[a]	^{144}Ba		
		112.3[b]	104±0		
		113.4[j]	141		
117.2	117.6	117.3[b]	144±1	117.3	(^{142}Ba)
		118[a]	^{140}Cs		
		118.7[j]	141		
		117.9[j]	142		
137.8	138.0	137.7[j]	141	137.9	^{141}Ba
144.8	144.7	(144.1)[b,g]	104^{+1}_{-0}	144.7	(^{104}Mo)
152.1	152.1	(151)[a]	^{106}Mo	152.1	^{106}Mo

MOLYBDENUM, BARIUM Cont'd

Present E_γ (keV)		Others		Assigned	
		E_γ (keV)	Mass	E_γ (keV)	Mass
Mo	Ba				
154.3					
	155.0				
	164.9				
(171.7)	171.9	172[2]	^{106}Mo	171.9	^{106}Mo
		171.7[d]	^{106}Mo		
		172.2[b]	106±0		
181.4		183[a]	^{144}Ba	181.4	(^{145}Ba)
		181.0[c]	^{146}Ba		
		183.5[b,g]	145±1		
	193.0	192[a]	^{106}Mo	193.0	(^{105}Mo)
		192.3[d]	^{104}Mo		
		193.6[b]	105±0		
200.0		199[a]	^{144}Ba	199.6	^{144}Ba
		198.4[j]	142		
		199.4[c]	^{144}Ba		

TECHNETIUM, CESIUM

Present E_γ (keV)		Others		Assigned	
		E_γ (keV)	Mass	E_γ (keV)	Mass
Tc	Cs				
	45.5				
46.1					
	49.1				
50.3					
51.0	50.7				
54.1					
	54.5				
55.1					
58.2	58.0				
	59.5				
61.7	61.5	61[a]	^{140}Cs	61.6	^{140}Cs
62.3					
64.4	64.1				
	66.8				
68.8	69.0	69[a]	^{108}Tc	68.9	^{108}Tc
71.6	71.4	69.4[j]	141	71.5	^{141}Cs
76.7	76.5	74.6[j]	141	76.5	^{141}Cs
78.7	78.5	78[a]	^{140}Cs	78.6	^{140}Cs
80.1	79.9	79.4[j]	^{140}Cs	80.0	^{140}Cs
81.9	81.5	81.8[j]	141	81.7	^{141}Cs
84.3	84.1				
85.7	85.4	85.6[b,k]	105^{+1}_{-0}	85.6	^{105}Tc

TECHNETIUM, CESIUM Cont'd

Present E_γ (keV)		Others		Assigned	
		E_γ (keV)	Mass	E_γ (keV)	Mass
Tc	Cs				
	86.2				
	88.9				
90.2		89.7[j]	141		
		90.5[b,l]	142±0	90.3	^{142}Cs
91.1	91.6	92.1[j]	^{142}Cs	91.4	^{142}Cs
96.7		97.0[b,l]	142±0	96.9	^{142}Cs
	102.8	102.8[b,k]	105±0	102.8	^{105}Tc
104.6					
106.1	105.9	106.1[j]	141	106.0	^{141}Cs
		106.0[b]	142±2		
108.1	107.8				
	109.8				
	115.1	115.6[b,m]	109±0	115.4	^{109}Tc
119.7	119.5	118[a]	^{140}Cs	119.6	^{109}Tc
		119.4[b,m]	109±0		
		118.7[j]	141		
123.2	122.9	123[a]	^{109}Tc	123.1	^{109}Tc
125.0	124.5				
137.3	136.8				
138.3	138.3	138.3[j]	138	138.3	^{138}Cs
154.0	154.3	154.3[j]	138	154.1	^{138}Cs
161.7		161.5[f]			

RUTHENIUM, XENON

Present E_γ (keV)		Others E_γ (keV)	Others Mass	Assigned E_γ (keV)	Assigned Mass
Ru	Xe				
50.7	50.6				
	58.1				
63.0					
70.8					
	71.7	72[a]	^{110}Ru	71.7	^{110}Ru
74.2	74.3				
	76.6				
	81.9				
82.6					
	94.7				
96.2		96.2[b,h]	$^{110}_{-1}$	96.2	^{110}Ru
98.3	98.4	98[a]	^{108}(Tc)	98.3	^{108}Ru
100.7					
102.7	102.6				
104.0	(104.1)	103.5[b]	$^{111}_{-1}$	103.7	^{111}Ru
108.6					
117.8					
131.9		131.8[b]	110±0	131.8	^{110}Ru
138.3					
142.7					
143.4					
150.5		150[a]	(^{110}Ru)	150.5	(^{111}Ru)
		150.5[b]	111±0		

RHODIUM, IODINE

Present E_γ (keV)		Others E_γ (keV)	Others Mass	Assigned E_γ (keV)	Assigned Mass
Rh	I				
45.7	45.6				
	49.8	49[a]	^{116}Rh	49.8	^{116}Rh
52.8					
	57.1				
58.8	58.8	59[a]	^{136}I	58.8	^{136}I
60.5	60.6	60.5[b]	121±1	60.5	^{112}Rh
65.8	65.5				
	68.3				
82.5	82.3				
87.4	87.4	(88)[a]	^{136}I	87.4	^{136}I
91.5					
96.0					
(112.1)	112.1				
116.8	116.8				
	118.3				
137.8					
	155.3	155.0[b]	137±0	155.1	^{137}I
	158.9				
159.5	159.8				
	161.4				
	162.1				
	212.7				
	230.2				

PALLADIUM

Present E_γ (keV)
48.6
58.3
178.5

ANTIMONY

Present E_γ (keV)
45.8
58.3
60.7
65.7
71.2
75.2
76.6
81.8
82.5
91.8
125.4
126.0
138.3

---

[a]See Ref. 3. (Energy uncertainty ∿ ± 1 keV).

[b]See Ref. 7. (Energy uncertainty ∿ ± 0.2 keV).

[c]See Ref. 2. (Energy resolution ∿ 1 keV at 122 keV).

[d]See Ref. 1. (Energy resolution ∿ 1 keV at 122 keV).

[e]See Ref. 9. (Energy uncertainty ∿ ± 3 keV).

[f]See Ref. 10. (Energy uncertainty ∿ ± 3 keV).

[g]May be Doppler shifted according to Ref. 7.

[h]Isomeric transition ($t_{1/2}$ > 80 nsecs) from Ref. 7.

[j]See Ref. 12. (Energy uncertainty ∿ ± 1.5 keV to ± 2.0 keV).

[klm]Identify pairs of γ-rays attributed to the same cascade by Ref. 7.

TABLE II

LOW ENERGY CASCADE TRANSITIONS

Even-Even Nuclei

	E_γ (keV)[a]		$2^\pm 0^+$ Observed?		$P_K^{2^+}$ (E2)	$P_K^{4^+}$ (E2)
	$2^\pm 0^+$	$4^\pm 2^+$	Complementary gated	Self gated		
^{110}Zr	152	327	yes	(wk)	0.18	0.014
^{102}Zr	213	352	yes	(wk)	0.05	0.009
^{148}Ce	159	300	yes	(wk)	0.23	0.04
^{150}Ce	97	209	yes	yes	0.58	0.11
^{104}Mo	172	351	yes	wk	0.13	0.012
^{144}Ba	199	331	yes	no	0.12	0.03
^{146}Ba	181	333	yes	no	0.16	0.03

Odd Z Nuclei

	E_γ[b] (keV)	$\gamma_{1/2}$[c]	Observed? Complimentary gated	Self gated	P_K (E1)	P_K (M1)	P_K (E2)
^{101}Y	91.0	19	yes	yes	0.1	0.2	0.6
	98.2	21	yes	yes	0.1	0.2	0.5
^{146}La	82.2	13	yes	yes	0.2	0.7	0.7
	167.7	16	yes	yes	0.04	0.1	0.2
^{147}La	58.1	8	yes	yes	0.5	0.8	0.8
	158.9	10	yes	yes	0.05	0.2	0.2
^{105}Tc	85.6	16	wk	yes	0.2	0.4	0.6
	102.8	15	yes	no	0.1	0.2	0.5
^{109}Tc	115.4	18	yes	(wk)	0.08	0.2	0.4
	119.6	16	yes	yes	0.07	0.1	0.4
^{142}Cs	90.3	15	yes	yes	0.2	0.5	0.6
	96.9	16	yes	no	0.2	0.4	0.6

[a] See Refs. 1 and 2. [b] Energies in this work presented as final values.
[c] See Ref. 7.

FIGURE CAPTIONS

Fig. 1 Schematic diagram of electronics.

Fig. 2 Total coincidence X-ray spectrum.

Fig. 3 (a) Windows set on X-rays from light fragments. (b) Windows set on X-rays from heavy fragments.

Fig. 4 Total coincidence γ-ray spectrum.

Fig. 5 (a) Sorted γ-ray spectrum from gate on yttrium. (b) Sorted γ-ray spectrum from gate praseodymium.

Fig. 6 (a) Sorted γ-ray spectrum from gate on zirconium. (b) Sorted γ-ray spectrum from gate on cerium.

Fig. 7 (a) Sorted γ-ray spectrum from gate on niobium. (b) Sorted γ-ray spectrum from gate on lanthanum.

Fig. 8 (a) Sorted γ-ray spectrum from gate on molybdenum. (b) Sorted γ-ray spectrum from gate on barium.

Fig. 9 (a) Sorted γ-ray spectrum from gate on technetium. (b) Sorted γ-ray spectrum from gate on cesium.

Fig. 10 (a) Sorted γ-ray spectrum from gate on ruthenium. (b) Sorted γ-ray spectrum from gate on xenon.

Fig. 11 (a) Sorted γ-ray spectrum from gate on rhodium. (b) Sorted γ-ray spectrum from gate on iodine.

Fig. 12 Sorted γ-ray spectrum from gate on palladium.

Fig. 13 Sorted γ-ray spectrum from gate on antimony.

Fig. 14 Generalized decay scheme for lower levels in the fission fragments. All of the indicated modes of X-ray - γ-ray coincidences were accepted in the system used in this experiment.

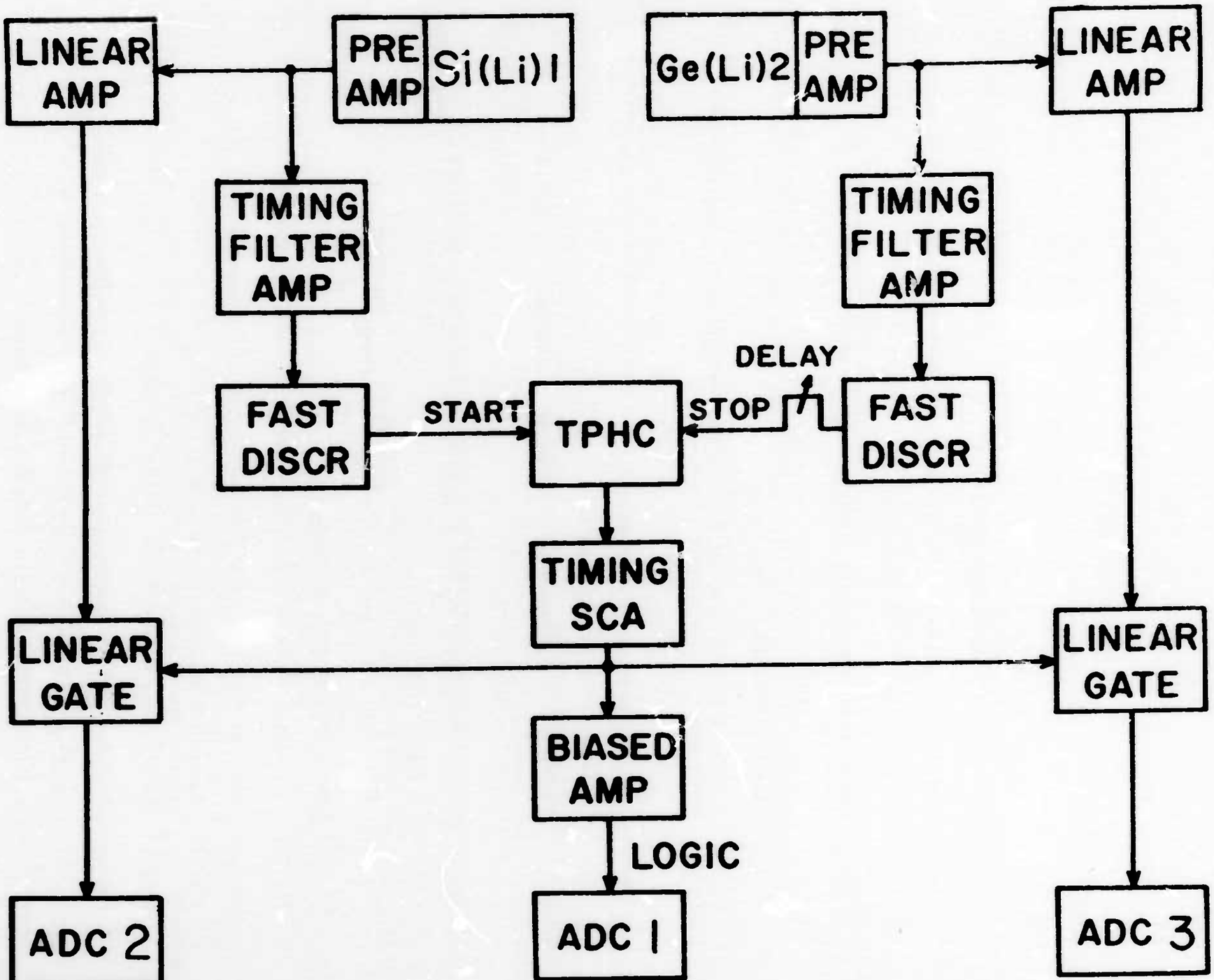
LINEAR AMP
PRE AMP
Si(Li) 1
Ge(Li)2
PRE AMP
LINEAR AMP
TIMING FILTER AMP
TIMING FILTER AMP
DELAY
FAST DISCR
START
TPHC
STOP
FAST DISCR
TIMING SCA
LINEAR GATE
LINEAR GATE
BIASED AMP
LOGIC
ADC 2
ADC 1
ADC 3

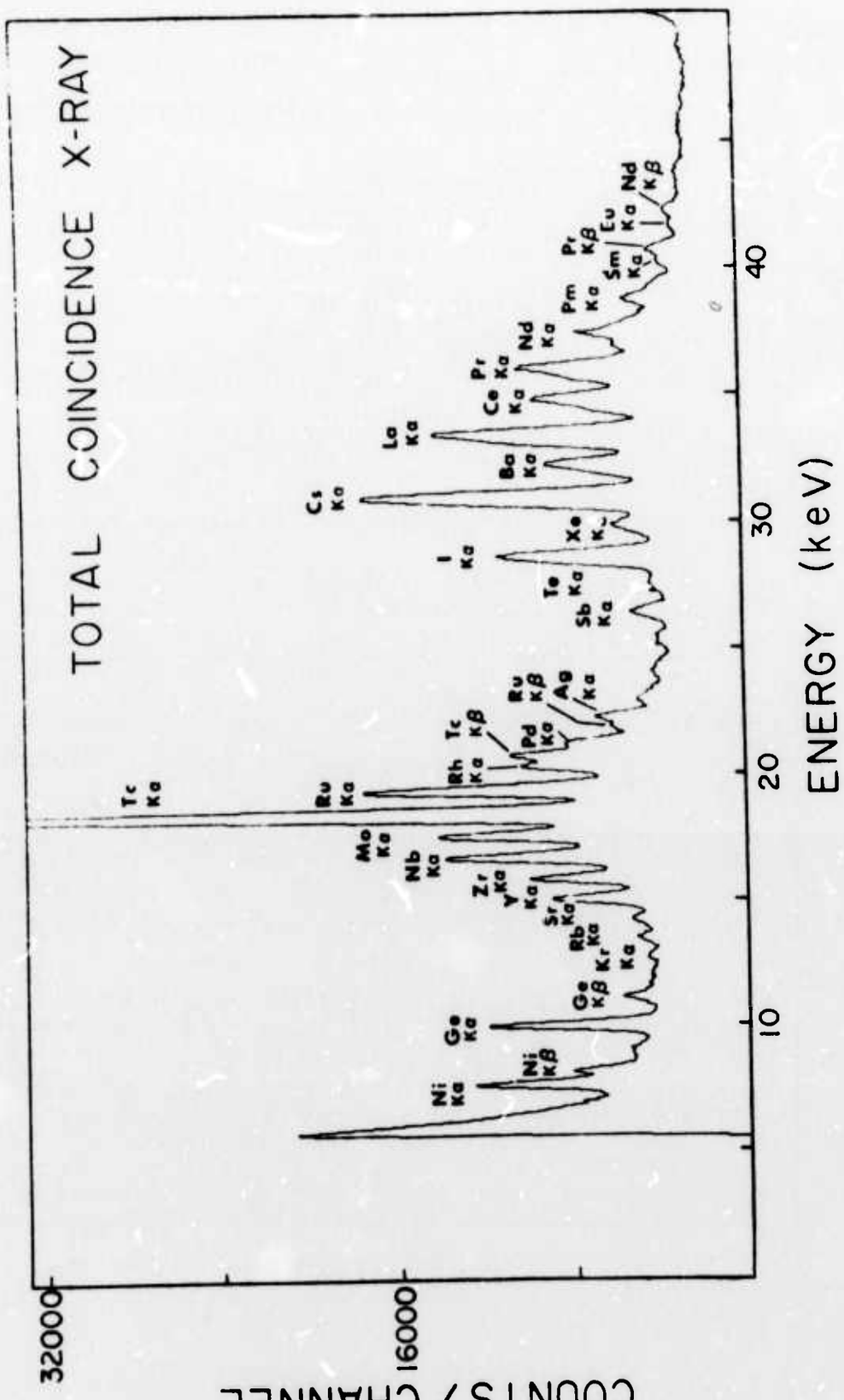
TOTAL COINCIDENCE X-RAY
COUNTS / CHANNEL
32000
16000
ENERGY (keV)
10
20
30
40
Tc Kα
Ru Kα
Rh Kα
Tc Kβ
Pd Kα
Ru Kβ
Ag Kα
Mo Kα
Nb Kα
Zr Kα
Y Kα
Sr Kα
Rb Kα
Kr Kα
Ge Kβ
Ge Kα
Ni Kβ
Ni Kα
Sb Kα
Te Kα
I Kα
Xe Kα
Cs Kα
Ba Kα
La Kα
Ce Kα
Pr Kα
Nd Kα
Pm Kα
Sm Kα
Eu Kα
Pr Kβ
Nd Kβ

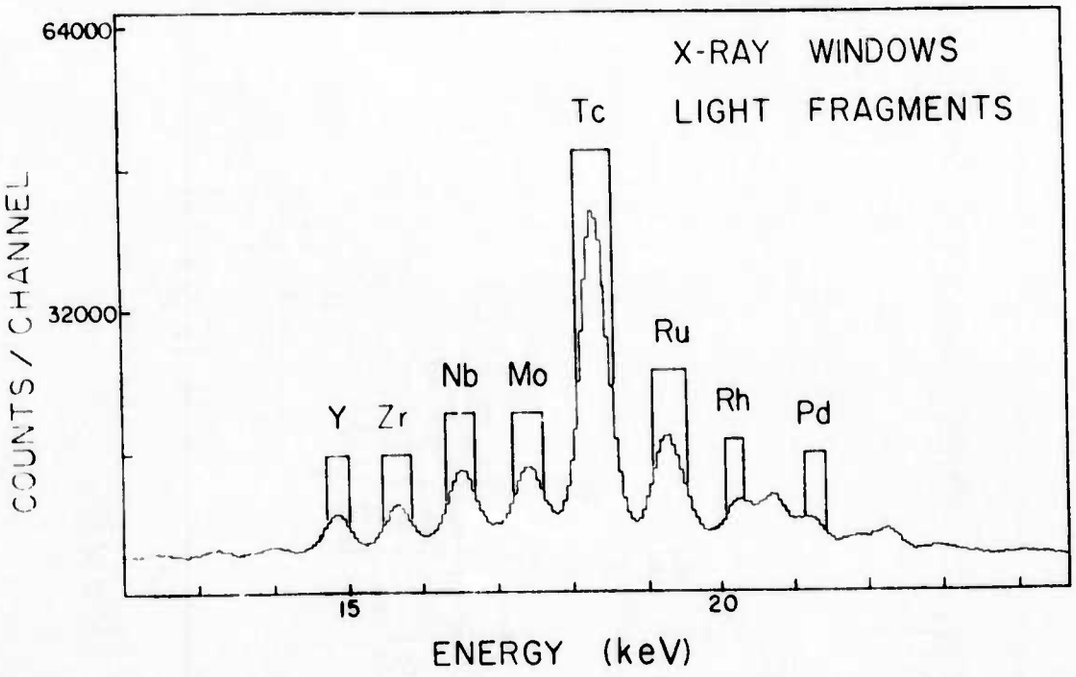
64000
32000
COUNTS / CHANNEL
X-RAY WINDOWS
LIGHT FRAGMENTS
Y
Zr
Nb
Mo
Tc
Ru
Rh
Pd
15
20
ENERGY (keV)

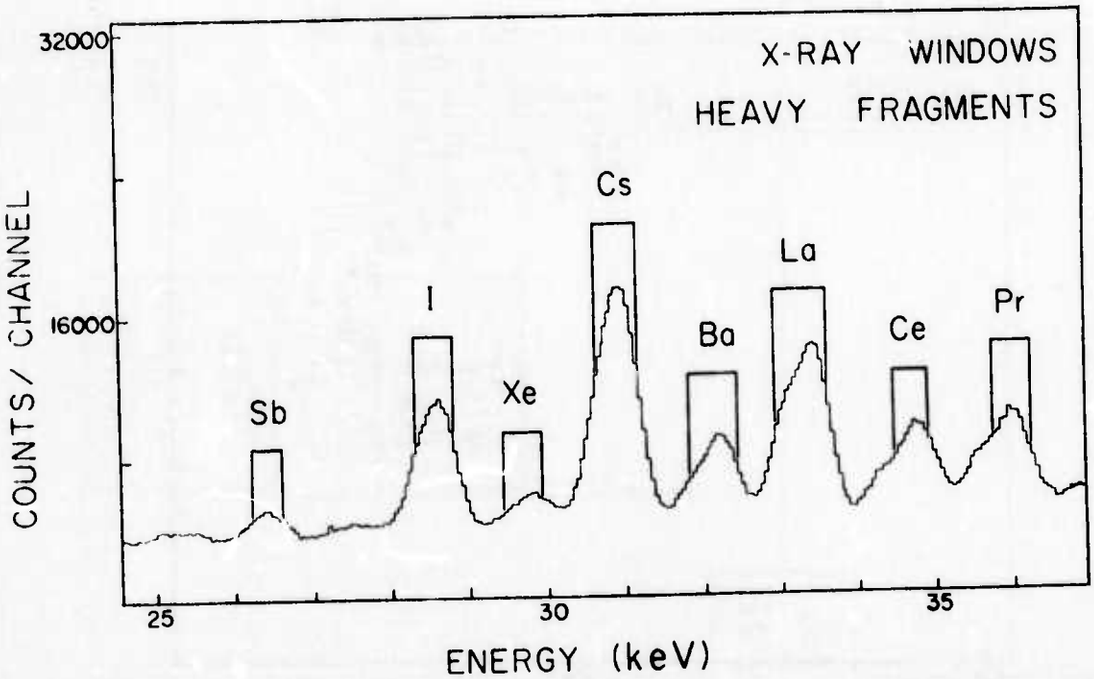
32000
16000
COUNTS / CHANNEL
X-RAY WINDOWS
HEAVY FRAGMENTS
Sb
I
Xe
Cs
Ba
La
Ce
Pr
25
30
35
ENERGY (keV)

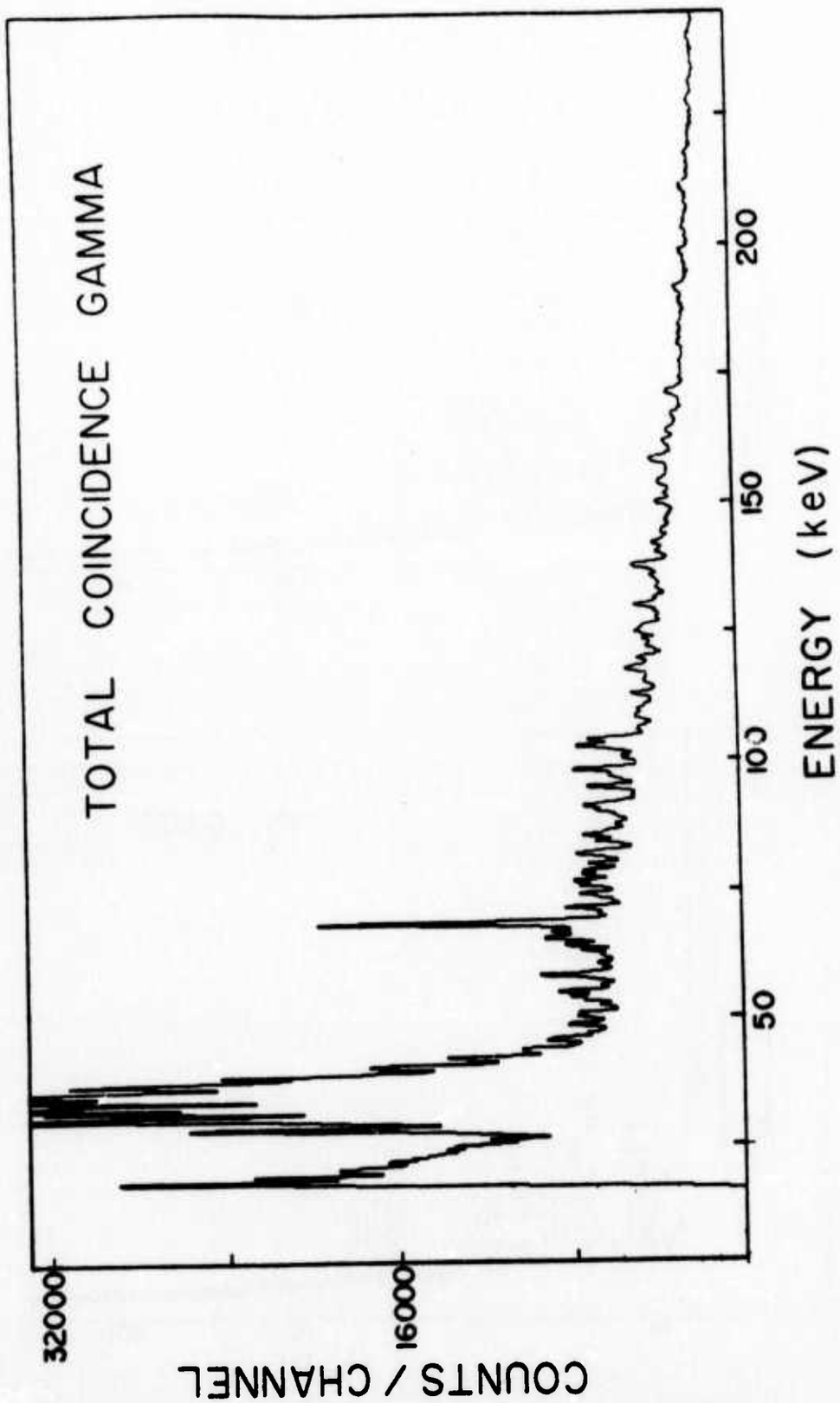
TOTAL COINCIDENCE GAMMA
COUNTS / CHANNEL
32000
16000
50
100
150
200
ENERGY (keV)

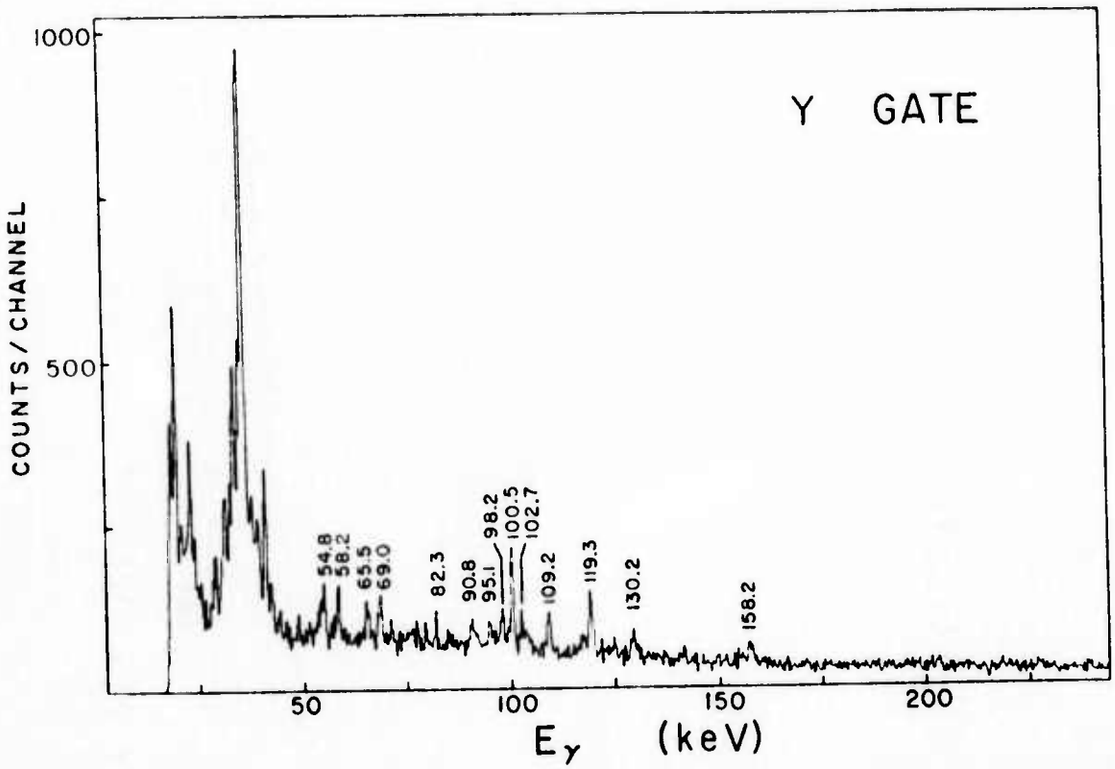
Y GATE
COUNTS / CHANNEL
1000
500
54.8
58.2
65.5
69.0
82.3
90.8
95.1
98.2
100.5
102.7
109.2
119.3
130.2
158.2
50
100
150
200
Eγ (keV)

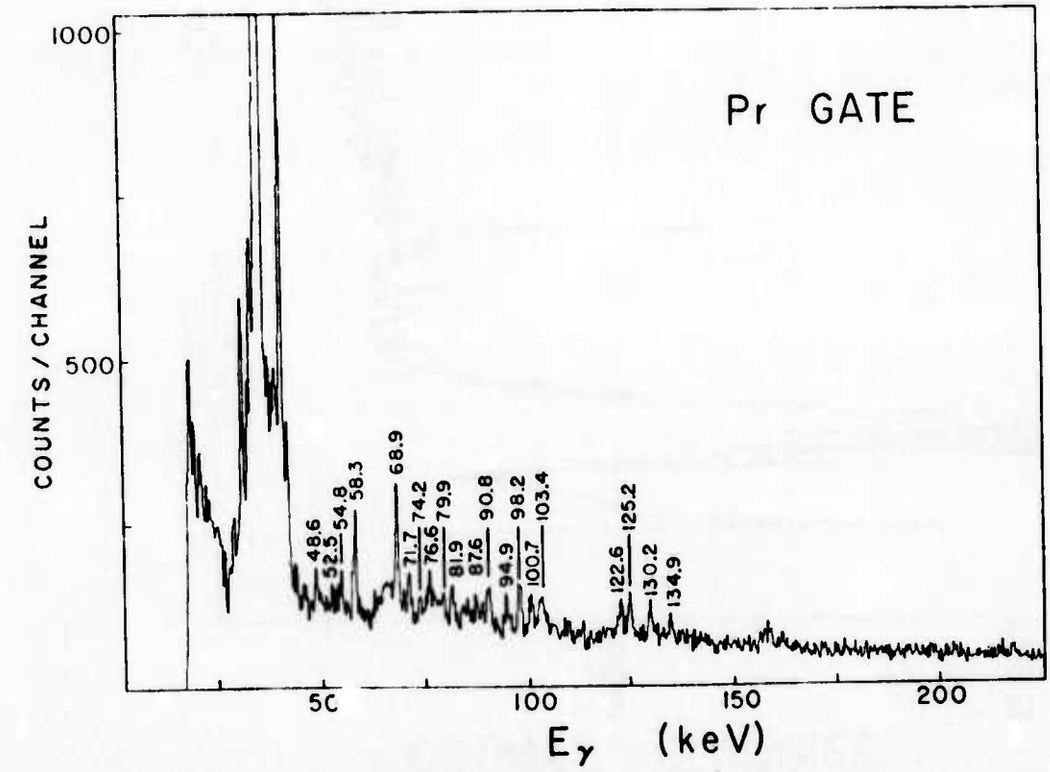
Pr GATE
COUNTS / CHANNEL
1000
500
48.6
52.5
54.8
58.3
68.9
71.7
74.2
76.6
79.9
81.9
87.6
90.8
94.9
98.2
100.7
103.4
122.6
125.2
130.2
134.9
50
100
150
200
Eγ (keV)

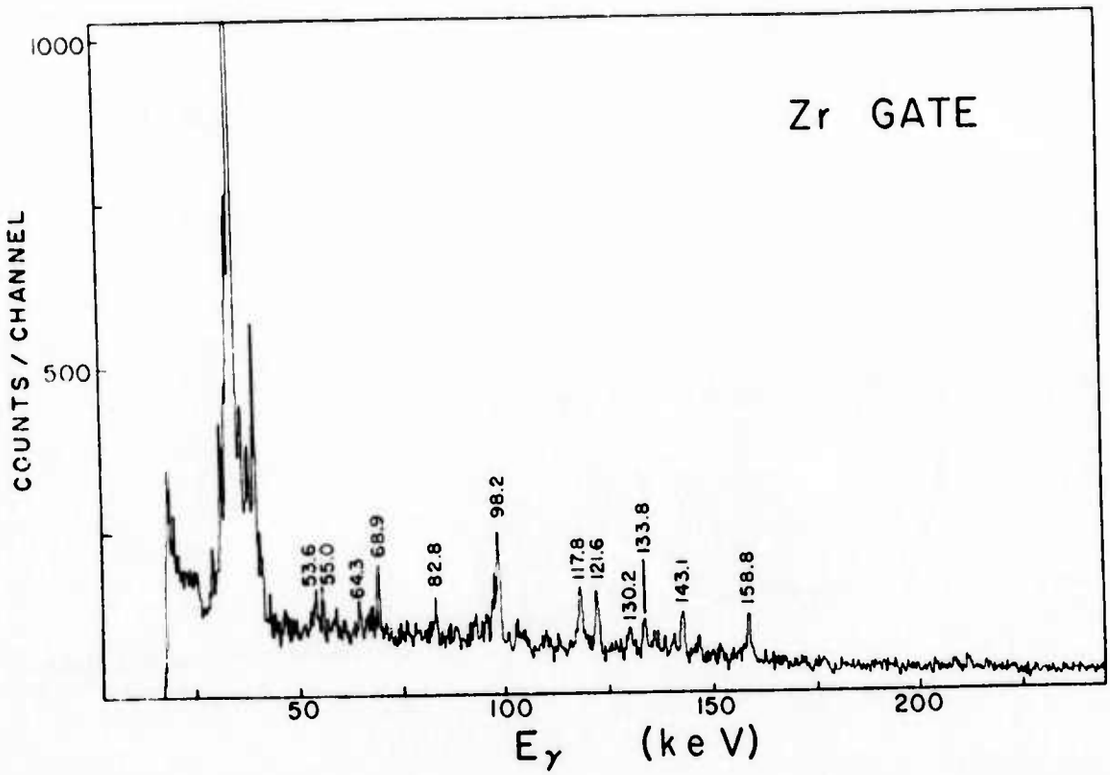
Zr GATE
COUNTS / CHANNEL
1000
500
50
100
150
200
E_γ (keV)
53.6
55.0
64.3
68.9
82.8
98.2
117.8
121.6
130.2
133.8
143.1
158.8

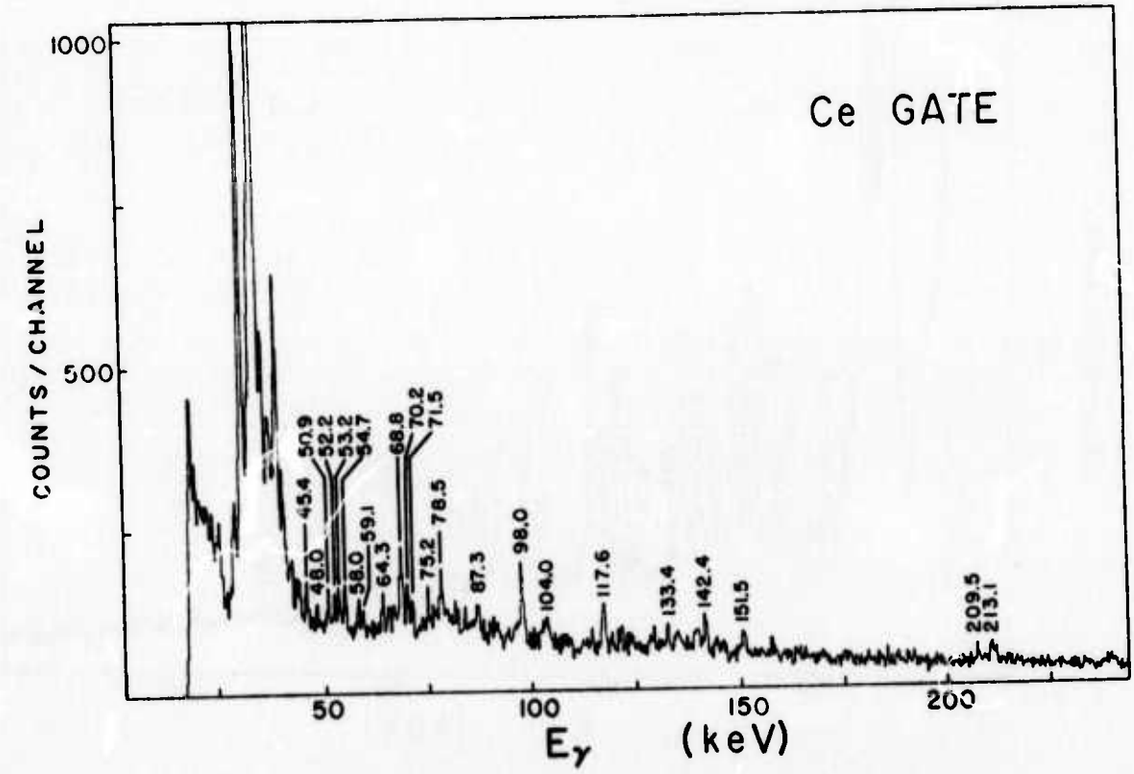
Ce GATE
COUNTS / CHANNEL
1000
500
50
100
150
200
E_γ (keV)
45.4
46.0
50.9
52.2
53.2
54.7
58.0
59.1
64.3
68.8
70.2
71.5
75.2
78.5
87.3
98.0
104.0
117.6
133.4
142.4
151.5
209.5
213.1

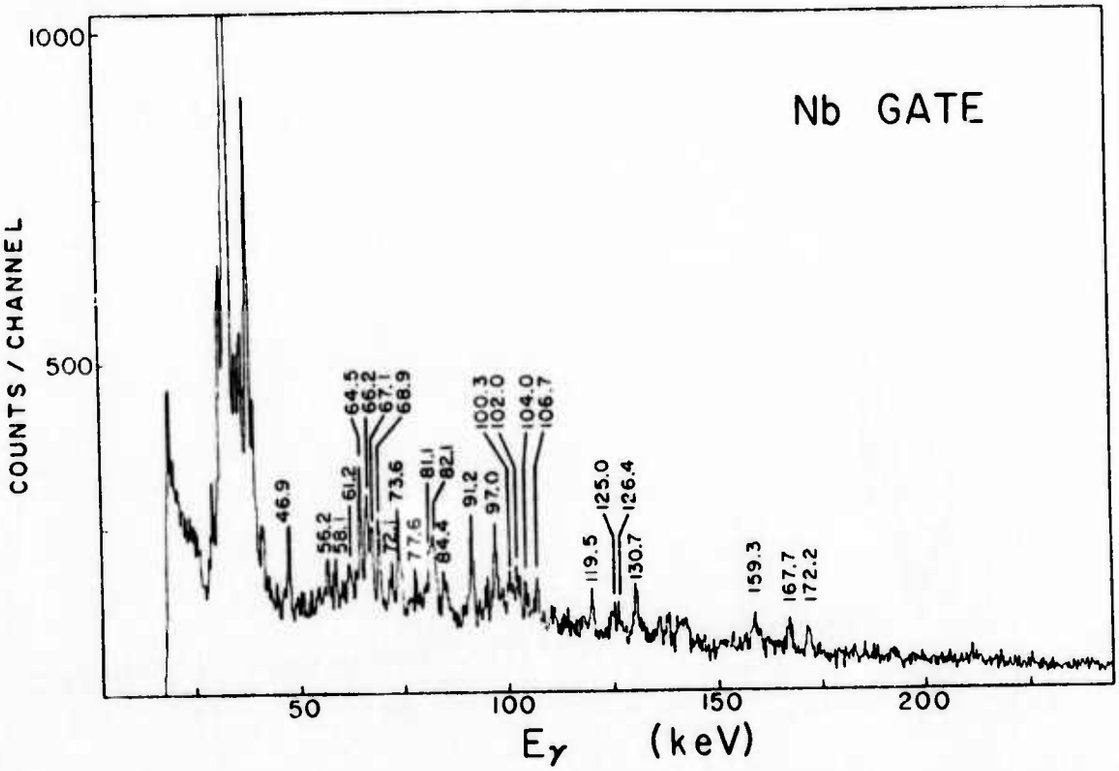
Nb GATE
COUNTS / CHANNEL
1000
500
50
100
150
200
E_γ (keV)
46.9
56.2
58.1
61.2
64.5
66.2
67.1
68.9
73.6
77.6
81.1
82.1
84.4
91.2
97.0
100.3
102.0
104.0
106.7
119.5
125.0
126.4
130.7
159.3
167.7
172.2

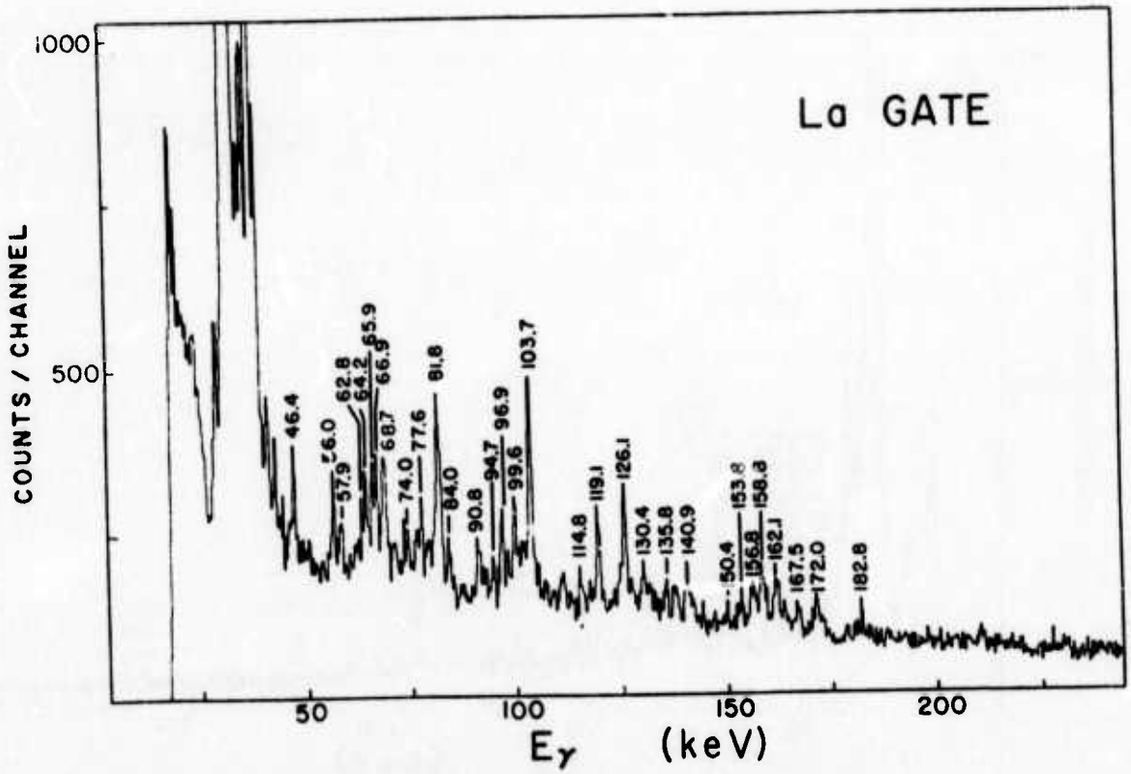
La GATE
COUNTS / CHANNEL
1000
500
50
100
150
200
E_γ (keV)
46.4
56.0
57.9
62.8
64.2
65.9
66.9
68.7
74.0
77.6
81.8
84.0
90.8
94.7
96.9
99.6
103.7
114.8
119.1
126.1
130.4
135.8
140.9
150.4
153.8
156.8
158.3
162.1
167.5
172.0
182.8

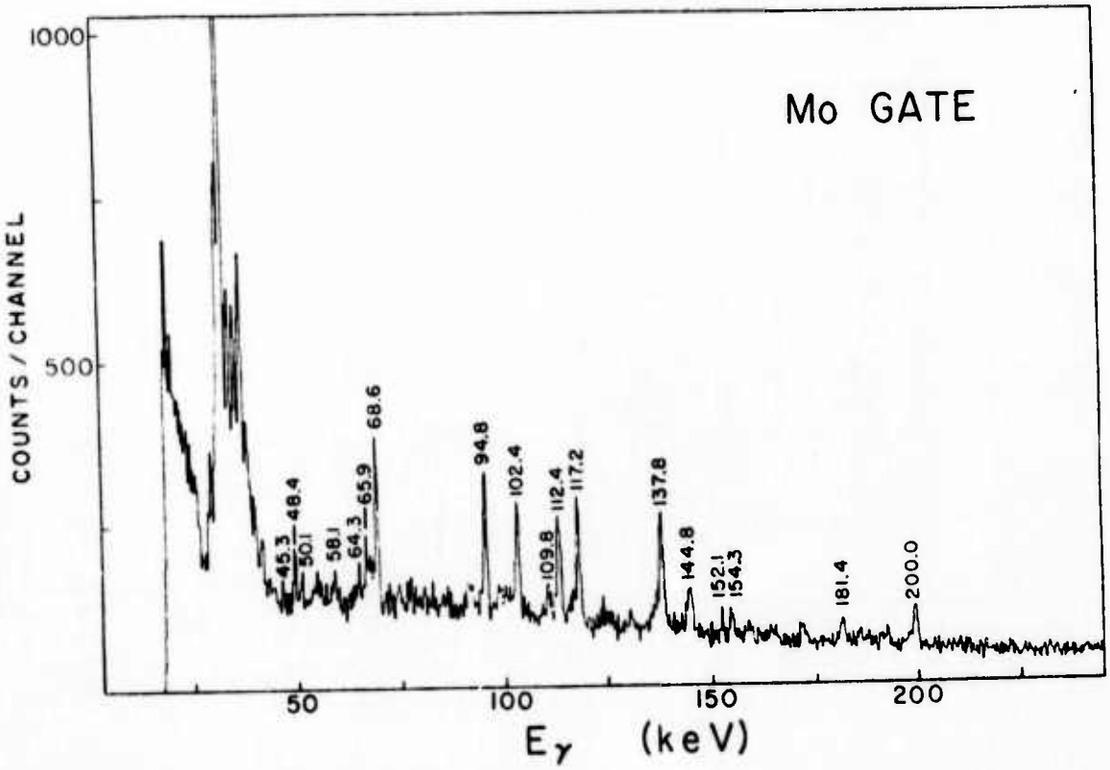
Mo GATE
COUNTS / CHANNEL
1000
500
45.3
48.4
50.1
58.1
64.3
65.9
68.6
94.8
102.4
109.8
112.4
117.2
137.8
144.8
152.1
154.3
181.4
200.0
50
100
150
200
Eγ (keV)

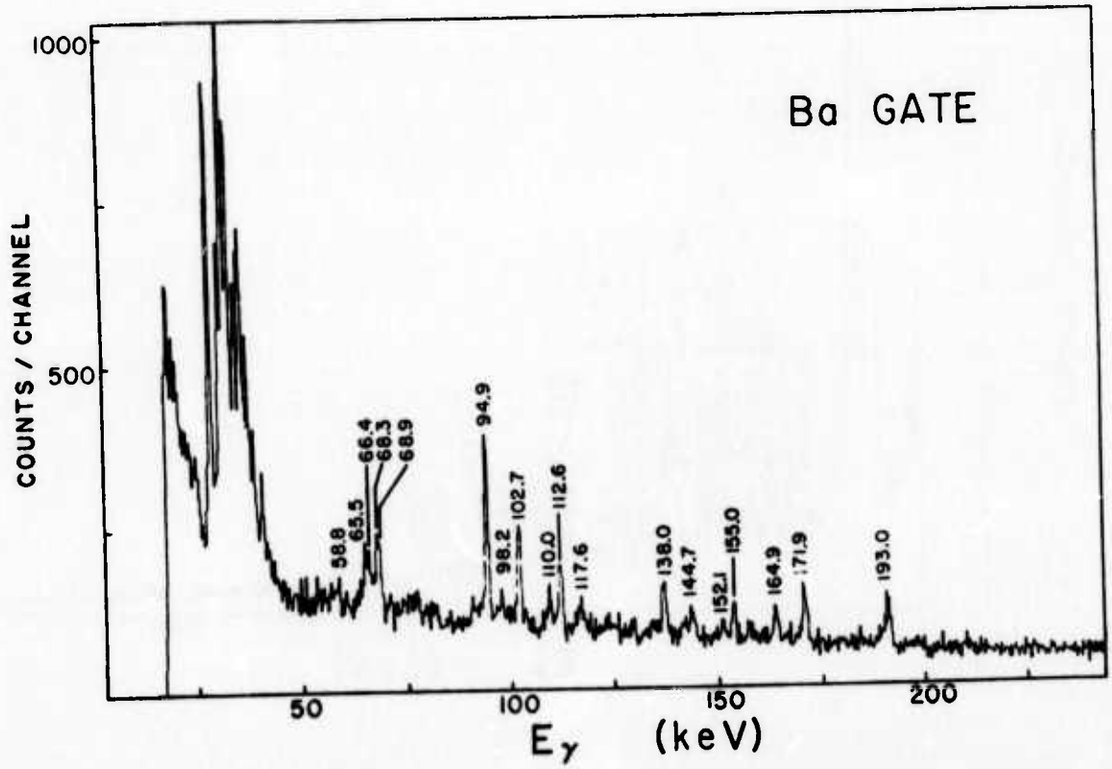
Ba GATE
COUNTS / CHANNEL
1000
500
58.8
65.5
66.4
68.3
68.9
94.9
98.2
102.7
110.0
112.6
117.6
138.0
144.7
152.1
155.0
164.9
171.9
193.0
50
100
150
200
Eγ (keV)

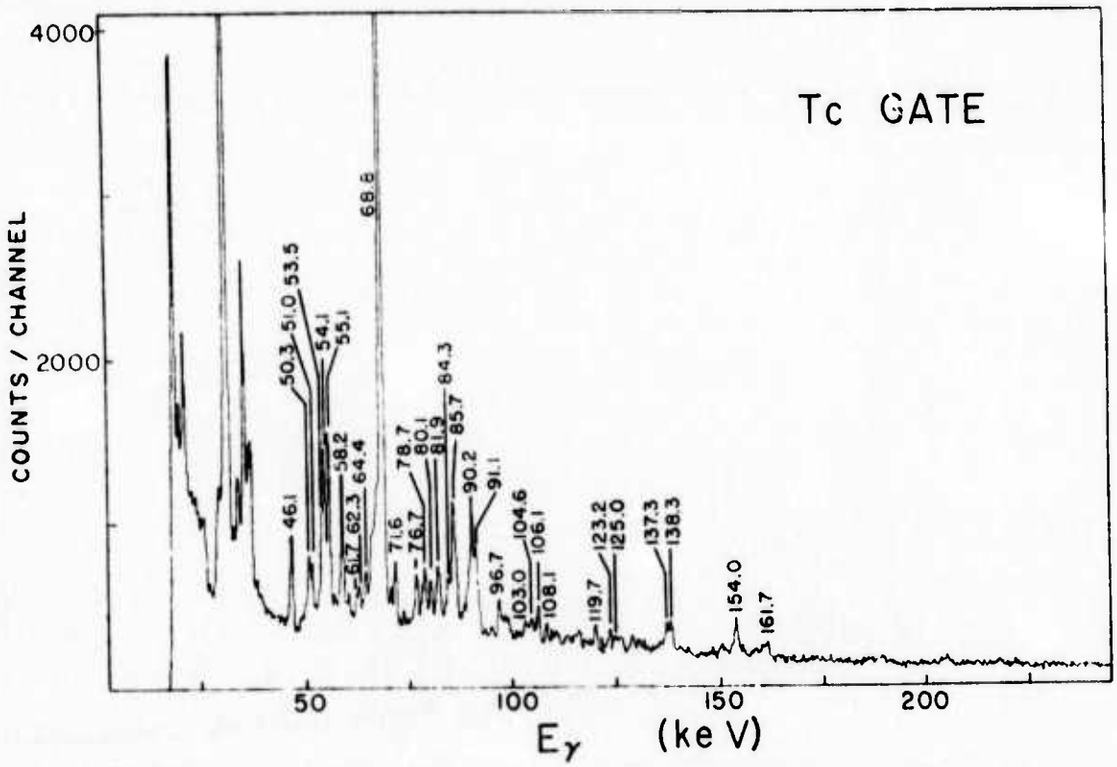
Tc GATE
COUNTS / CHANNEL
4000
2000
50
100
150
200
Eγ (keV)
46.1
50.3
51.0
53.5
54.1
55.1
58.2
61.7
62.3
64.4
68.8
71.6
76.7
78.7
80.1
81.9
84.3
85.7
90.2
91.1
96.7
103.0
104.6
106.1
108.1
119.7
123.2
125.0
137.3
138.3
154.0
161.7

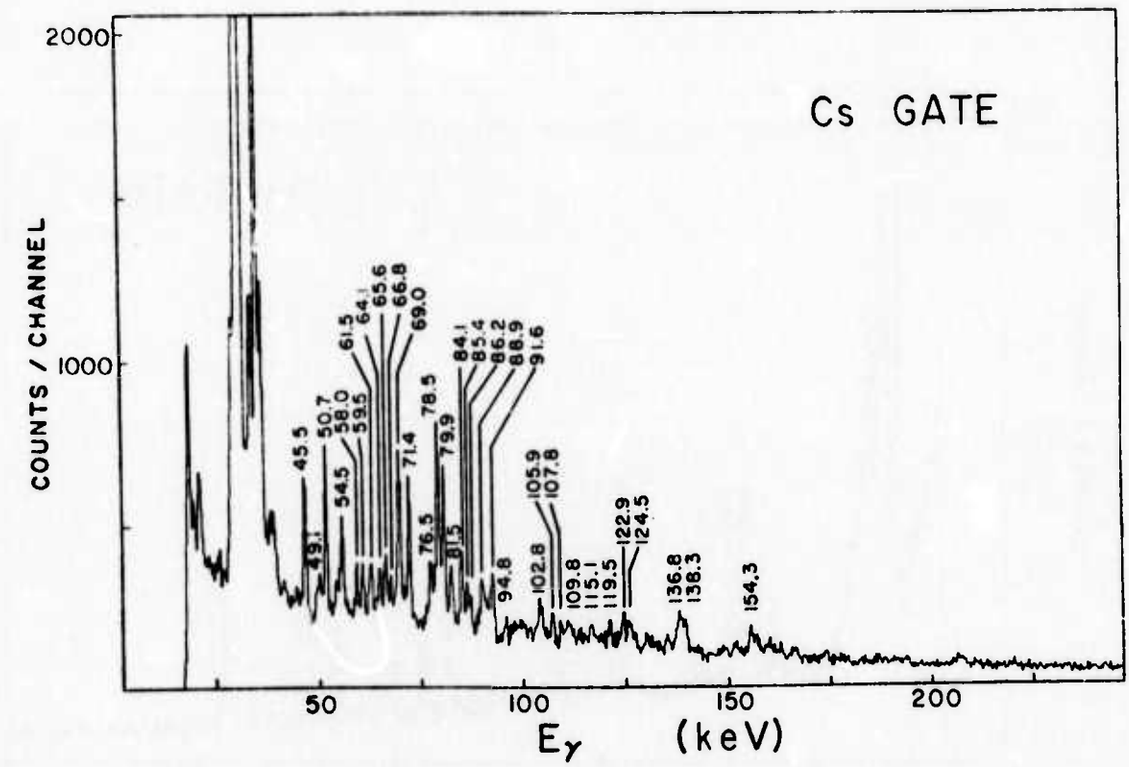
Cs GATE
COUNTS / CHANNEL
2000
1000
50
100
150
200
Eγ (keV)
45.5
49.1
50.7
54.5
58.0
59.5
61.5
64.1
65.6
66.8
69.0
71.4
76.5
78.5
79.9
81.5
84.1
85.4
86.2
88.9
91.6
94.8
102.8
105.9
107.8
109.8
115.1
119.5
122.9
124.5
136.8
138.3
154.3

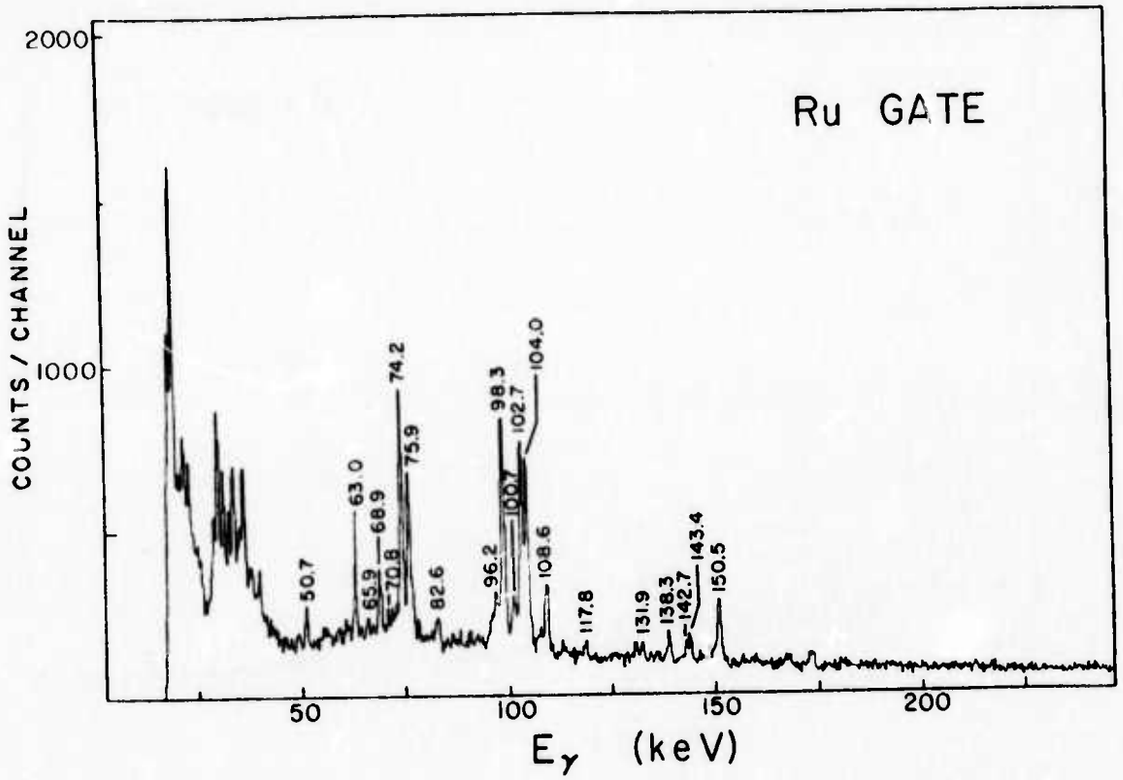
Ru GATE
COUNTS / CHANNEL
2000
1000
50.7
63.0
65.9
68.9
70.8
74.2
75.9
82.6
96.2
98.3
100.7
102.7
104.0
108.6
117.8
131.9
138.3
142.7
143.4
150.5
50
100
150
200
Eγ (keV)

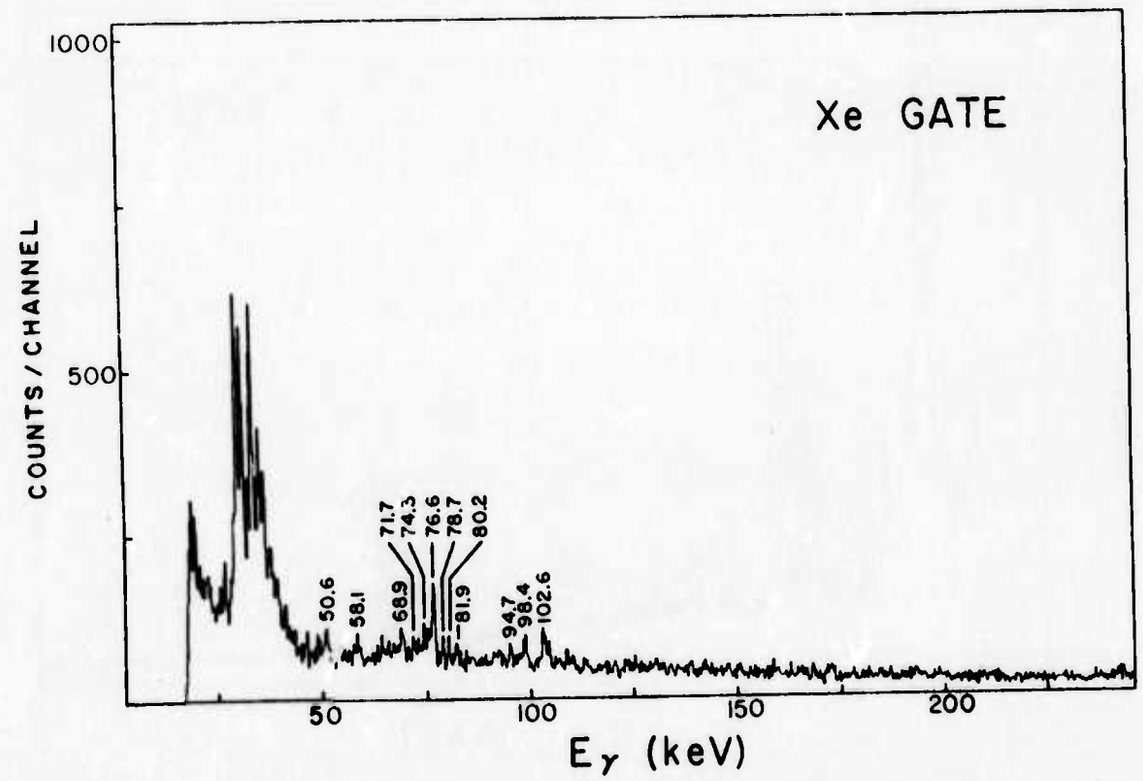
Xe GATE
COUNTS / CHANNEL
1000
500
50.6
58.1
68.9
71.7
74.3
76.6
78.7
80.2
81.9
94.7
98.4
102.6
50
100
150
200
Eγ (keV)

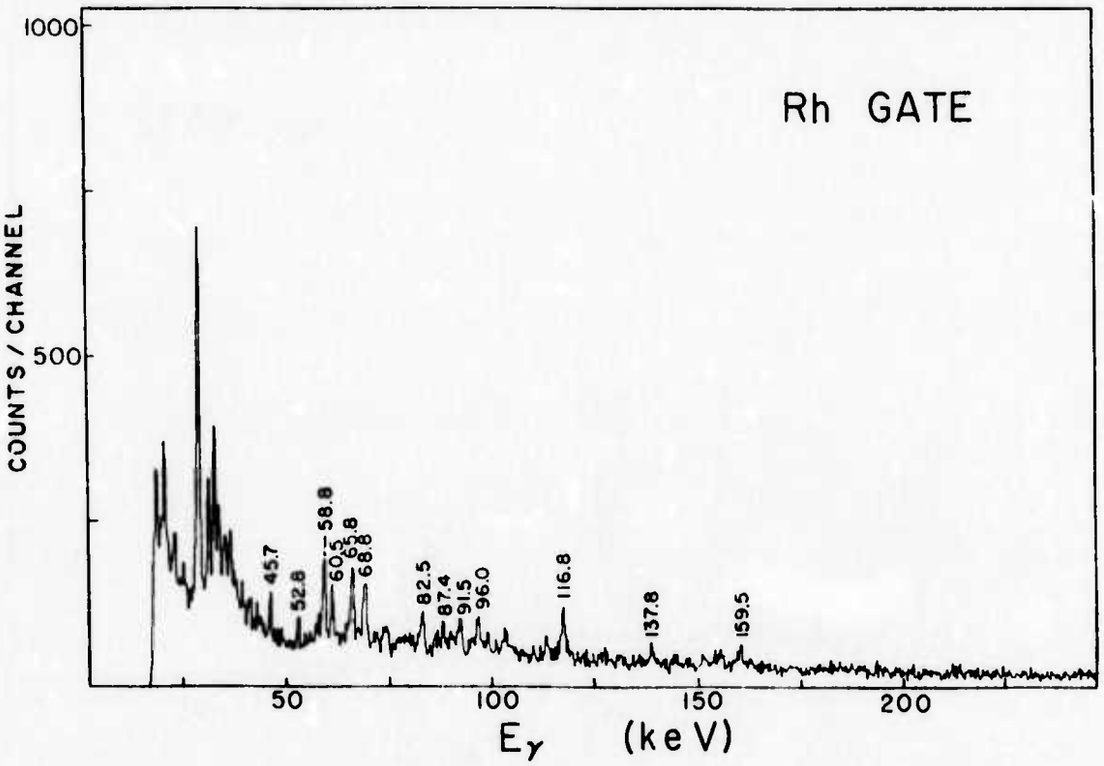
Rh GATE
COUNTS / CHANNEL
1000
500
45.7
52.8
58.8
68.8
82.5
87.4
91.5
96.0
116.8
137.8
159.5
50
100
150
200
Eγ (keV)

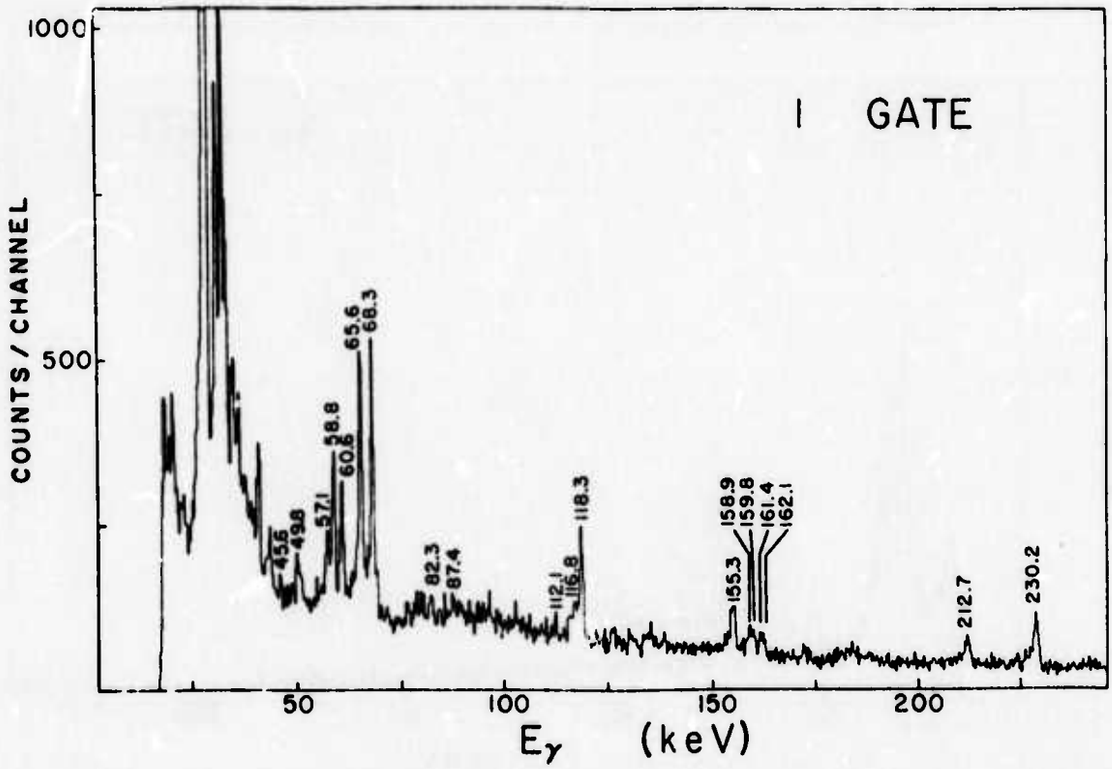
I GATE
COUNTS / CHANNEL
1000
500
45.5
49.8
57.1
58.8
60.8
65.6
68.3
82.3
87.4
112.1
116.8
118.3
155.3
158.9
159.8
161.4
162.1
212.7
230.2
50
100
150
200
Eγ (keV)

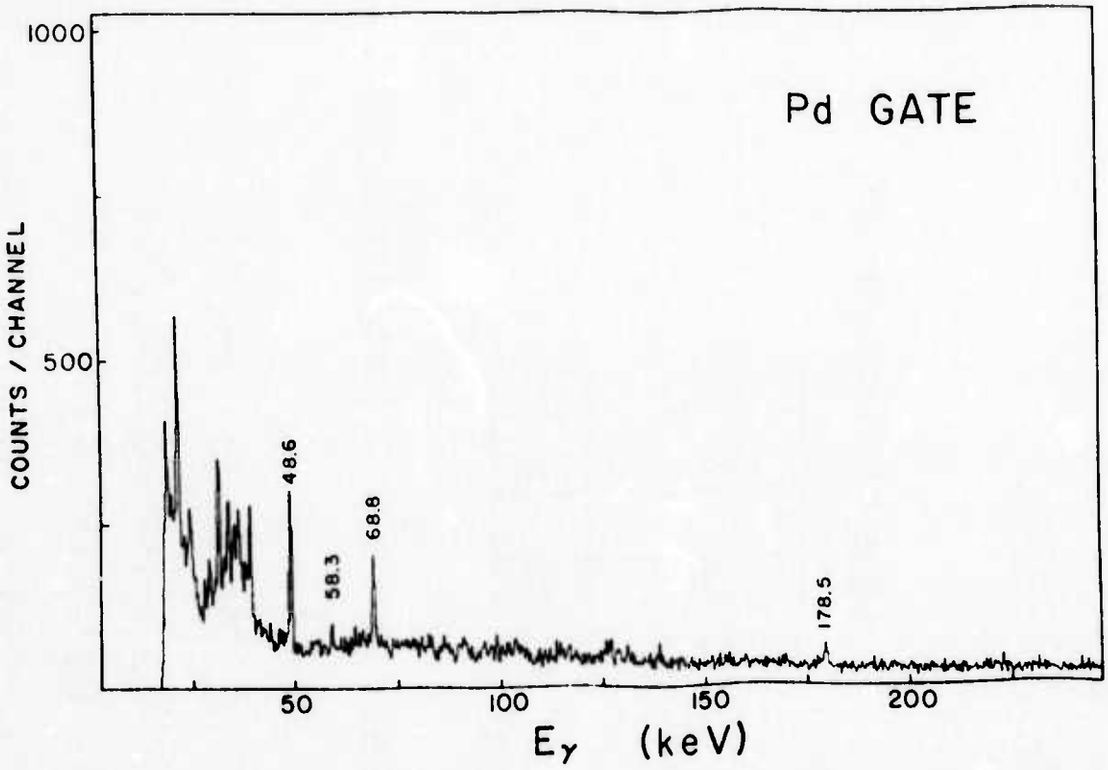
Pd GATE
COUNTS / CHANNEL
1000
500
48.6
58.3
68.8
178.5
50
100
150
200
Eγ (keV)

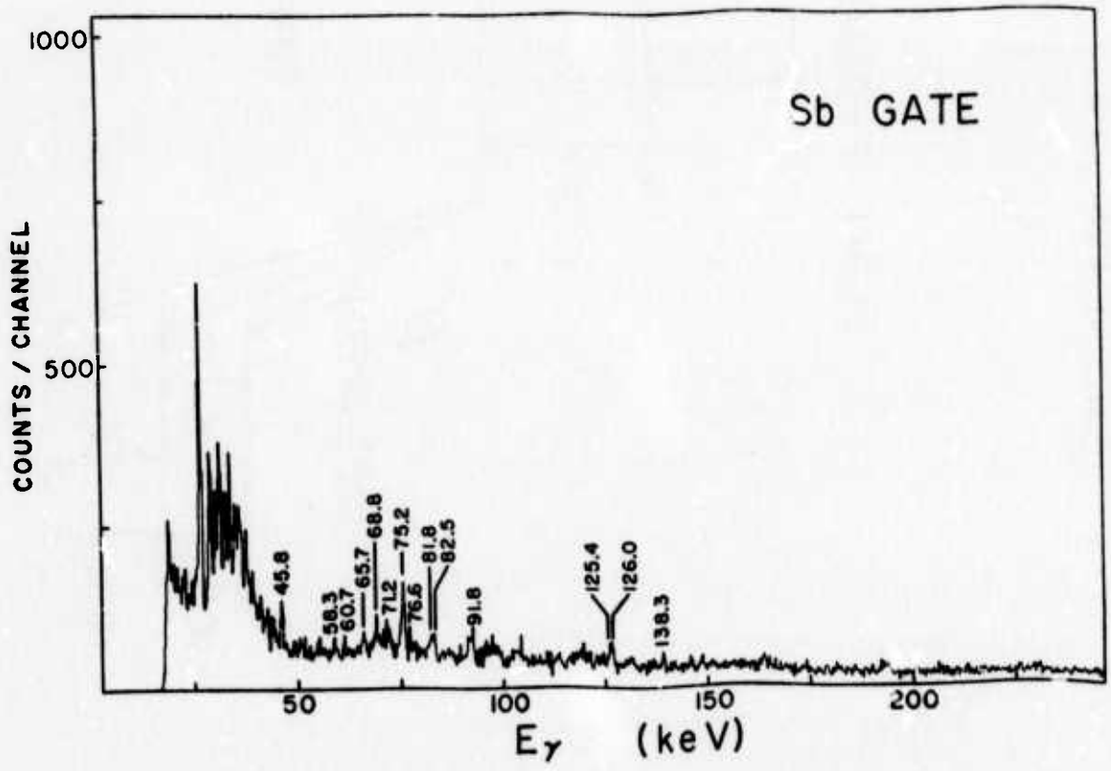
Sb GATE
COUNTS / CHANNEL
1000
500
45.8
58.3
60.7
65.7
68.8
71.2
75.2
76.6
81.8
82.5
91.8
125.4
126.0
138.3
50
100
150
200
Eγ (keV)

GENERALIZED DECAY SCHEME (POST NEUTRON)

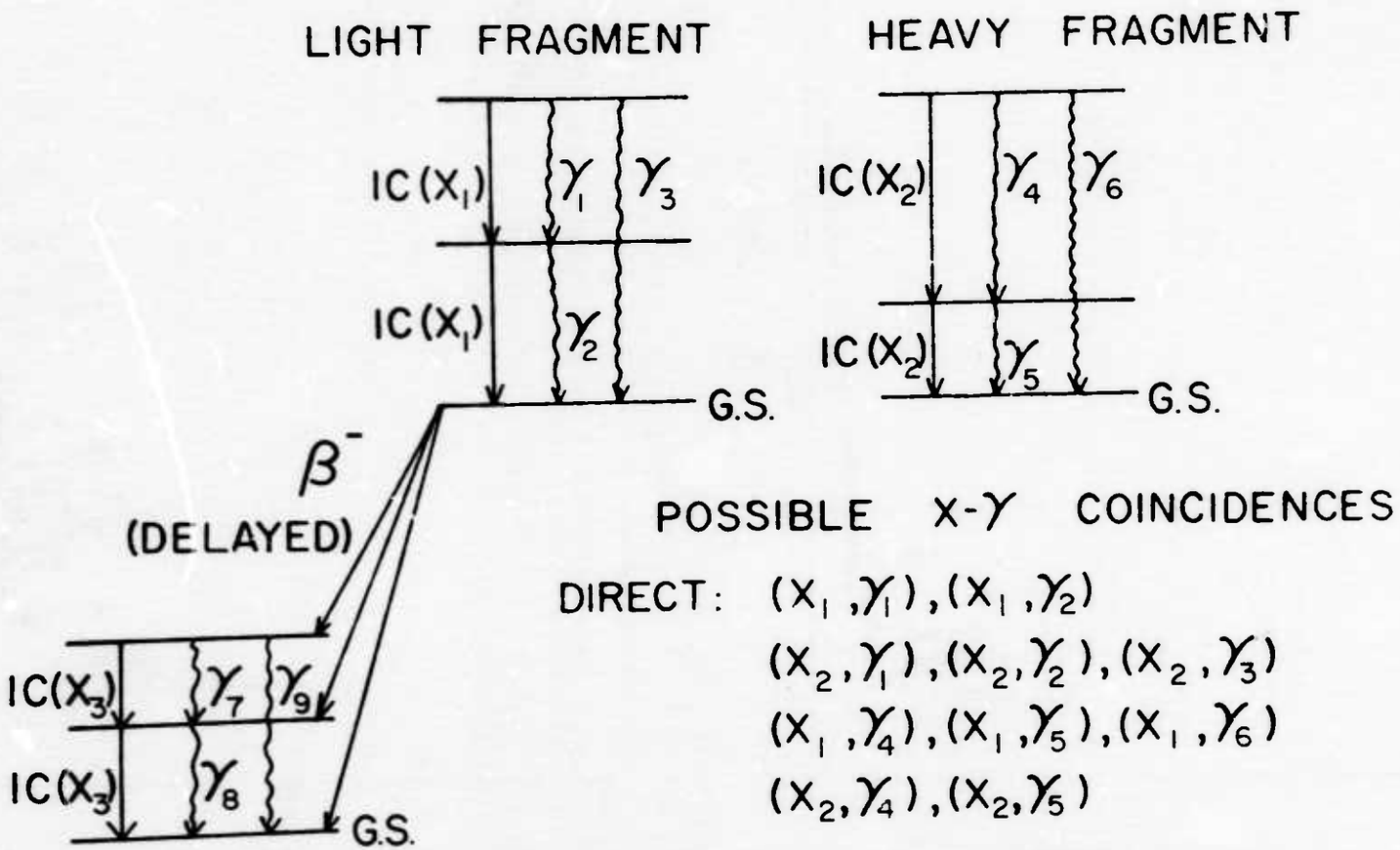

POSSIBLE X-γ COINCIDENCES

DIRECT: $(X_1, \gamma_1), (X_1, \gamma_2)$
$(X_2, \gamma_1), (X_2, \gamma_2), (X_2, \gamma_3)$
$(X_1, \gamma_4), (X_1, \gamma_5), (X_1, \gamma_6)$
$(X_2, \gamma_4), (X_2, \gamma_5)$

DELAYED: $(X_3, \gamma_7), (X_3, \gamma_8)$